APPLICATION OF HEAT CAPACITY MAPPING MISSION DATA TO REGIONAL GEOLOGIC ANALYSIS FOR MINERAL AND ENERGY RESOURCE EVALUATION

DECEMBER 1983
Final Report - HCMM Investigation S-79678-B

Submitted by: Kenneth Watson[1] - Principal Investigator
Susanne Hummer-Miller[1]
Daniel H. Knepper, Jr.[1]
M. Dennis Krohn[2]
Melvin H. Podwysocki[2]
Howard H. Pohn[2]
Gary L. Raines[1]
Lawrence C. Rowan[2]

[1] U.S. Geological Survey
MS 964, Box 25046, DFC
Denver, CO 80225

[2] U.S. Geological Survey
MS 927 National Center
Reston, VA 22092

FEB 1984 RECEIVED NASA STI FACILITY ACQ BRANCH

Prepared for: GODDARD SPACE FLIGHT CENTER
HCMM Investigations
Greenbelt, MD 20771

Prints of the images in this report may be inspected at U.S. Geological Survey Libraries in Reston, VA., Denver, CO, and Menlo Park, CA. Duplicate prints are available, at cost, from the U.S. Geological Survey Photo Library, Box 25046, DFC, MS 914, Denver, CO 80225.

0272-101

REPORT DOCUMENTATION PAGE	1. REPORT NO.	2.	3. Recipient's Accession No.

4. Title and Subtitle
Application of Heat Capacity Mapping Mission data to regional geologic analysis for mineral and energy resource evaluation.

5. Report Date
December 1983

6.

7. Author(s) K. Watson, S. Hummer-Miller, D.H. Knepper, Jr., M.D. Krohn M.H. Podwysocki, H.H. Pohn, G.L. Raines, and L.C. Rowan

8. Performing Organization Rept. No.

9. Performing Organization Name and Address
U.S. Geological Survey
Geophysics Branch
Box 25046, DFC, MS 964
Denver, CO 80225

10. Project/Task/Work Unit No.

11. Contract(C) or Grant(G) No.
(C) S-79678-B
(G)

12. Sponsoring Organization Name and Address
Locke Stuart
NASA - HCMM Investigative Support
Goddard Space Flight Center, Code 902
Greenbelt, MD 20771

13. Type of Report & Period Covered
Type III, Final Report

14.

15. Supplementary Notes

16. Abstract (Limit: 200 words)

HCMM thermal-inertia images of a diversity of terranes and geologic settings have been examined in conjunction with topographic, geologic, geophysical, and Landsat data. The images were found to have attributes similar to bedrock maps. In the Cascades region, two new features were identified and a method was developed to characterize regional terranes using linear feature data. Two northeast-trending lineaments were discovered in the Overthrust Belt of Montana and Idaho. The longer of the two extends from the Idaho-Oregon border, through the Idaho batholith and across the Lewis thrust. It coincides, along segments, with mapped faults and an aeromagnetic pattern change. A major lineament crossing the Colorado Plateau and the Southern Rocky Mountains was detected on several thermal-inertia images and evidence was found for the existence of a geologic discontinuity. Thermal inertias of igneous rocks in the Richfield, Utah, quadrangle were consistent with previous results, and this led to the development of a simple 3 component model. Sedimentary rocks in Richfield and the Appalachian Mountains were found to have thermal inertias consistent with literature values. Vegetation-covered areas in Richfield and the Silver City quadrangle (Arizona and New Mexico) displayed thermal-inertia differences within heavily vegetated areas although no appreciable correlation was found between vegetation cover and thermal inertia. Resistant ridges and knolls have high thermal inertias and thermal-inertia contrasts occurred at lithologic and fault contacts. In the heavily vegetated Pinaleno Mountains, Arizona, a lithologic unit obscured on Landsat MSS data due to the vegetation cover, exhibited a thermal-inertia contrast with it surroundings and in the Appalachian Mountains several resistant geologic units could be traced. These results indicate that thermal-inertia mapping may have greater potential in vegetated areas than previously recognized.

17. Document Analysis a. Descriptors

b. Identifiers/Open-Ended Terms

c. COSATI Field/Group

18. Availability Statement:	19. Security Class (This Report)	21. No. of Pages
	20. Security Class (This Page)	22. Price

CONTENTS

ILLUSTRATIONS

ABSTRACT

Heat Capacity Mapping Mission (HCMM) data of a diversity of terranes and geologic settings have been examined to evaluate their use for detecting and mapping geologic features in support of energy and mineral resource studies. Thermal-inertia images were prepared from the day and night HCMM digital data using an algorithm developed previously by us, and analyzed by comparing to topographic, geologic, and geophysical maps and other available data. Selected Landsat and digital terrain data sets were also co-registered with HCMM data in order to study the effects of vegetation and topography.

In the Cascade region, general thermal-inertia and reflectance statistics show differences between several large physiographic units. Analysis for structural and tectonic features indicates the complementary nature of HCMM and Landsat images. Two new features were identified and a method was developed that may be useful for recognizing and characterizing regional geologic terranes from linear features data.

HCMM data of the Overthrust Belt of Montana and Idaho was examined for expression of the structural framework. Overall structural style of folds and faults of the Overthrust Belt was clearly delineated from surrounding terrain, and two long northeast-trending linear features were discovered. One, in the Butte quadrangle, may be related to a bedrock-alluvium contact and occurs in an area of great interest for placer deposits. The other lineament extends southwest from near Frances Lake, Montana, across the Lewis thrust and the Montana lineament and through the Idaho Batholith. Mapped faults occur along segments of the lineament and along its extension to the Idaho-Oregon border a sharp change in the aeromagnetic patterns coincide with the extension.

The Colorado Plateau in the Richfield, Utah, area was examined for the thermal-inertia variations between several rock types. Sedimentary rocks

produce the expected relationships, with quartzites and orthoquartzites having the highest values, followed by dolomites and then shales and limestone. Granites were found to have higher thermal inertias than other igneous rocks, and a weak but consistent trend was observed among the other igneous rock types. Areas of hydrothermal alteration are generally too small to be observed on HCMM, although one thermal-inertia high was tentatively identified as an area of silicification.

A major lineament crossing the Colorado Plateau and the Southern Rocky Mountains was detected on several thermal-inertia images. The existence of a geologic discontinuity along the lineament is supported by gravity, aeromagnetic, seismic, geologic and topographic data; however, the nature of the discontinuity is unknown. The lineament extends from southwestern Arizona to northeastern Colorado and passes through the Hopi Buttes volcanic field, Arizona, a volcanic plug at Shiprock, New Mexico, the Creede and Cripple Creek mineral districts and the Pikes Peak batholith, Colorado.

Studies in the Basin and Range province focused on two 1^{o} by 2^{o} quadrangles: Silver City (Arizona and New Mexico) and Walker Lake (Nevada and California). In the Silver City quadrangle area, prominent northeast trending linear features and thermal-inertia differences were observed in both alluvial and bedrock areas. Of particular interest was the detection of thermal-inertia differences in vegetation-covered bedrock areas; on Landsat MSS data, those areas have relatively uniform reflectance values dominated by vegetation. The observed thermal-inertia differences are believed to be associated with resistant rock masses and, in one case, thermal-inertia differences correspond with a mapped lithologic difference. At Walker Lake, the two main linear trends seen on the HCMM data (northeast and northwest) coincide with the most prominent directions previously seen on Landsat data.

No consistant pattern was observed between thermal inertia and altered bedrock due, we believe, to the competing effects of silicification and leaching in the altered areas.

Studies in more heavily vegetated terrain of the eastern U.S. confirm that observed thermal-inertia differences in the Appalachian Mountains correlate with geologic units. Among a sequence of sedimentary units, orthoquartzites were observed to have the highest thermal inertias. On individual day and night thermal images of the Allegheny Plateau, the structures detected included two lineaments with expression on gravity and magnetic maps. Aspects of soil moisture were seen which did not appear to correlate with the vegetation canopy, and the Piedmont drainages were found to be better defined than those of the Coastal plains.

The study also considered a number of aspects of the construction of thermal-inertia images, including an evaluation of the parameters used in the thermal inertia algorithm, an extension of the algorithm to include slope and elevation corrections, and an examination of several aspects of image registration. A model explaining the thermal-inertia behavior of igneous rocks, based on the components of quartz, glass, and mafic minerals, was recognized from the HCMM observations and found to fit controlled laboratory measurements reported in the literature. A study of the effects of vegetation was conducted, because thermal-inertia differences were observed in vegetated areas that had relatively uniform reflectance on Landsat images. In the Richfield, Utah, image area, a comparison between vegetation index values derived from Landsat data and thermal-inertia values yielded a correlation coefficient of only 0.08, indicating that observed thermal-inertia variations are not strongly controlled by vegetation. The method was also tested in small, cultivated areas, which were probably dominated by the effects of

irrigation, and correlations 4 to 5 times higher were observed.

We conclude from these studies that HCMM thermal-inertia images have attributes similar to bedrock maps. Even in heavily vegetated terrain, where the bedrock and soil appear obscured on Landsat data, we have developed some evidence to suggest that resistant rock masses and, in one case, a lithologic difference can be observed. Generally, thermal-inertia differences among sedimentary rock units are as expected, but subtle differences among igneous rock units were observed that are consistent with a simple three component model. Little success was achieved in detecting areas of alteration because of the low ground resolution and the opposing effects of silicification and leaching on the thermal inertia. Structural studies resulted in the detection of several lineaments that have not been previously recognized, illustrating that the scale, resolution, and thermal aspects of these data provide information which is complementary to Landsat MSS data in studying the regional tectonic framework.

I INTRODUCTION

The principal objective of this study was to investigate the use of HCMM (Heat Capacity Mapping Mission) data for detecting and mapping geologic features in support of energy and mineral resource exploration and evaluation. Other related objectives involved the development and refinement of techniques and approaches in thermal modelling and image processing.

In our first study (Watson and others, 1981), we investigated the utility of using HCMM data, as well as thermal-inertia data constructed from the satellite data, to detect and map geologic features. We demonstrated that some rock type discrimination is possible among metasedimentary rocks, mafic rocks, and felsic rocks in the arid environment of southwestern Arizona. We were also able to detect narrow geologic units in the Powder River Basin, Wyoming, by their thermal-inertia contrast with their surroundings. The most important results involved delineation of tectonic framework elements, some of which were not previously recognized. In that initial study, we gained the necessary knowledge and understanding of HCMM data to extend our analysis to other geologic areas with different geologic settings, more extensive vegetation, and more rugged terrain.

This report focuses on five such areas: the Cascade Range, the Colorado Plateau, the Basin and Range province, the Allegheny Plateau and Appalachian Mountains, and the Overthrust Belt in Montana and Idaho. These areas were selected primarily because ongoing programs of the U.S. Geological Survey provide a substantial knowledge base from which to draw and unique data sets with which to compare our results. In most cases we were able to readily address the objectives of our investigation. In a few cases we were able to conduct only rudimentary analysis due to unavailability of required image products. However, as the investigation progressed, new objectives were

addressed as unexpected new features were observed and new methods of analysis developed. These extensions to our study, we feel, greatly enhance the scope of our investigations and illustrate our belief that HCMM data provide new insight for regional investigation.

This report is intended to define more precisely the role of thermal and thermal-inertia studies in regional geologic exploration, both independently and in combination with other data, including remote sensing data sets and conventional geologic, geophysical, and geochemical data. The report contains both an examination of HCMM data in five diverse areas and a general analysis of several aspects that are not site specific and apply generally to various terranes. For site studies we provide a brief description of the geologic setting and the objectives of the analysis of the HCMM data. Although our original plan was to use only the NASA-supplied relative thermal-inertia images, in many cases we employed our own registration procedures and an extension of our modelling algorithm to produce thermal-inertia images. The general analysis section provides a discussion of thermal modelling, registration, vegetation and topographic effects, and thermal inertias of igneous rocks that arose from our collective experiments developed from this and the previous HCMM investigation.

2 GEOLOGIC STUDY AREAS

2.1 CASCADE RANGE and VICINITY

The Cascade Range of Washington, Oregon, and northern California (Figure 1) is a constructional mountain range built by extensive volcanism beginning in Tertiary time. The recent phreatic eruptions, seismic activity, and ground swelling at Mt. St. Helens, Washington, testify to the continued volcanic activity associated with the range. An older series of andesitic volcanic rocks (early and middle Tertiary) are exposed along the western margin of the range (Western Cascades). These rocks are known to be overlapped in places by Miocene lavas of the Columbia River flood basalts erupted from sources east of the present Cascade Range and north of the High Lava Plains. Capping both rock series is a line of modern andesitic stratovolcanoes (e.g., Mt. Rainier, Mt. St. Helens, Mt. Hood, Mt. Lassen) that form the backbone of the Cascade Range (High Cascades). Each of the rock series is a complex of volcanic and volcanoclastic rocks formed in response to tectonic events associated with continued interaction between the North American, Pacific, and Farallon plates.

The High Lava Plains of Oregon is an east-southeast trending belt of Cenozoic volcanic rocks extending from Newberry volcano in Oregon into southern Idaho (Figure 2). This belt is characterized by basalts with less voluminous rhyolitic domes, lava flows, and ash flows that decrease in age from east to west (Christiansen and McKee, 1978). The High Lava Plains mark the northern extent of the Basin and Range province. In Oregon the Basin and Range province is characterized by north-northeast trending linear ranges of Tertiary volcanic and Mesozoic sedimentary rocks, separated by linear valleys containing alluvial fill. North of the High Lava Plains is the Blue Mountains province, a structurally complex area of dominantly Tertiary basalts, with

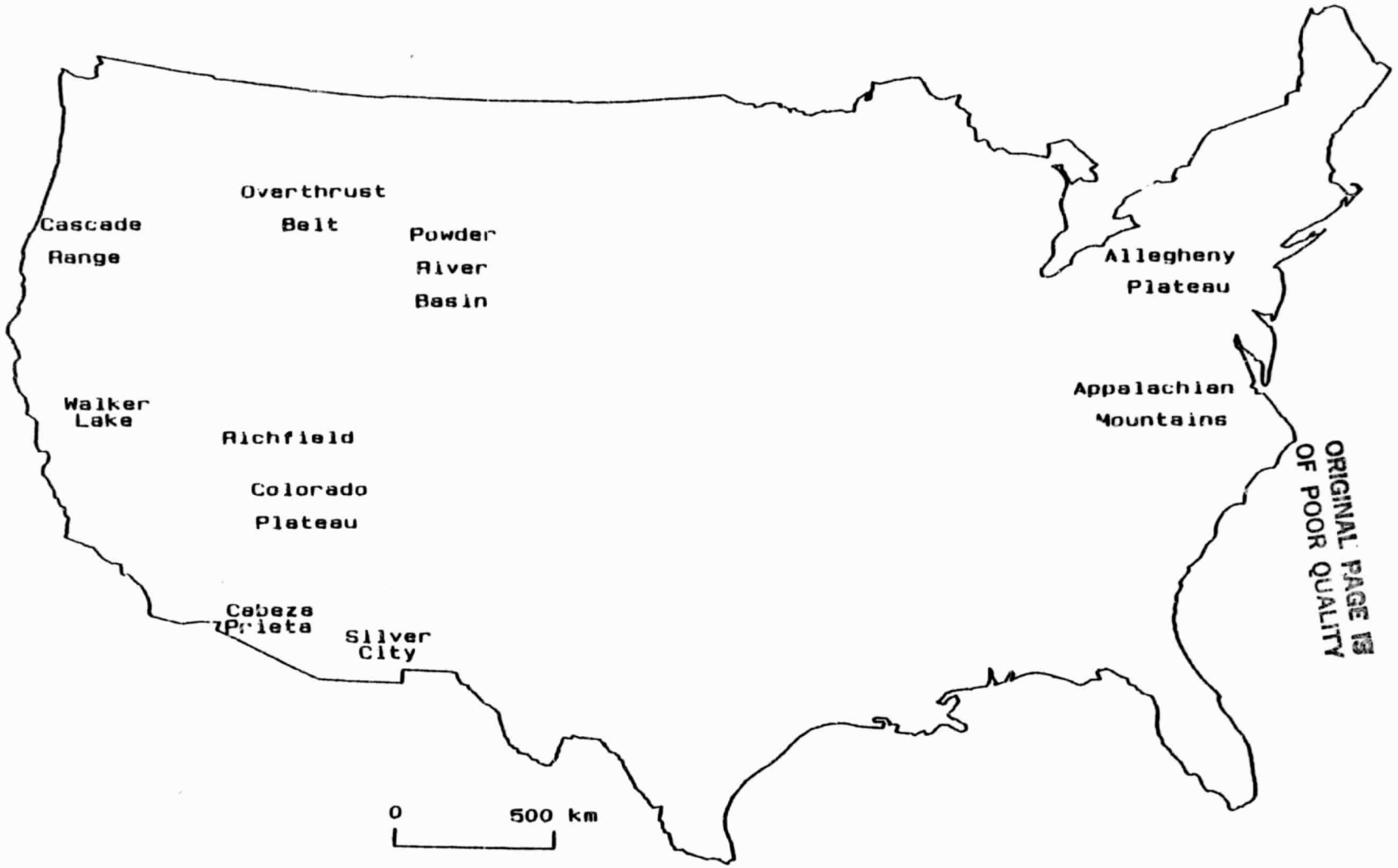

Figure 1.--HCMM study areas. Two of the areas, Powder River Basin and Cabeza Prieta, were discussed in a previous report (Watson and others, 1981).

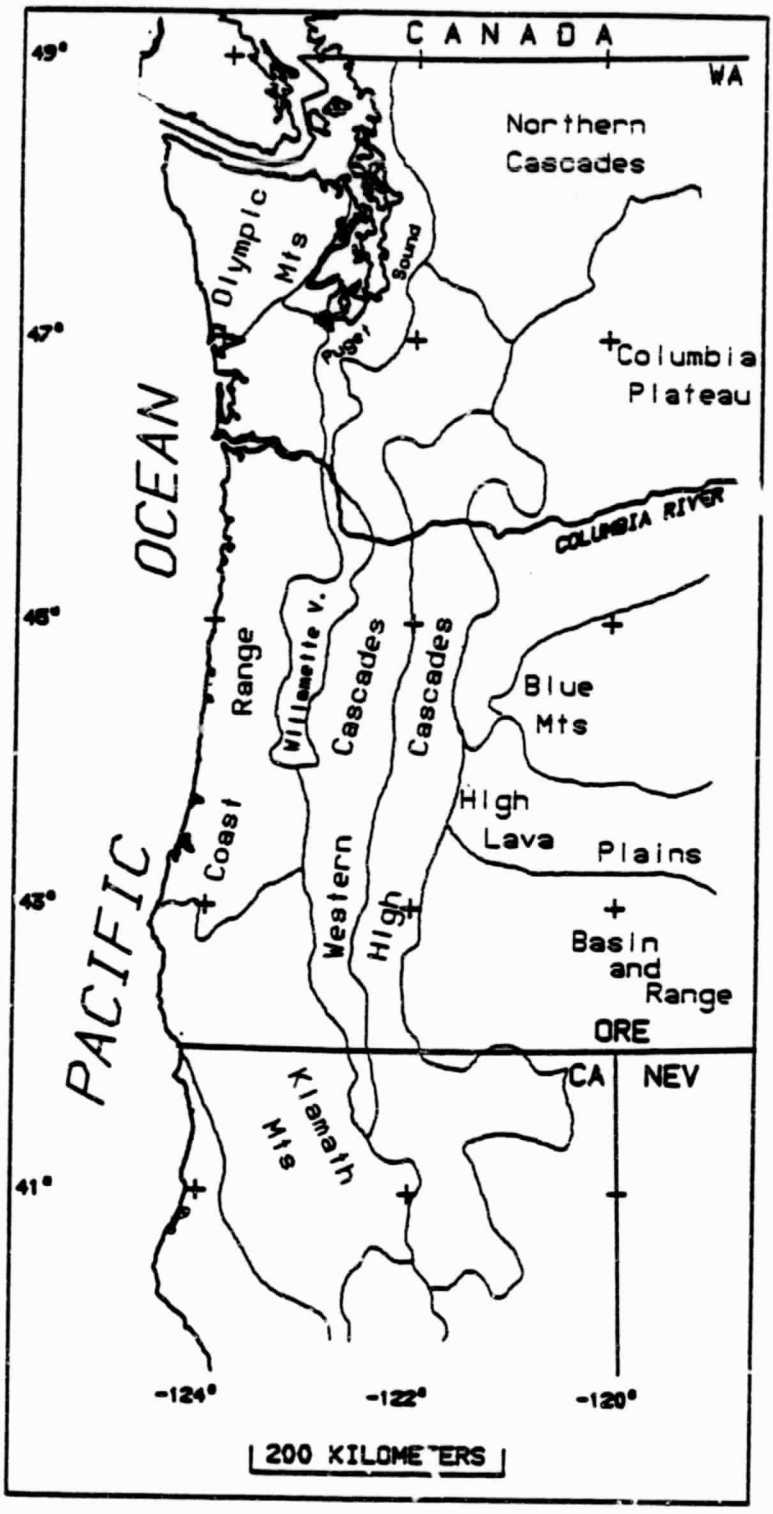

Figure 2.--Physiographic provinces of northwestern continental United States.

abundant exposures of Paleozoic and Mesozoic sedimentary, igneous, and metamorphic rocks as well. The Columbia Plateau province is a vast, generally flat area underlain by Miocene flood basalts that are incised by the major drainages.

Detailed analysis of HCMM images in the Pacific Northwest was largely limited to that portion of the Cascade range south of the Columbia River, including portions of the adjoining High Lava Plains, Basin and Range, Blue Mountains, and Columbia Plateau provinces (Figure 2). HCMM data in the various provinces were studied to determine if differences in thermal inertia could be detected among the main physiographic units and to evaluate the structural geologic content of the individual band images.

Day (NASA scene ID AA0169-21270-2) and night (NASA scene ID AA0402-09360-3) HCMM thermal images covering the central and southern Cascade Range were examined for geologic structure; unfortunately, the companion HCMM visible data contained abundant system noise and were not usable in the study. The computer-enhanced HCMM images were interpreted for linear features, which are distinct linear elements observable on the images (Figures 3 and 4); no attempt was made to define more diffusely expressed, broad-scale lineaments. The linear feature data were digitized and the length- and strike-frequency distributions were determined for a subset of the HCMM data that coincides with a linear features data set previously mapped on computer-enhanced Landsat images (Figure 5). Fewer linear features were mapped on the HCMM images than on the Landsat images, and the HCMM linear features are longer on the average. The linear feature data from both the day and the night HCMM images have prominent northwest and east-northeast trends (Figure 6), similar to the Landsat linear feature data, but a distinct north-south trend in the Landsat linear feature data is conspicuously missing from both HCMM data sets; in fact, this trend is a prominent minimum on the HCMM data.

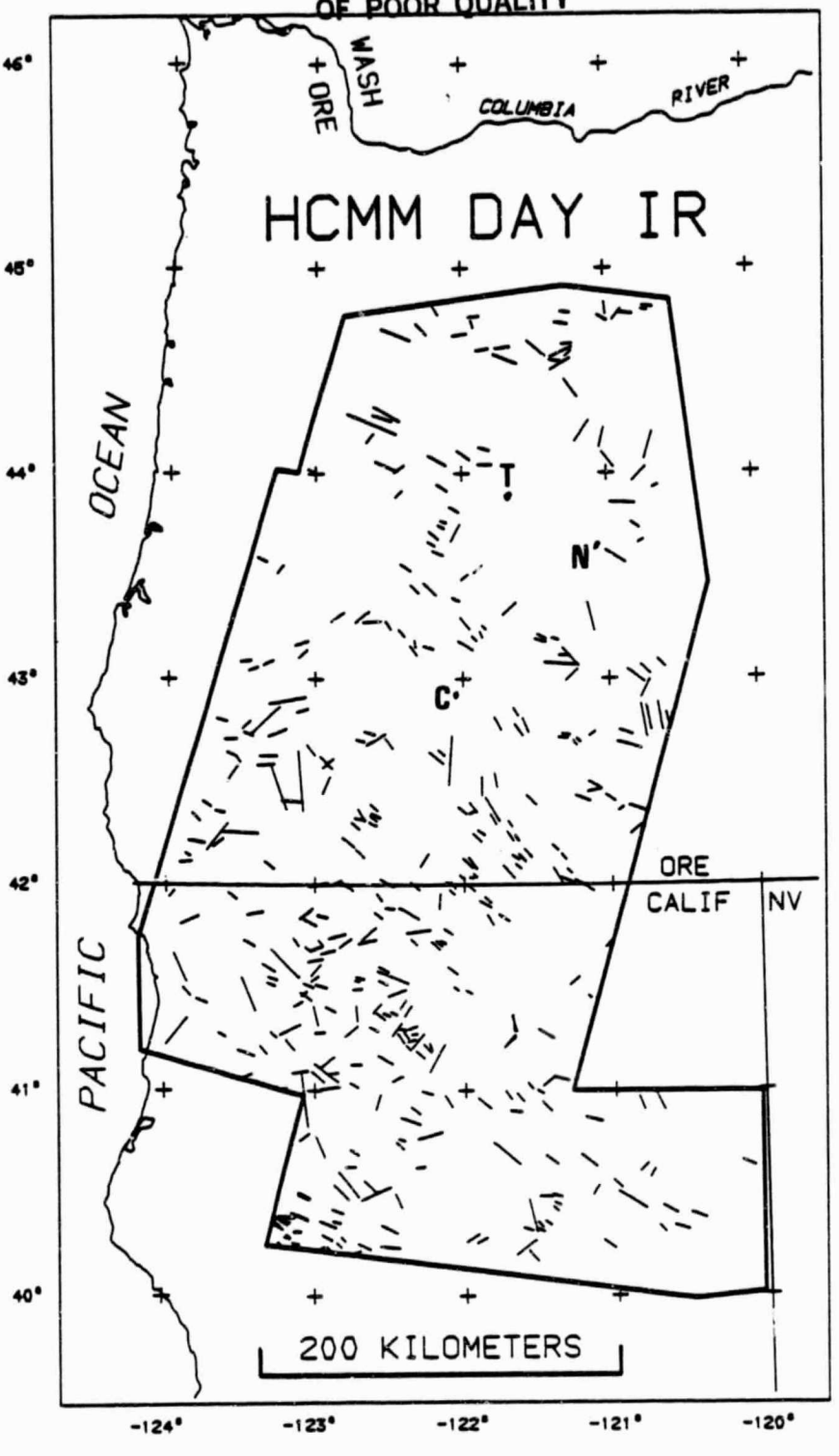

Figure 3.--Linear features map of an HCMM day thermal image. Locations referred to in text are: C - Crater Lake, N - Newberry Caldera, T - Three Sisters Volcanics.

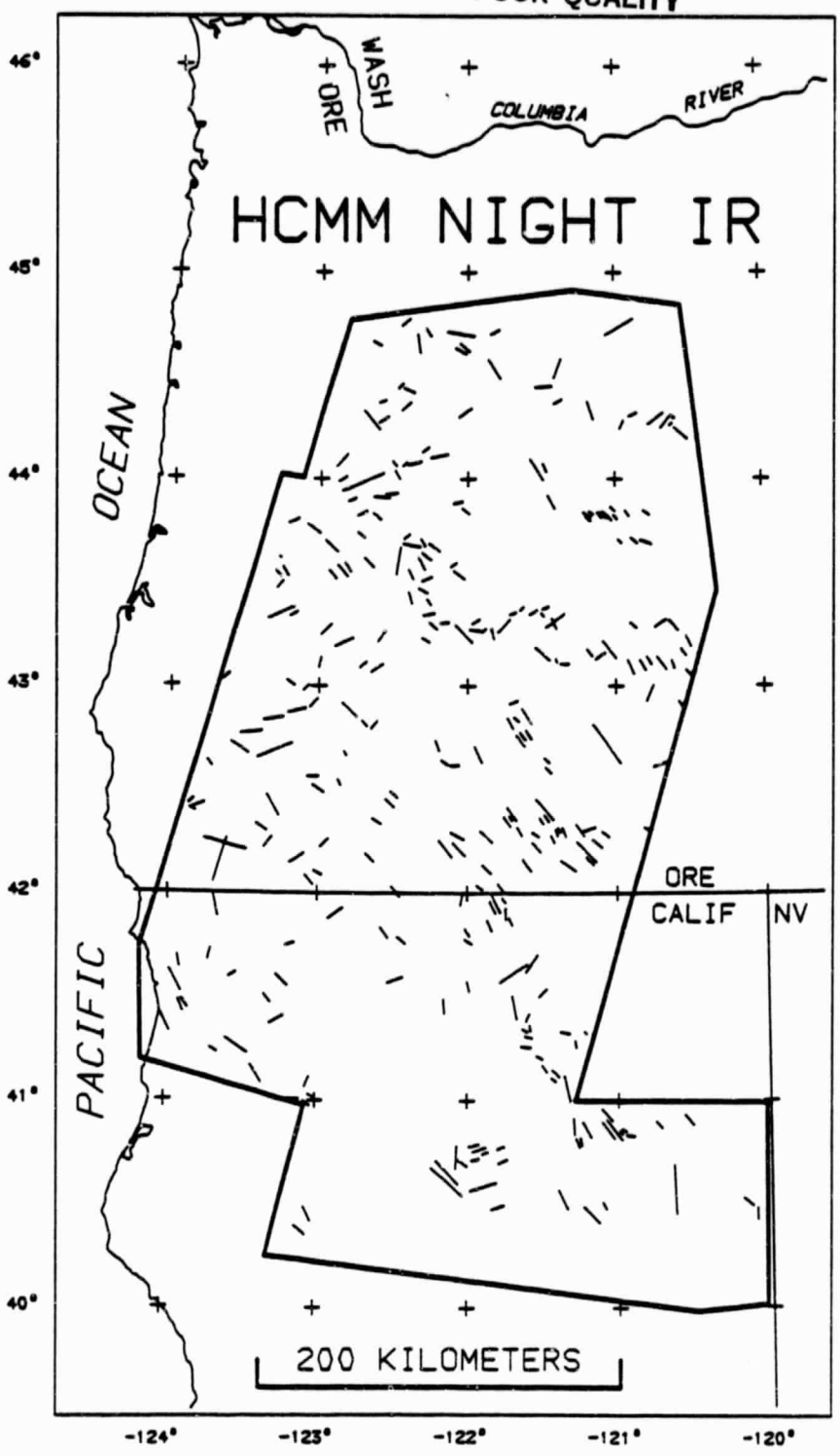

Figure 4.--Linear feaures map of an HCMM nighttime image.

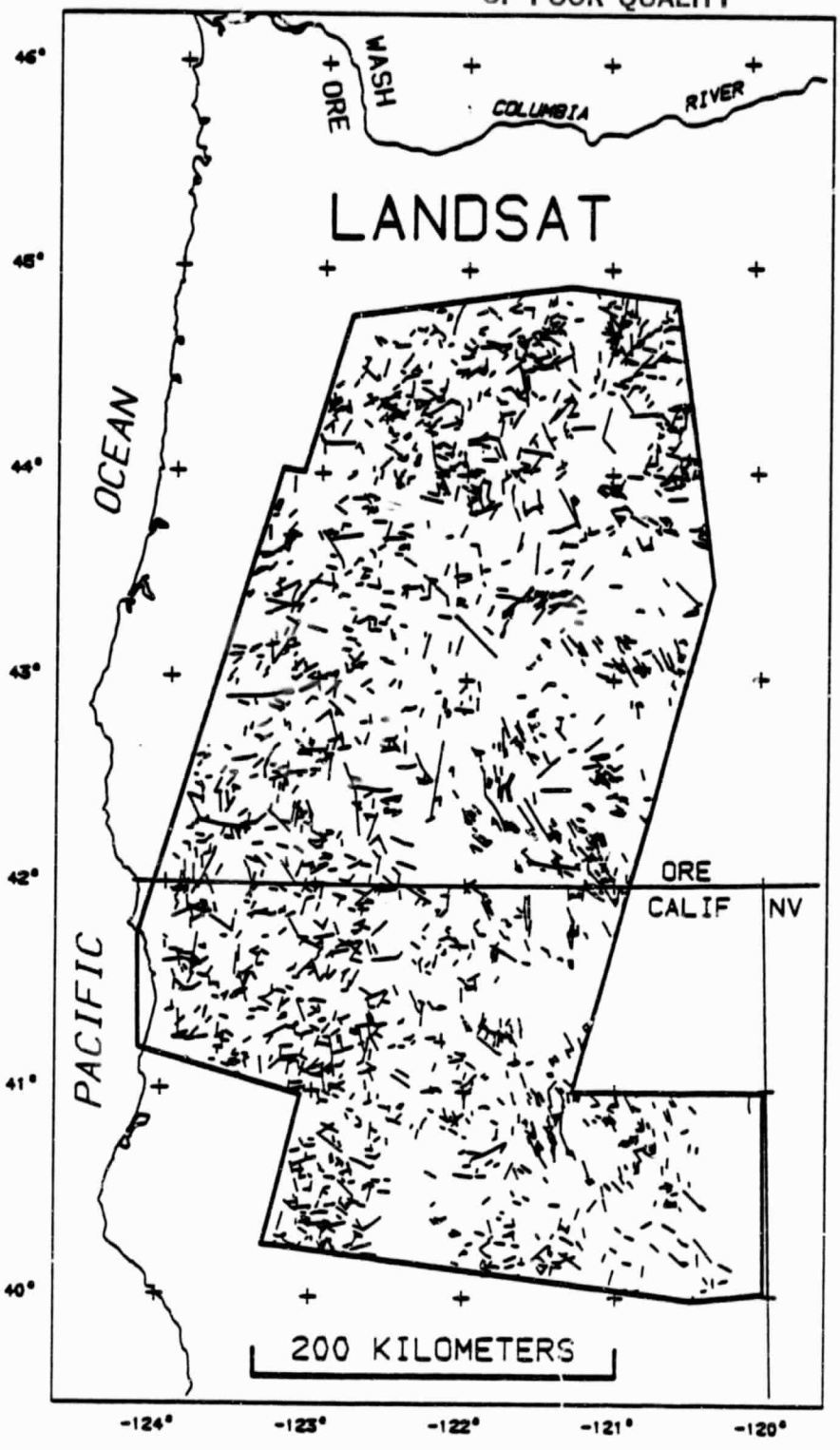

Figure 5.--Linear features map of a Landsat image.

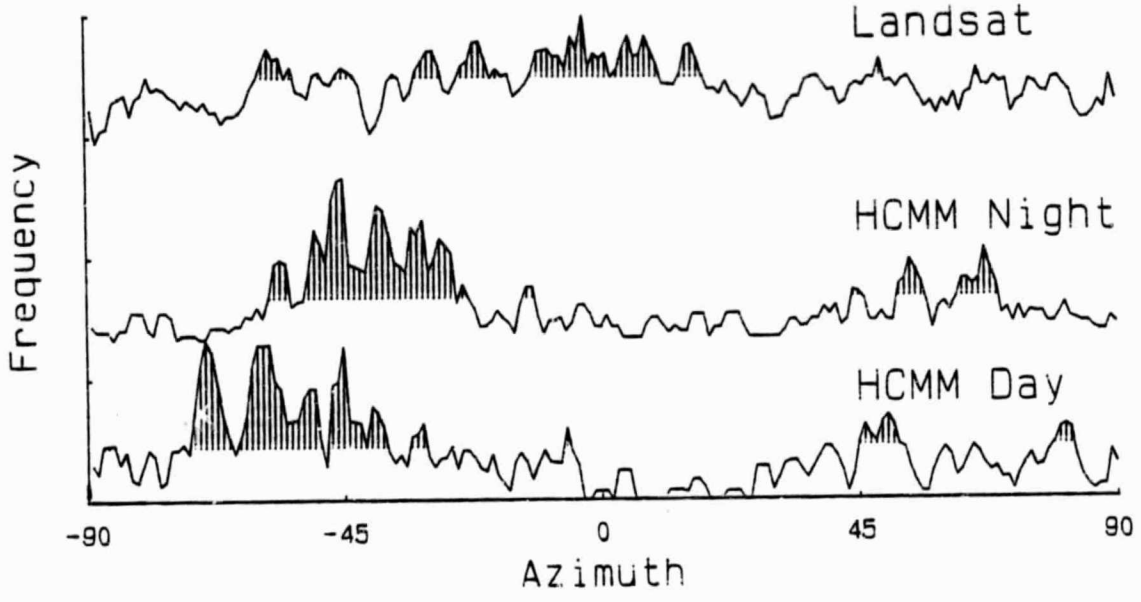

Figure 6.--Linear features frequency versus azimuth for the Cascade area. Shaded areas are for frequencies which are above the 90% significance level.

Because the resolutions of the Landsat and HCMM systems are quite different, we wanted to develop some means to compare linear feature data derived from analysis of these images. The method we decided to employ had been previously developed to examine crater distributions on planetary surfaces (Shoemaker and others, 1962). The cumulative frequency at specified lengths (i.e., the number of features with lengths greater than that length) were computed and displayed on a log-log plot. A number of such plots were constructed for data from HCMM, Landsat, and fault maps, and all were found to have the same characteristic shape: a linear slope in the middle, an asymptotic flattening at short lengths, and a falloff from the linear projection at long lengths. The linear section was then least-squares fitted to compute a slope value.

Even though different azimuthal trends are present in the Landsat and HCMM linear features data sets and the number and lengths of the linear features are quite different, it is interesting that the straight-line portion of the respective plots have similar slopes (Figures 7). The asymptotic portion on the left (short length) side of each curve is probably a function of the system resolution and image scale, while the falloff portion on the right (long length) end is a complex function of several factors including the individual interpreter, the size of the image, and the discreteness of the process. The straight-line portion of each curve may be indicative of the particular study area, its structure, lithology, and general geologic environment, and may provide a means of semi-quantitatively characterizing terranes.

Although numerous structural patterns can be seen on the HCMM images and the linear feature data, two deserve special mention. The first is a roughly circular feature (45 km diameter) surrounding Newberry Caldera, Oregon, on the

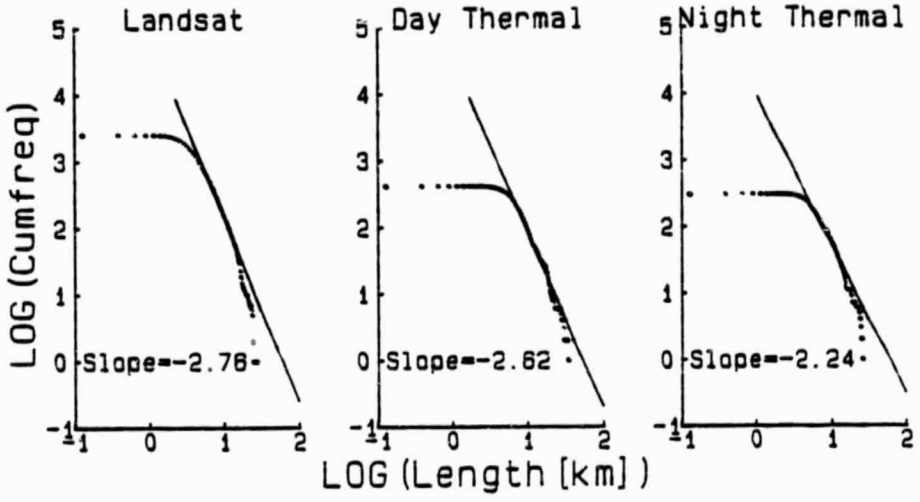

Figure 7.--Cumulative frequency distributions of the Cascade region for Landsat and HCMM data. The slopes are computed from a least squares fit to the linear segment of the data.

night thermal image (Figure 8) that has no obvious counterpart on the Landsat image. It roughly coincides with the 5,000 ft (1,667 m) contour on the Crescent topographic map and correlates, in a very general sense, with the distribution of the volcanic flows. It is expressed in places by topographic changes and changes in vegetation pattern. The feature includes the main field of cinder cones, which are north and northwest of the caldera, and also the most highly dissected terrain. The pattern may be related to subsidence during outflow from the main magma chamber, which acted to limit the distribution of the lava flows.

On a broader scale, a second pattern is defined on the HCMM images by an absence of linear features in a region roughly bounded by The Three Sisters Volcanics, Newberry Caldera, and Crater Lake (Figures 3 and 4). The region is centered about 50 km to the west of Newberry Caldera and has a diameter of roughly 80 km. The linear features on the periphery are generally either radial or tangential to the boundary. This conspicuous lack of linear features may be due to a youthful, unfractured volcanic cover that masks the regional distribution of linear features with sufficient length to be seen on the HCMM images. Alternatively, this region may be anomalously devoid of fractures. Magnetic data have been interpreted as implying a shallowing of the Curie isotherm in this region (Connard and others, 1983); this suggests that perhaps the rocks might be more ductile in this region and that fracture development at depth, with subsequent propagation to the surface, may indeed be retarded.

Apparent thermal-inertia and reflectivity statistics constructed from the June 2, 1979, image (AA0402-09360-3, AA0402-20310-1,2) for areas within several of the major lithologic/physiographic provinces in the Pacific Northwest were computed to determine whether important differences exist

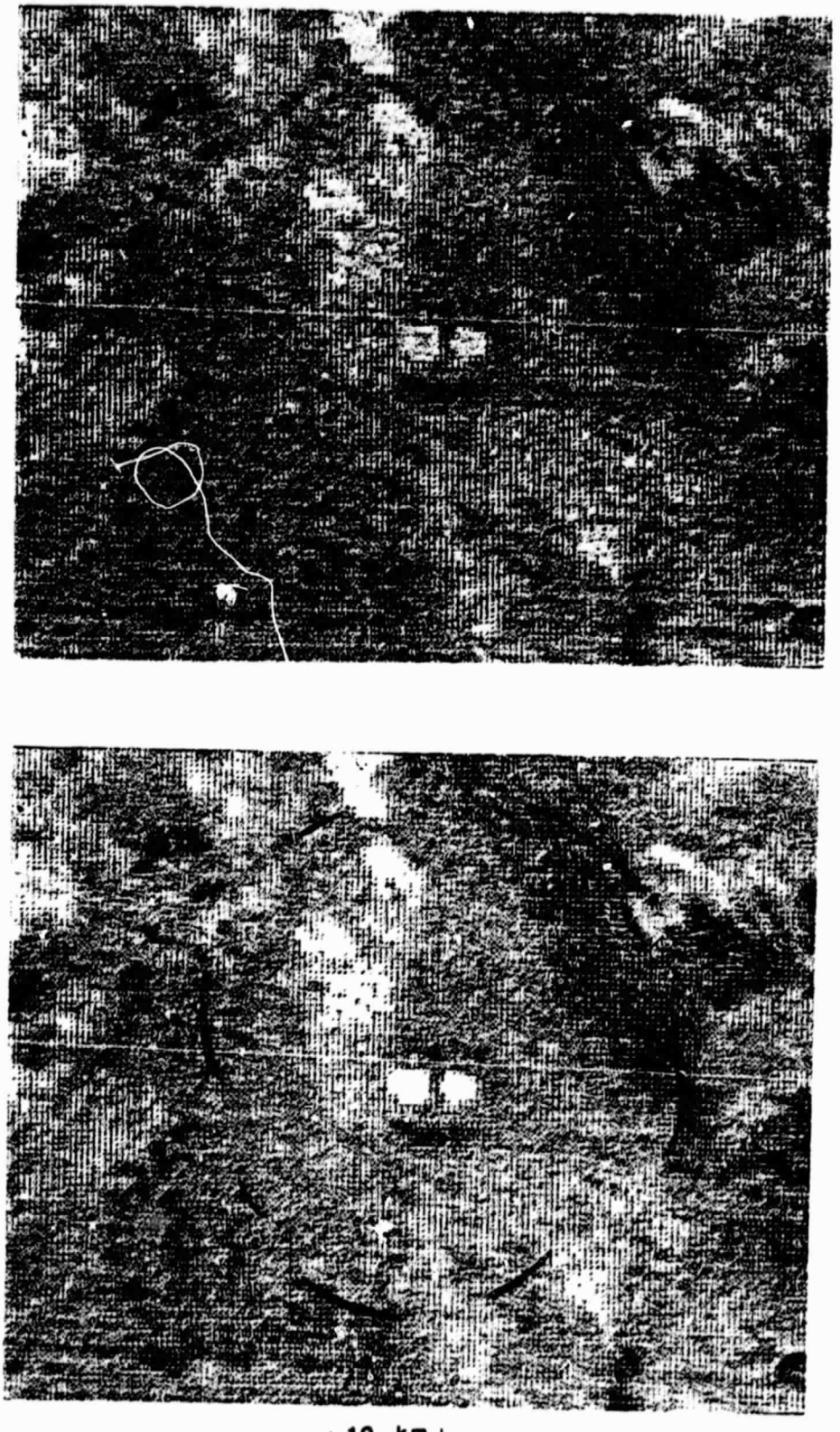

Figure 8.--HCMM night thermal image of Newberry Caldera, Oregon (lat 43.7°, long 121.2°). The feature discussed in the text is outlined on the bottom image by curved line segments.

(Figure 9). In general, the thermal-inertia statistics are in three clusters: (1) the Cascades, (2) the Blue Mountains, and (3) a grouping of the High Lava Plains, the Columbia Plateau, and the Basin and Range provinces. In the Cascade Range cluster, there is some separation of the mean values for areas in the High Cascades and the Western Cascades, but there is a considerable overlap in the two distributions. An insert in the figure shows the statistics for the Mt. Hood volcano (High Cascades), which is anomalous because of the snow cover present when the HCMM data were acquired. Two separate areas were analyzed in the Blue Mountains province to determine whether a statistical difference could be observed on opposite sides of an apparent discontinuity seen on the thermal-inertia image. The difference appears slight. The third cluster, including the High Lava Plains, Columbia Plateau, and Basin and Range data, has the highest reflectivities and lowest apparent thermal inertias. The mean apparent thermal inertias are not greatly different; however, the ranges of reflectivity are quite broad.

This study has illustrated that thermal-inertia differences exist among large physiographic units of the Cascade region and that thermal data can supply structural information which is additional to and thus complementary to Landsat data. A new technique has been used in this study to compare lineament data acquired from systems with different resolutions, and it may have broad application to the interpretation of linear feature data.

2.2 OVERTHRUST BELT

The Montana/Idaho part of the western Overthrust Belt (Figure 1) is characterized by the presence of numerous northerly trending imbricate thrust plates. These plates, consisting mainly of Precambrian and Paleozoic sedimentary rocks, have been intruded by plutons of Mesozoic and Tertiary age. Relatively non-resistant Cretaceous and Tertiary sedimentary rocks are

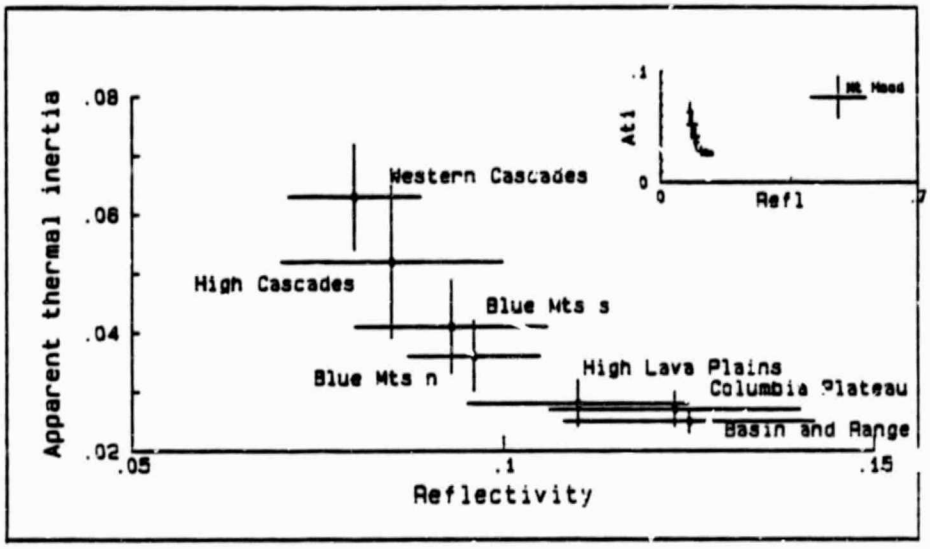

Figure 9.--Apparent thermal inertia, reflectance statistics for physiographic units in northwestern United States. Vertical and horizontal lines indicate standard deviations. An insert shows the values for Mt. Hood (see text).

present in the northeastern part of the study area. A major west-northwest trending zone of right-lateral strike-slip displacement, including the Osburn, Ninemile, and St. Joe faults, transects the area. South of this zone, crystalline rocks are more widespread, the thrust plates are fragmented by numerous faults, and irregularly shaped basins are filled with complex depositional patterns of alluvium of Cenozoic age. The northern part of the Overthrust Belt has high potential for precious and base-metal and petroleum products. The metal deposits in the area include stratabound sulfide, vein and replacement, and placer deposits.

Our studies were primarily directed towards gaining an understanding of the expression of structural framework in HCMM thermal-inertia data. We were also interested in evaluating the use of these data to study the development of the drainage network and the deposition of alluvial deposits in the basins because of their potential for placer deposits. For the analysis, a relative thermal-inertia image was constructed (Figure 10a) using HCMM data acquired October 9, 1978 (AA0166-09370-3 and AA0166-20340-1,2).

A pronounced structural feature (Figure 10a and 10b) which can be seen on the thermal-inertia image is the Lewis and Clark "line" (often referred to as the Montana lineament), a west-northwest trending zone of large high-angle faults (Wallace and others, 1960). Linear features which match the Osborn and Placer Creek faults are clearly visible. The Osborn Fault has many associated faults, some of which are mineralized, and igneous activity and mineralization in the Coeur d'Alene mining district were localized along its course (Anderson. 1948).

In the northeastern part of the image is located the Lewis thrust and an intense band of overthrust faults, east of Flathead Lake (Figure 11). Crossing these thrusts can be seen a number of generally northeast-trending

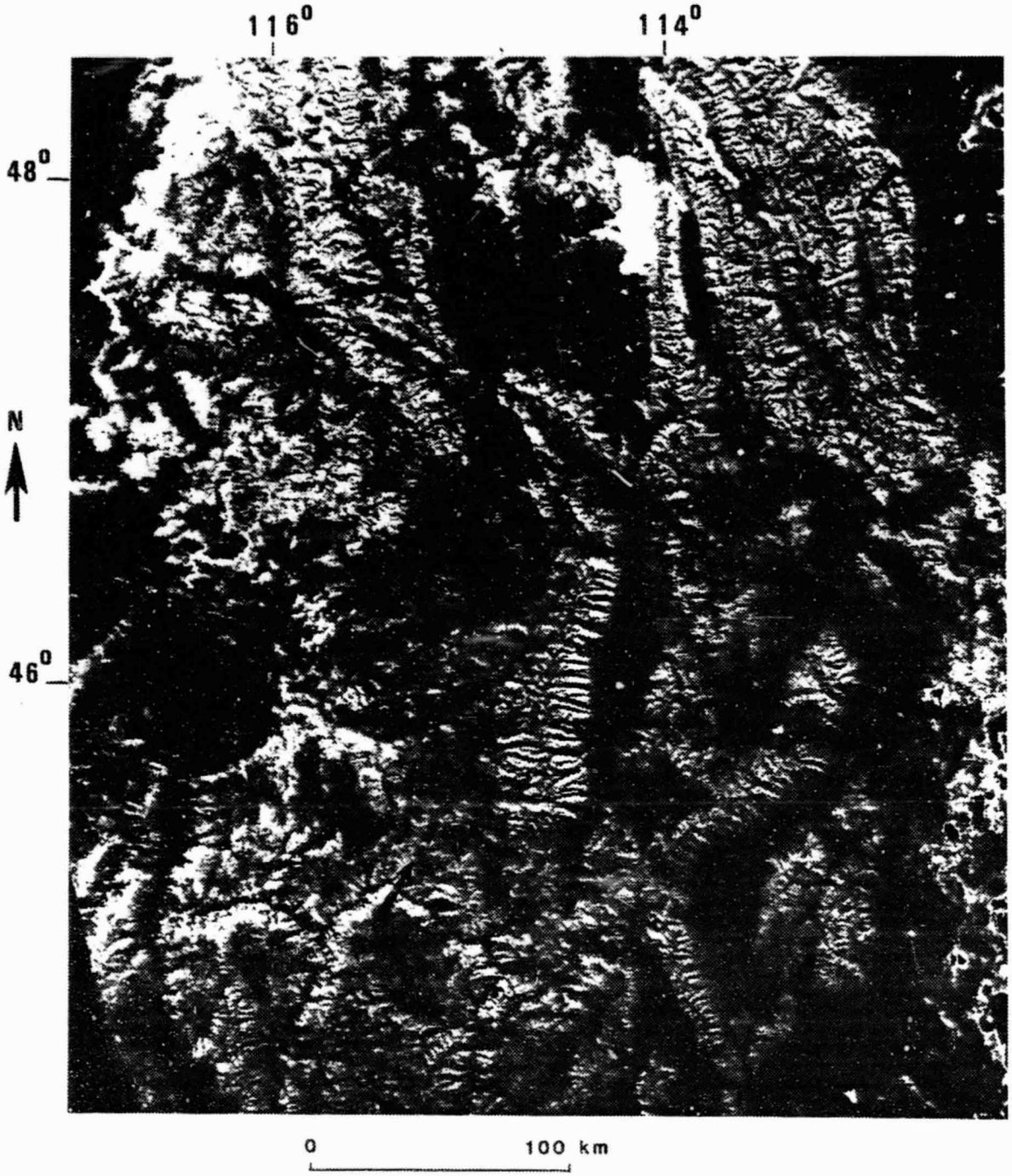

Figure 10a.--Thermal-inertia image of the Overthrust Belt in Montana/Idaho. Clouds appear as dark areas along the eastern edge of the image (fringed with a bright edge) and in a north-south zone roughly 70 km west of Flathead Lake (see Figure 10b) and extending southward about 100 km. A northeast-trending lineament described in the test extends across the center towards the upper right hand corner of the image.

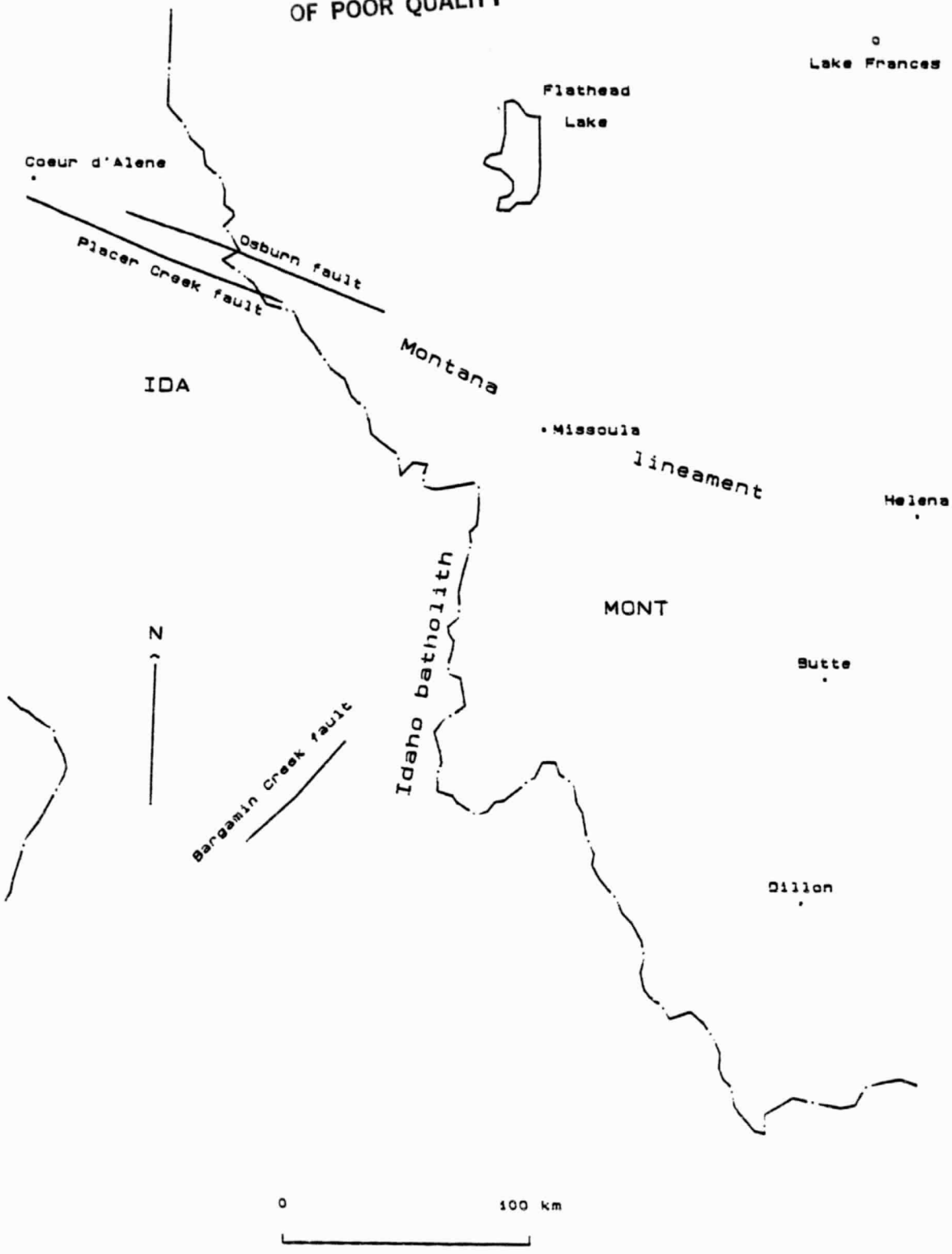

Figure 10b.--Location map of features in the Overthrust Belt described in the text.

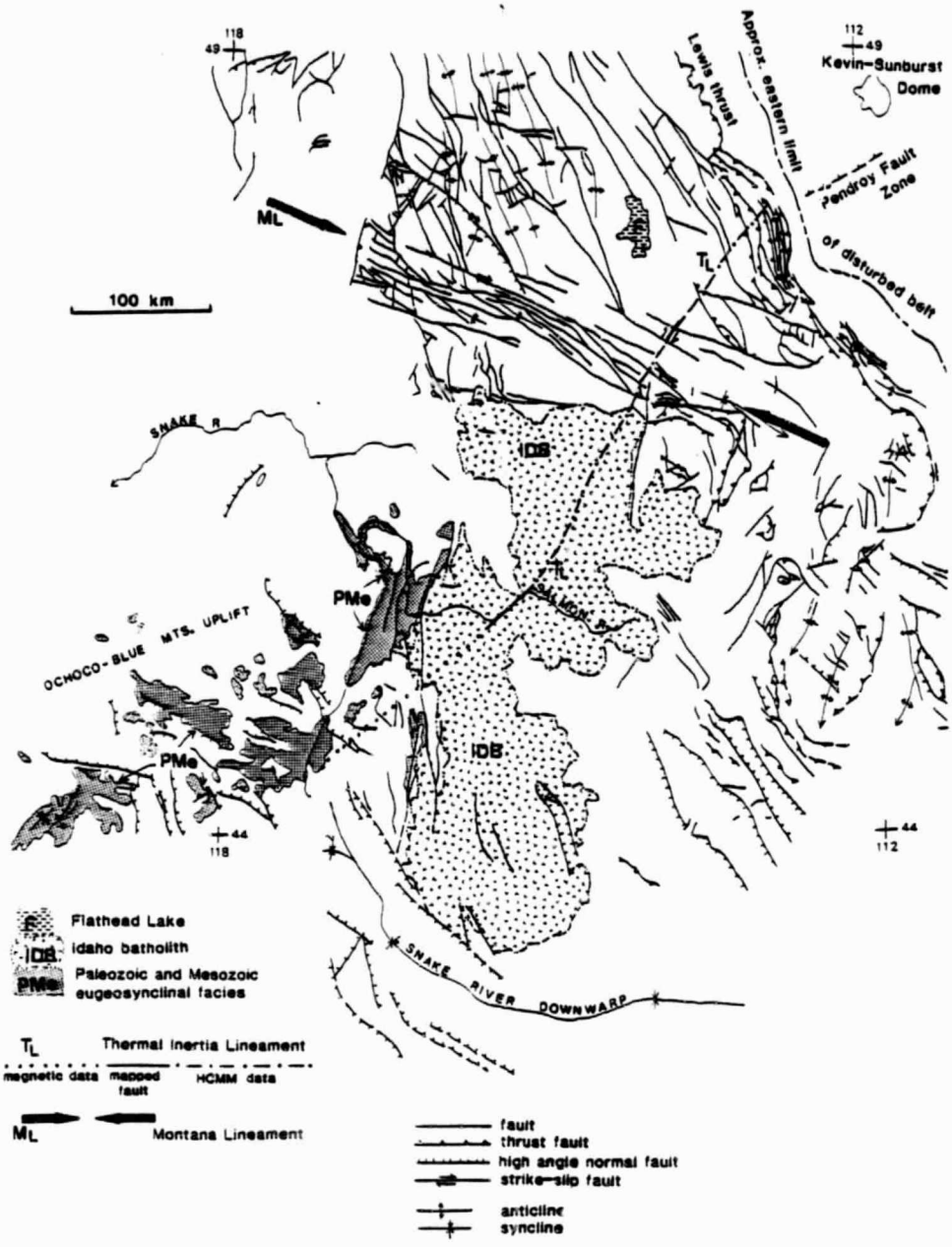

Figure 11.--Map showing the lineament described in the text and a number of associated features. The lineament extends from the Ochoco-Blue Mountain uplift in Oregon to just southwest of the Kevin-Sunburst Dome in Montana.

linear features. The most prominent one extends from Francis Lake, Montana, through the Idaho Batholith for about 300 km (Figures 10a and 11). No continuous expression of this feature can be found on the 1:2,500,000 scale geologic and tectonic maps of the United States. At its southwestern end it coincides with the Bargamin Creek fault (Cater and others, 1973) within the Idaho batholith, where it is expressed by several drainages. The lineament crosses the Montana lineament just north of Missoula and appears to coincide with a short mapped fault, breaks in topography, and northeast-trending drainages. The Montana lineament zone is quite diffuse and locally may be as wide as 50 km (McMannis, 1959). In the general vicinity of Missoula, where the linear feature crosses the zone, the Montana lineament changes both in character and direction (Weidman, 1965).

We examined a number of detailed geologic and gravity and magnetic anomaly maps to evaluate this feature. In the north part of the Choteau 2° quadrangle (Figure 12), a set of secondary lineaments that are subparallel with the main lineament extend into the Pendroy Fault zone (Figure 11), and the north-trending continental divide bends sharply to the east-northeast where the main lineament crosses the divide (lat 47° 55′N., long 113°W.). Further to the southwest, the main lineament roughly coincides with an indentation in the trace of a northwest-trending fault, and further southwest with a mapped fault (lat 47° 15′N., long 113°, 45′W.).

Continuing southwest, into the Hamilton 2° quadrangle (Figure 12), the lineament coincides with a zone of short (<5 km) faults in a region 20 km southwest of Missoula. Further southwest is a region where no evidence for the lineament is found on the existing geologic mapping. However, much of the mapping is incomplete due to the extremely rugged terrain in the Selway Bitterroot Wilderness Area.

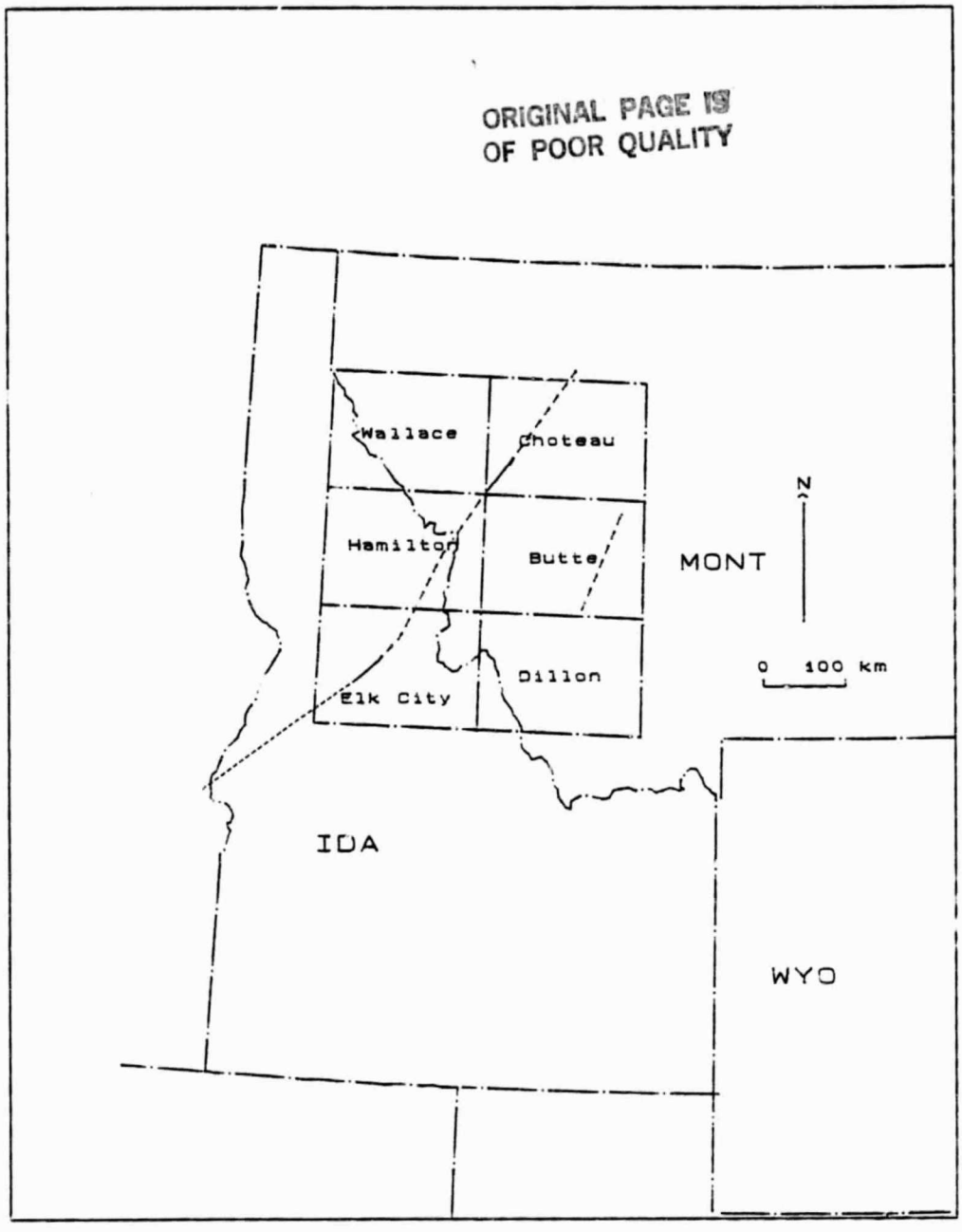

Figure 12.--Quadrangle location map for the Overthrust Belt. Two lineaments discussed in the text are shown as dashed lines (solid when coinciding with mapped faults) and dotted lines (when projected using aeromagnetic data).

The southwestward extension of the feature, in the Elk City 2° quadrangle (Figure 12), provides the most convincing evidence for a geologic origin for the lineament. There the lineament is roughly coincident with a geologic contact and then coincides with the northeast-trending Bargamin Creek fault, which the Salmon River drainage follows for about 50 km (Figure 11).

Gravity (Figure 13) and magnetic (Figure 14) maps provide some supportive evidence for geologic expression along the lineament in the form of truncation of patterns, coincidences with small local anomalies, and some parallelism of trends. The Idaho State aeromagnetic map also suggests structural control of this feature. A projection of this trend southwest to the Idaho-Oregon border passes through a region where there is a sharp break in the spatial frequency character of the anomalies. The patterns to the north have high spatial frequencies associated with shallow sources, and those to the south have much lower frequencies suggesting a fundamentally different geologic character. The trend can be projected westward on the basis of regional gravity data. The proposed lineament appears to have two bends in its trend. One occurs near Missoula, Montana, where the lineament crosses the Montana lineament; the other bend, in the vicinity of the Clearwater Mountains (about 150 km to the southwest), is near a pronounced northwestern trend on the aeromagnetic map. The sense of deflection is sinstral. The lineament roughly parallels the Great Falls lineament (O'Neill and Lopez, 1983) and two other unnamed lineaments (Ruppel, 1982) which lie about 100 km, 200 km, and 300 km, respectively, to the southeast.

A linear features map of the Dillon 2° quadrangle (Montana-Idaho) was also constructed from the HCMM thermal-inertia data (Figure 15b). The data were compared with the geologic map (Ruppel and others, 1982) for corresponding faults and lithologic contacts. Because of scale and projection

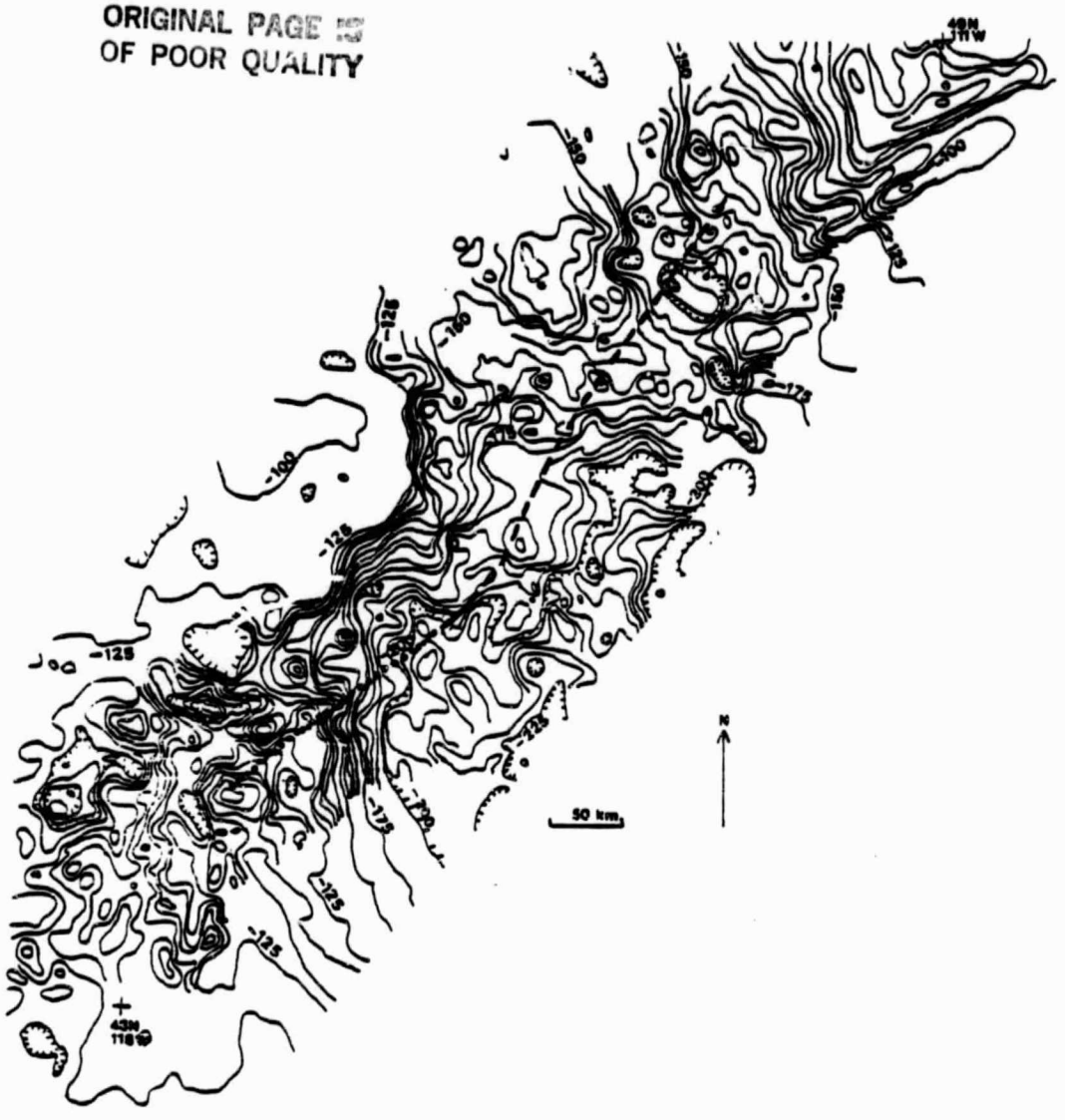

Figure 13.--Simplified gravity anomaly map of the Overthrust Belt. Main contours on 25 mgal contours from the U.S. Gravity anomaly map (Society of Exploration Geophysicists, 1982). The linear feature follows general trends in the Idaho batholith and appears to be expressed locally in the intermediate 5 mgal contours shown in the vicinity of the linear feature.

Figure 14.--Aeromagnetic map of north-central Idaho and western Montana (Zietz and others, 1978, 1980) showing color-coded total intensity magnetic field with a 100 gamma contour interval. The linear feature described in the text is shown as a broken solid line where expressed on HCMM data and as a dotted line where extended using aeromagnetic data.

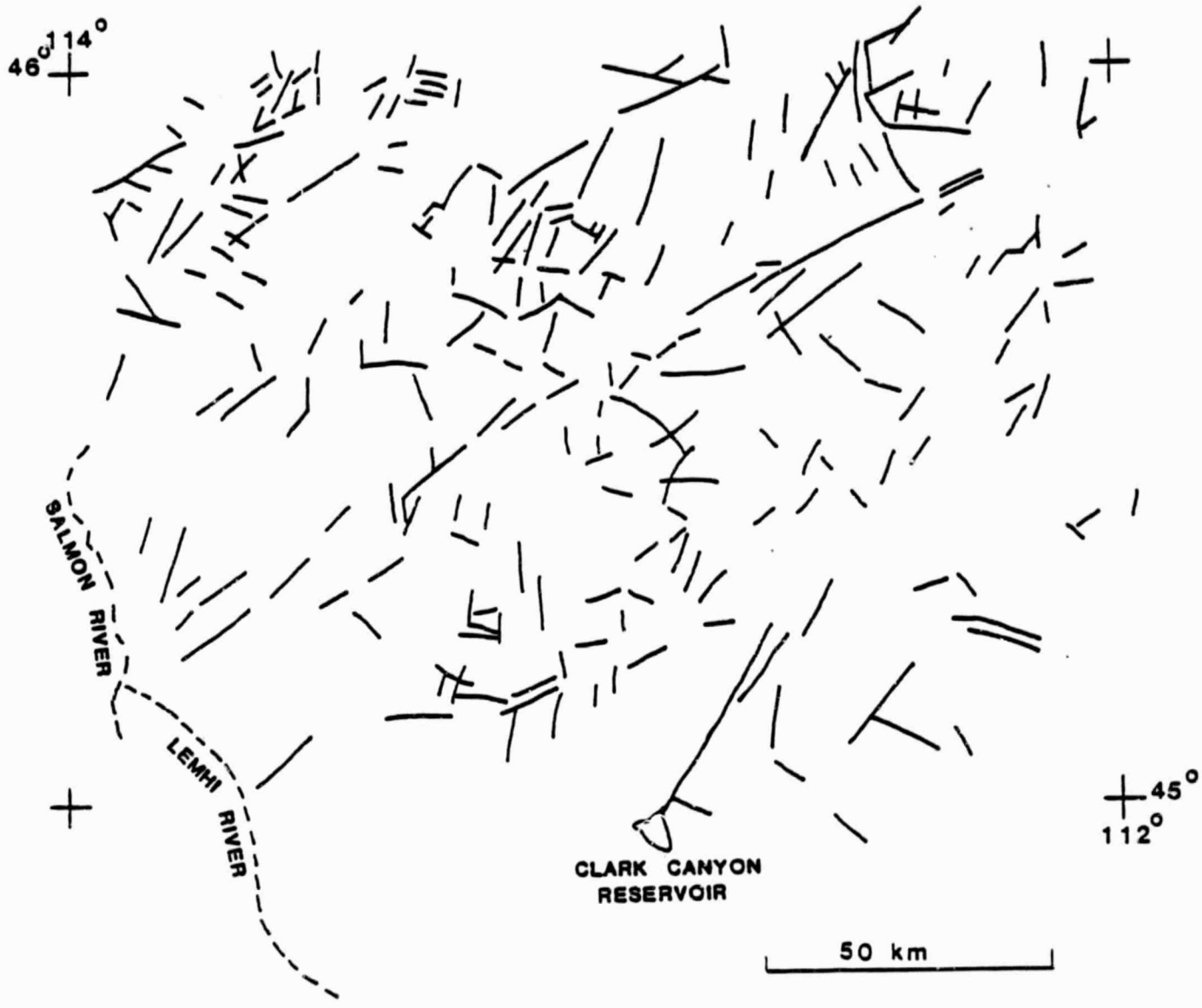

Figure 15a.--Linear features map of the Dillon 2° quadrangle (Montana and Idaho) from Landsat MSS 7 mosaic.

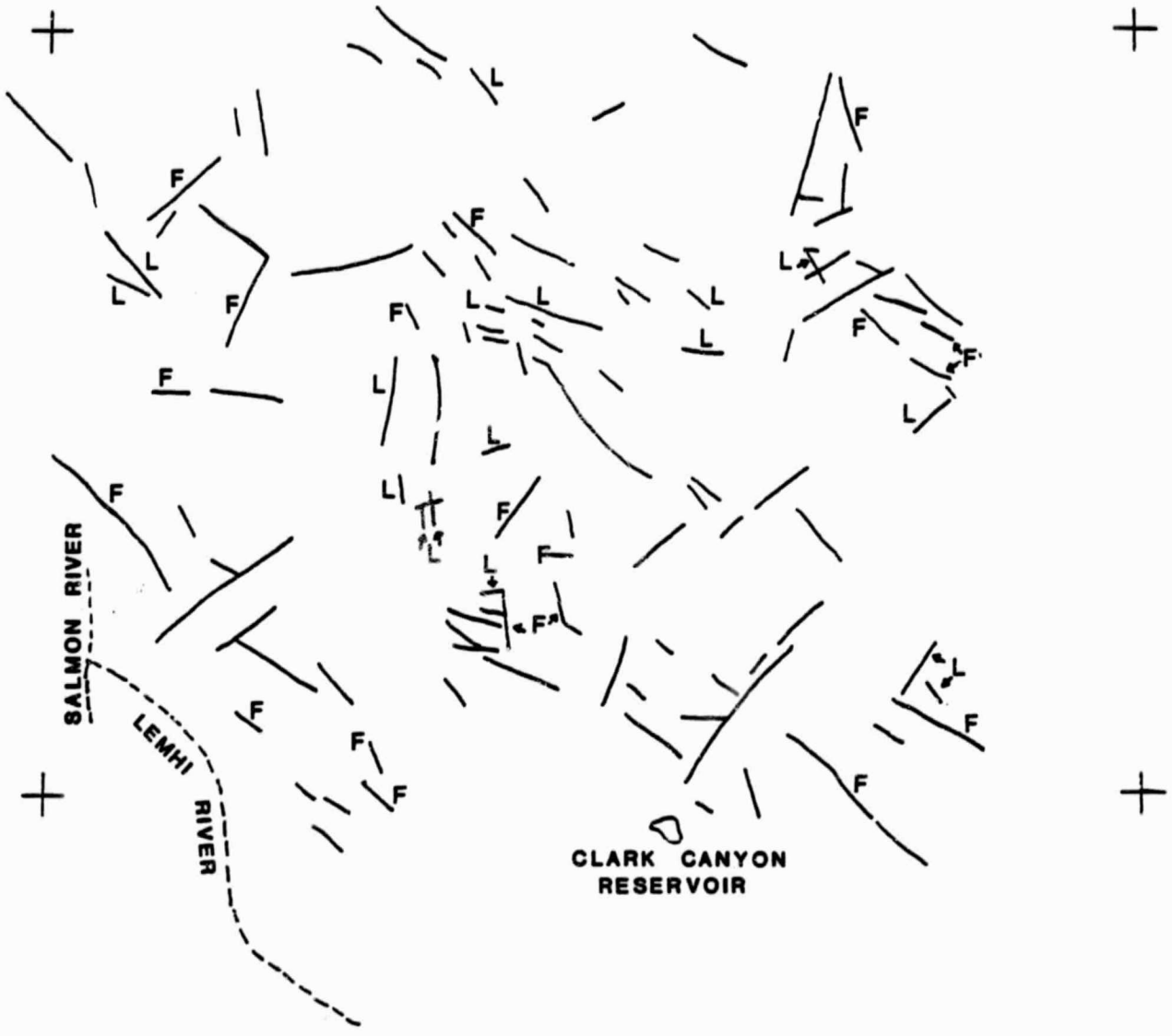

Figure 15b.--Linear features map of the Dillon 2° quadrangle (Montana - Idaho) from the HCMM black and white thermal-inertia image. Tick mark locations and scale are approximately the same as Figure 15a. Many of the features are mapped faults (F) and others appear to be lithologic contacts (L).

differences, a detailed comparison was not feasible, however, many of the features identified are mapped faults (F) and others appear to be lithologic contrasts (L). The HCMM linear features map was also compared with a linear features map constructed from the Landsat MSS band 7 mosaic at 1:2,500,000 scale (Figure 15a). Obviously, there are many more features on the Landsat scene due to the higher resolution. Some of these lineaments are very long and, we believe, represent fracture zones, especially the very long northeast-trending feature across the central part of the quadrangle. On the other hand, many of the faults and lithologic contacts observed in the HCMM image are not evident on the Landsat mosaic and indicate the additional and complementary aspects of these data. Another difference in the two linear features maps is that the HCMM map is dominated by northwest trends whereas northeast-trending lineaments are more prominent on the Landsat map.

The thermal-inertia HCMM image (Figure 10a) coverage of the Butte 2° quadrangle, Montana, was examined to study possible geologic relations to the placer gold deposit at Carpenter Creek. Carpenter Creek is 4 km east of Avon, Montana, and flows 8 km south-southwest to join the Blackfoot River just west of the Continental Divide. The placer deposits of Carpenter Creek are some of the richest in the area, having yielded over 250,000 oz of gold (7775 kg) from bench and creek placers following the first four years of discovery in 1865 (Lyden, 1948). One of the unresolved geologic problems concerning the deposit as stated by Lyden (1948, p. 127) is that:

"For its full length the terrace placers on Carpenter Creek are found only on the west bank, the benches on the east bank being virtually barren."

Recent detailed mapping (M. R. Waters, 1982, oral commun.) has confirmed this observation and has furthermore suggested that the gold is probably of local origin, being reworked from the Tertiary alluvial fan deposits and gold

occurrences to the north associated with the Blackfoot City granodiorite stock (Wallace and others, 1981).

The HCMM thermal-inertia image shows a lineament trending N. 18° E. from the east side of Deerlodge Valley, through Avon Valley, to Canyon Creek Valley northwest of Helena, Montana, a distance of approximately 100 km (Figure 10, 11). It transects Avon Valley and is coincident with Carpenter Creek. The lineament aligns with an asymmetric northeast-trending gravity low along the eastern side of Deerlodge Valley (Kouizeski and others, 1968). One of the more interesting aspects of the lineament is that in Deerlodge Valley the terrain shows a sense of normal displacement, down to the west, along the eastern escarpment of Deerlodge Valley. There are at least two possible mechanisms whereby a northeast-trending normal structure could affect the concentration of placer gold on the west side of Carpenter Creek. If the structure was present in the Tertiary, the initial concentration of placer gold in the alluvial fans may have been preferentially concentrated on the west side. Alternatively, if a small topographic low resulted from a northeast-trending structure during the Quaternary period when the bench and creek terraces were being deposited, the gold may have been preferentially concentrated on the west side of Carpenter Creek. The HCMM images provide information that is relevant to this geologic problem, but additional analysis is needed.

Our results for this area suggest that HCMM thermal-inertia data contain new information which can complement and--for certain directions, geologic settings, and length of features--supplement Landsat data for study of regional structural framework.

2.3 COLORADO PLATEAU

2.3.1 Richfield Quadrangle in Utah

The Richfield, Utah, 1^{o} by 2^{o} quadrangle (Figure 1) contains a relatively diverse range of igneous and sedimentary rocks. The eastern third of the quadrangle, including the Sevier Plateau and the Tushar Range, lies within the High Plateau section of the Colorado Plateaus province (Figure 16a). These physiographic entities form a transition zone between the flat-lying rocks of the Colorado Plateaus province to the east, and the Basin and Range province, which occupies the western two-thirds of the quadrangle. The geology of the quadrangle is quite complex and is difficult to portray on a map at small scale. The northern half of the quadrangle is underlain principally by dolomites, limestones, and shales of Paleozoic age in the west (Confusion, House, and Cricket Ranges) and by Paleozoic and Mesozoic carbonates and clastic rocks in the east (Pavant Range). The few igneous rocks that occur in the northern area are primarily Late Tertiary to Quaternary basaltic and rhyolitic volcanics in the sedimentary basin fill of the Sevier Desert. South of a west-northwest oriented line (Figure 16a) defined by the junctions of the Pavant and Tushar Ranges on the east and the Confusion and Wah Wah Ranges on the west, exposed rocks are predominately igneous, except for the northern part of the Needle and Wah Wah Ranges, which are composed primarily of Paleozoic sedimentary carbonates. The igneous rocks are predominantly volcanic, consisting of Tertiary volcanic vent complexes and extensive regional ashfall units. The only exceptions are the central part of the Mineral Mountains, which contains a Tertiary granitic batholith, and several small Tertiary stocks scattered throughout the ranges. Most of the southern and central ranges are extensively mineralized and contain many exposures of rocks that have been hydrothermally altered to argillic, advanced argillic,

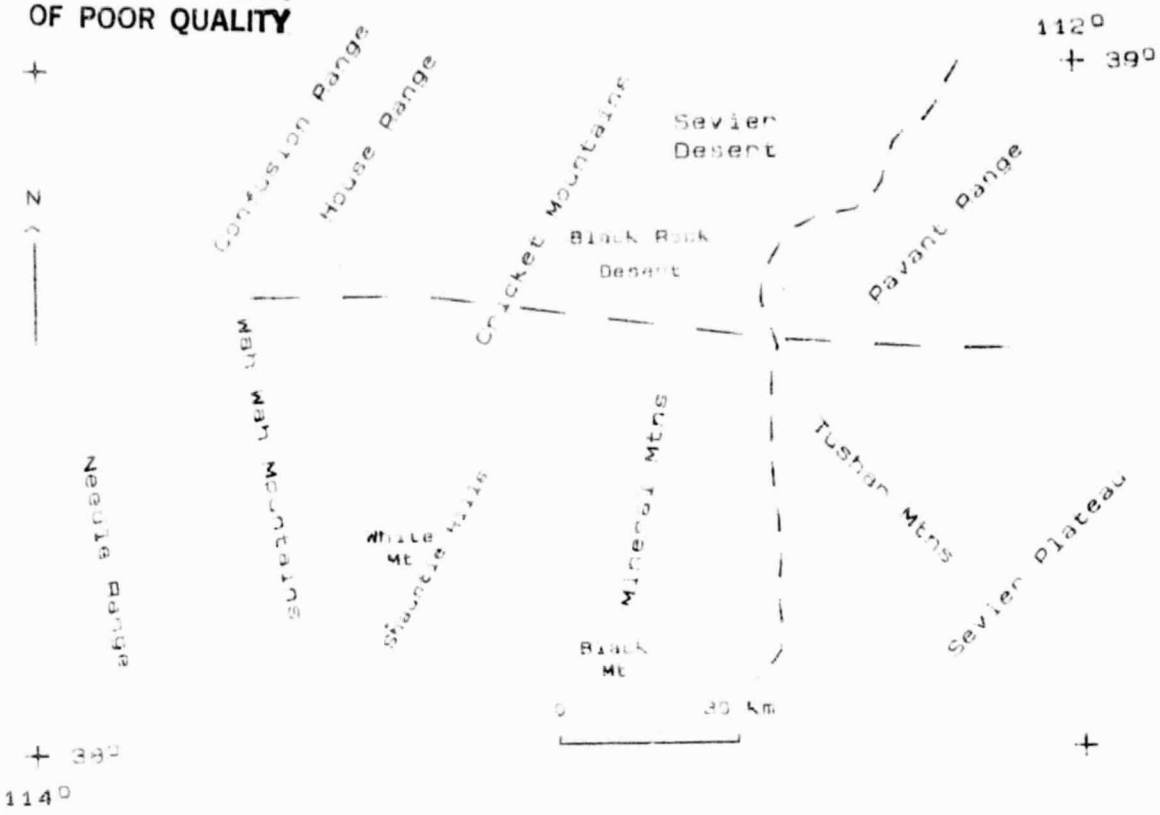

Figure 16a.--Location map of physiographic features in the Richfield quadrangle. Basin and Range - Colorado Plateaus boundary is shown by the short-dashed line. The long-dashed horizontal line represents the general boundary separating the sedimentary rocks to the north from the igneous rocks to the south (see text).

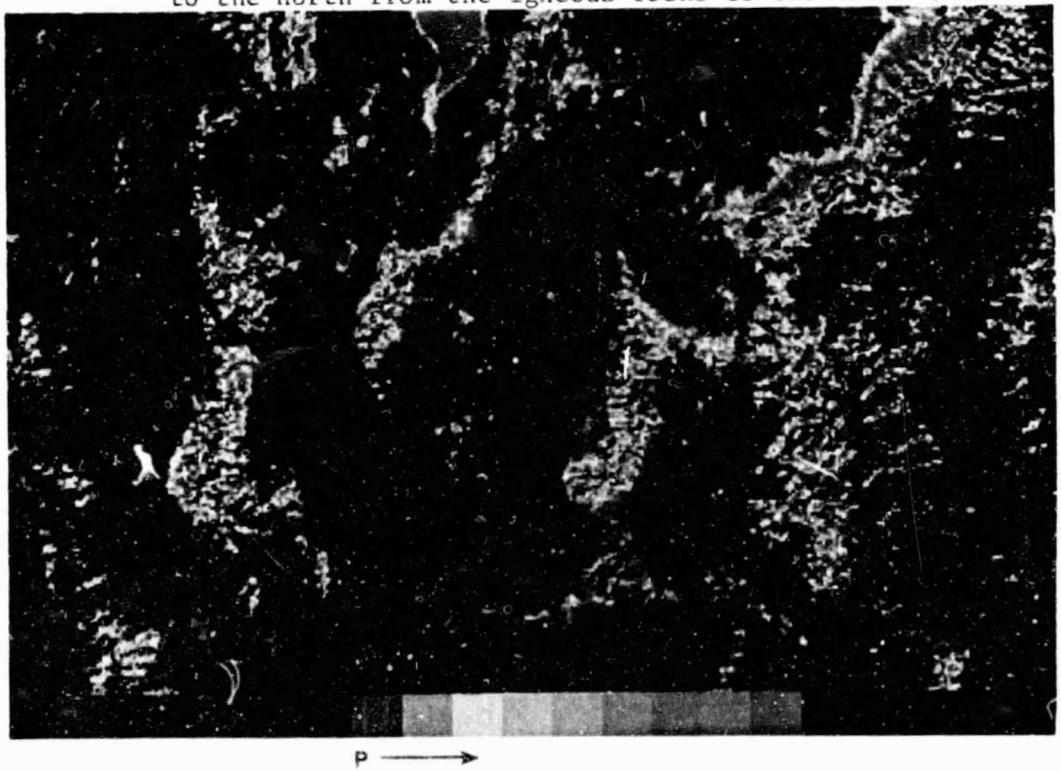

Figure 16b.--A topographically-corrected thermal-inertia image of the Richfield 2° quadrangle (Utah). Scale and boundaries are the same as on (a).

and sericitic stages. Altered areas occur in the Shauntie Hills, Wah Wah, Needle and Tushar Ranges. The Sevier Plateau contains mostly Mesozoic clastic sedimentary rocks with some Tertiary volcanic vent and flow facies.

The sedimentary rocks for most of the region have been affected by large-scale eastward thrusting during the Mesozoic. Late Tertiary Basin and Range normal faulting oriented mainly north-south has affected both the igneous and sedimentary rocks.

Heavy vegetation (>40% cover) typically is found in the uplands at elevations greater than 1830 m (6,000 ft). It consists mostly of stands of pinyon pine and Utah juniper with ponderosa pine, aspen, and mountain mahogany at the higher levels where the rainfall is greater. Lowland vegetation tends to be more sparse, except in irrigated cropland areas, and consists of scattered grasses, sagebrush, rabbitbrush and some salt desert shrubs in more alkaline soils. Hence, some of the better areas to examine for lithologic discrimination without the confounding aspect of heavy vegetation on the thermal-inertia image are the rhyolites and basalts of the Black Rock Desert and the dolomites, limestones and quartzites at the lower elevations in the House Range and Cricket Mountains. Other areas that are relatively barren of thick vegetation cover include the lower elevations of the Wah Wah and Black Mountains, where intermediate to acidic volcanic rocks are predominant.

An analysis was conducted of the thermal inertia and reflectance for several igneous and sedimentary units in the Richfield, Utah, quadrangle. For this study a thermal-inertia image was constructed from images acquired September 23, 1978, (AA0150-09410-3 amd AA0150-20350-1,2). These HCMM images were registered to digital terrain data (Defense Mapping Agency), and a topographically corrected thermal-inertia image (Figure 16b) was generated (see section 3.1) on a color plotter at a scale of 1:250,000 to match other

geologic, geophysical, and topographic maps. Statistics for several igneous and sedimentary rock types were computed using the geologic map (Steven and Morris, 1983) as a base to locate units. Rock type values were obtained by combining the statistics for several similar units (Figure 17).

Although the reflectivity values for the sedimentary rocks show complete overlap, some separation can be seen in the thermal-inertia values (Figure 17). In order of increasing thermal inertia they rank: shale (Sh) and limestone (Ls), dolomite (D), and quartzite-sandstone (Qz, Ss). The sandstone is considered together with the quartzite because the values were determined for the Navajo Sandstone, and this is closer to an orthoquartzite, being described as "locally converted to hard quartzite" (Steven and Morris, 1983). The ranking agrees with thermal inertias computed from literature values (Miller and Watson, 1977). The statistics for the igneous rock units, however, show considerable overlap and little discriminability (Figure 18). Generally the granites (G) are distinguishable from the other igneous rock types by their higher thermal inertias, but there appears to be a large overlap among the remaining igneous rock types. There is a trend, however, among the mean values of the thermal inertias: granite (G) > basalt (B) > andesite (A) and rhyolite (R) > quartz latite (QL). Although the statistical ranges overlap each other, indicating that classification schemes are unlikely to be successful, a model has been proposed (see section 3.3) that provides a basis for interpretation of observable thermal-inertia differences in igneous rock terrane.

Silicified hydrothermally altered volcanic rocks might be expected to show an increased thermal inertia compared to the unaltered parent rock due to the high thermal inertia of quartz. One relatively small area (approximately 1 km^2) of dominantly silicified volcanic rocks is present about 5 km west of

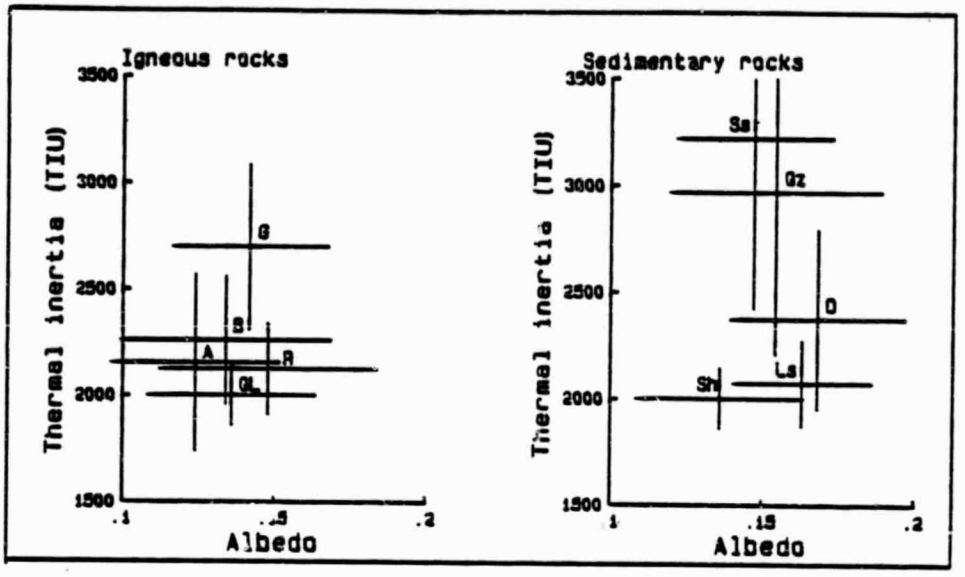

Figure 17.--Statistics for selected rock types in Richfield, Utah. Standard deviations are indicated by vertical and horizontal lines. Symbols indicate rock types. Igneous rocks: A - Andesite, B - Basalt, G - Granite, QL - Quartz latite, R - Rhyolite. Sedimentary rocks: D - Dolomite, Ls - Limestone, Qz - Quartzite, Sh - Shale, Ss - Sandstone (see text).

White Mountain in the southern Shauntie Hills of the Richfield quadrangle. A small thermal-inertia high can be located in the scene within this area, however, uncertainties in the exact registration of the image to the map base preclude an unequivocal relationship between the anomaly and the silicified area. Larger exposures of the sedimentary Prospect Mountain Quartzite, a rock of equivalent silica content, do show high thermal-inertia values and support our hypothesis. In general the altered areas in this quadrangle are too small to be analyzed (registered and sampled) with the 500 m resolution HCMM data.

Several important general aspects have resulted from our analysis of co-registered data sets of the Richfield quadrangle area. A model of the thermal-inertia behavior of igneous rocks has been developed (section 3.3) and this arose, to a significant degree, from the analysis of these co-registered data. A method for topographically correcting thermal data for elevation and slope effects was developed using these Richfield data (section 3.1), and one additional result from this area has been the development of a method to form simulated HCMM thermal images at any time in the diurnal cycle. This result has been presented at an international colloquium (Watson, 1983). Also we have also used these data to conduct a study of the relationship between vegetation cover and thermal inertia using co-registered topography, HCMM, and Landsat digital data (section 3.2). The study indicates that thermal data may be useful for geologic studies even where dense vegetation masks the spectral reflectance of rocks and soils.

2.3.2 A Major Linear Feature Transecting the Colorado Plateau

As part of our previous HCMM investigation (Watson and others, 1981), we had produced a thermal-inertia image (April 3/4, 1979, data AA0342-09150-3 and AA0343-20230-1,2) of an area within the Basin and Range province of southwestern Arizona to examine the thermal-inertia variation of igneous

rocks. During the present contract study, we were able to acquire additional HCMM data of that area (May 25/28, 1978, data AA0029-13330-8), and, although not part of our proposed work plan, these data provided an opportunity to examine two thermal-inertia images nearly one year apart. Because the area is quite arid, a detailed examination of meteorological data from weather stations in the area indicated that during the overpasses, and for several days prior, there had been clear skies with no rainfall. We decided to register the two thermal-inertia images and compute a difference image.

Computer enhancement of this difference image (Figure 18) lead to the recognition of a feature shown as a very subtle thermal-inertia change. The southern boundary of the feature is very straight and forms an acute angle with the Gila River. No coincident structure is indicated on geologic maps of this region and the feature cannot be seen on Skylab photography (Figure 19), Landsat MSS data, or X band radar images (Figure 20). The feature does cross the exposed bedrock ridges of this part of the Basin and Range province, where geologic contacts occur. Detailed examination of several HCMM images along the feature has led to the distinct identification of two additional segments of the proposed feature (Figure 21), one in the Hopi Buttes area of northeastern Arizona (AA0170-09160-3, AA0170-20240-1,2) and the other northeast of the Creede mineral district in southwestern Colorado (AA0017-20560-2). A further examination of regional geological and geophysical information of the southwestern U.S. has led to the interpretation a possible major lineament with a length of over 1,400 km extending from southwestern Arizona, across the Colorado Plateau and the Southern Rocky Mountains and into the plains of northeastern Colorado (Figure 22). The most direct evidence for the feature can be found on the aeromagnetic maps of the states of Arizona (Figure 23a) and Colorado (Figure 23b), where a linear element with bilateral

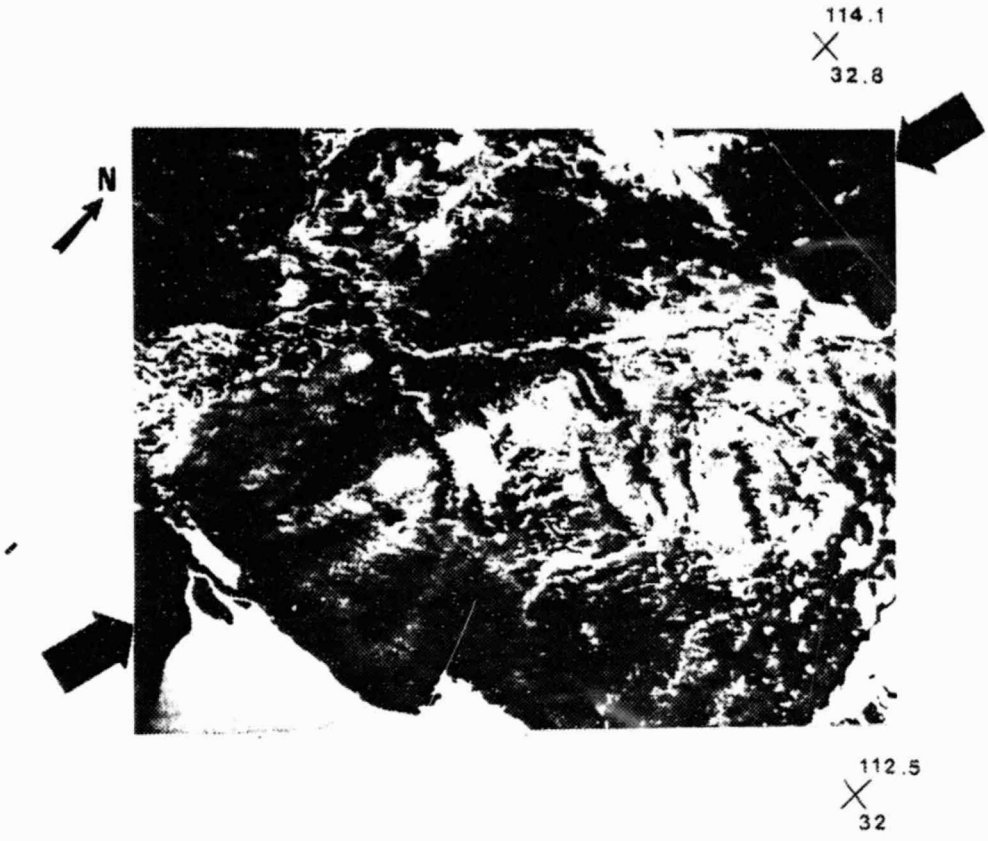

Figure 18.--Thermal-inertia difference image of the Cabeza Prieta area. The image was formed by subtracting a June 1978 thermal-inertia image from an April 1979 image. The difference image is adjusted so that areas with little change appear grey. The southern boundary of the anomalous area (dark triangle) represents the linear feature discussed in the text.

ORIGINAL PAGE
COLOR PHOTOGRAPH

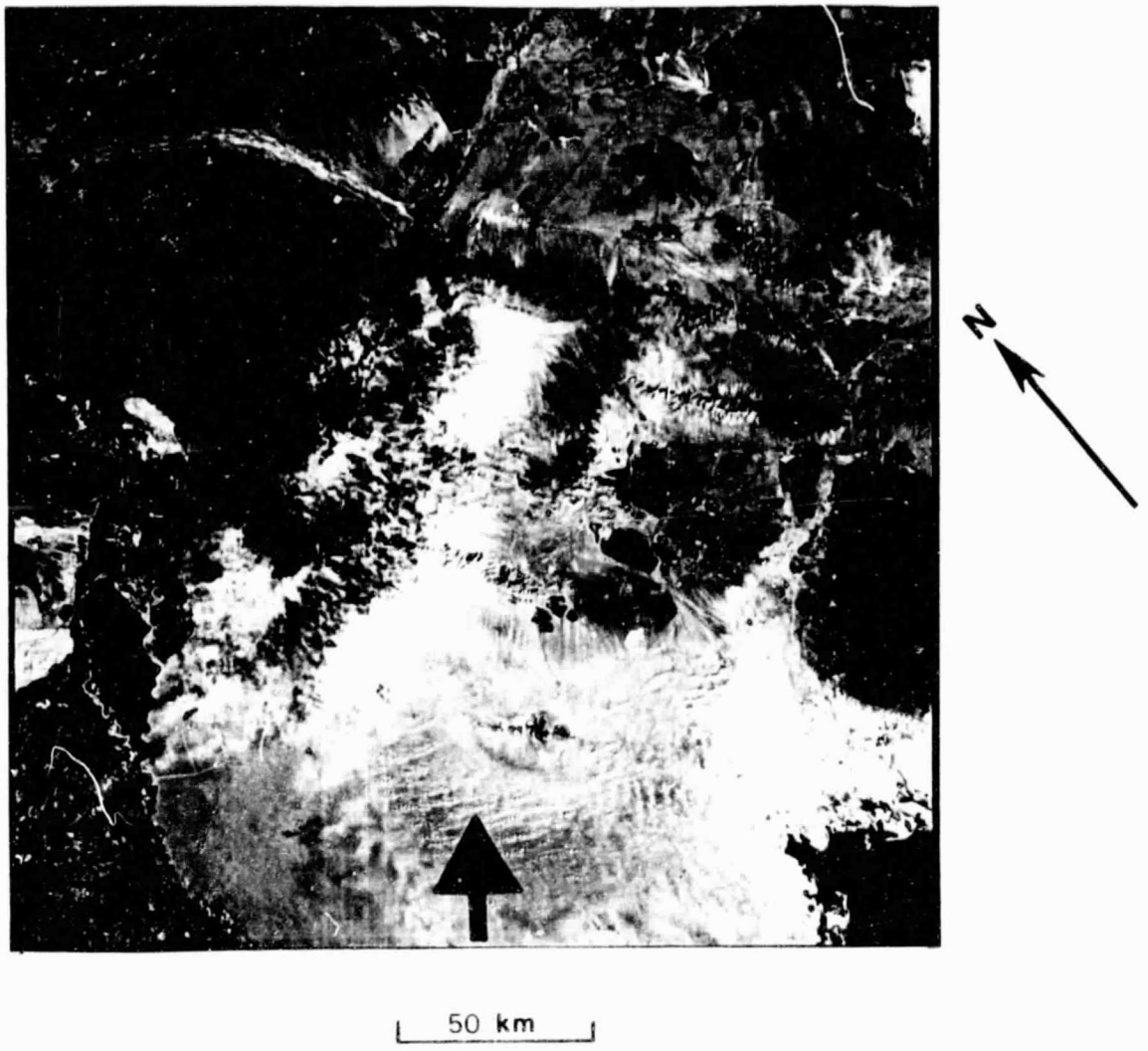

Figure 19.--Skylab photograph of southwestern Arizona area. There appears to be no expression of the linear feature which is described in the text and whose location is indicated by the facing arrows.

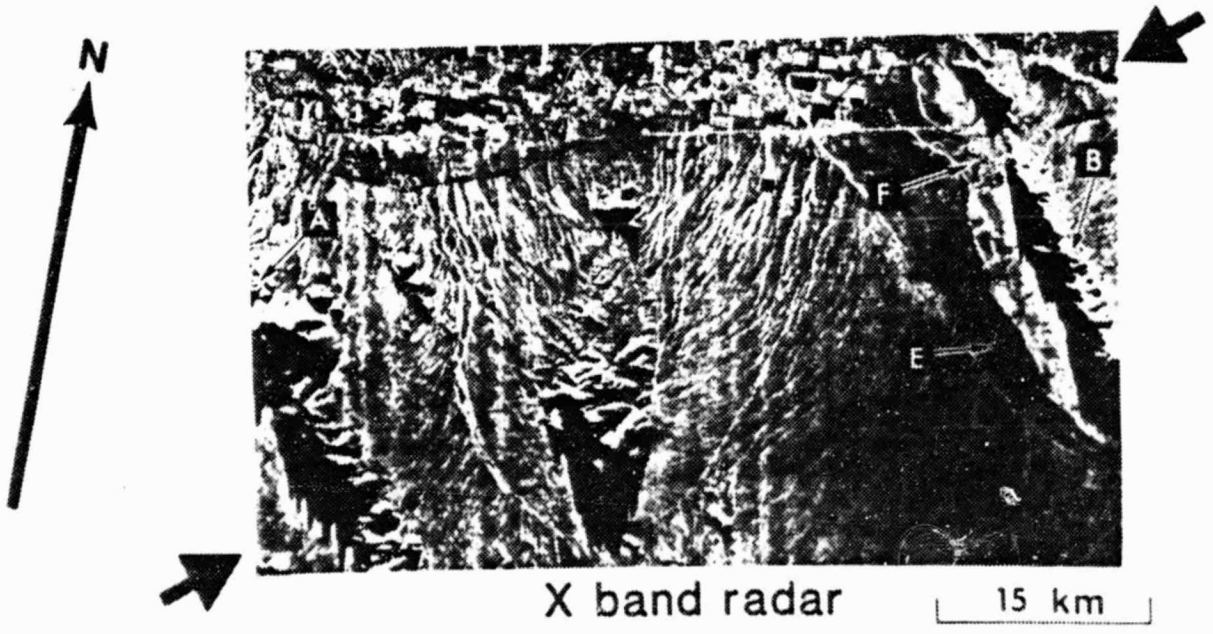

Figure 20.--Landsat and X band radar image of southwestern Arizona. The linear feature of Figure 18 does not appear to be expressed on the Landsat image, but where it crossed the exposed bedr ck, there appears to be geomorphic expression on the radar image. Letters on the radar image apply only to the original reference (Goodyear Aerospace, 1973).

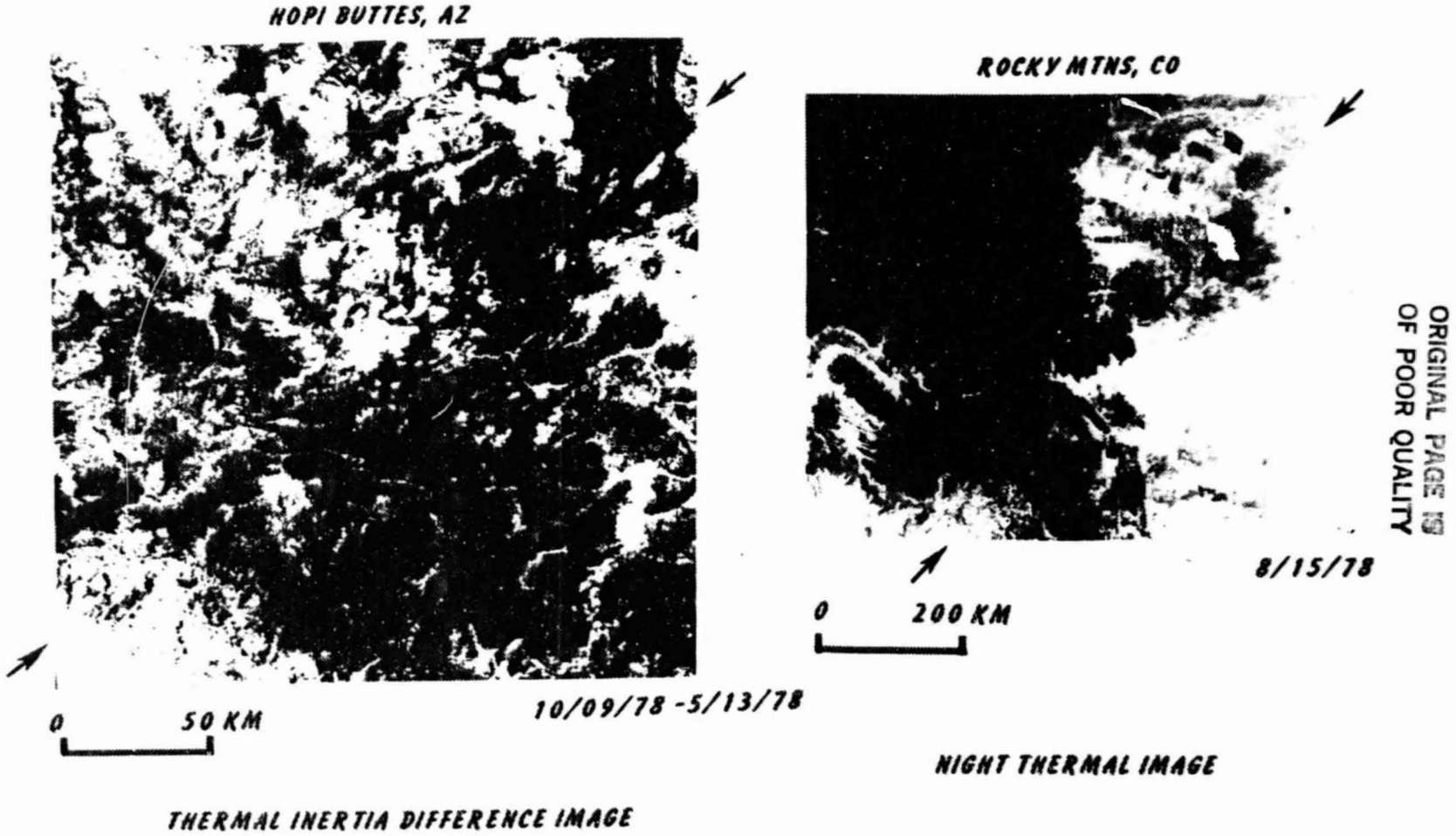

Figure 21.--Thermal lineament on HCMM data of the Hopi Buttes, Arizona, and the Colorado Rocky Mountains. The Hopi Buttes scene is a thermal-inertia difference image constructed using data from the indicated dates. The Rocky Mountains scene is a night thermal image. Colorado Springs is near the center of this image.

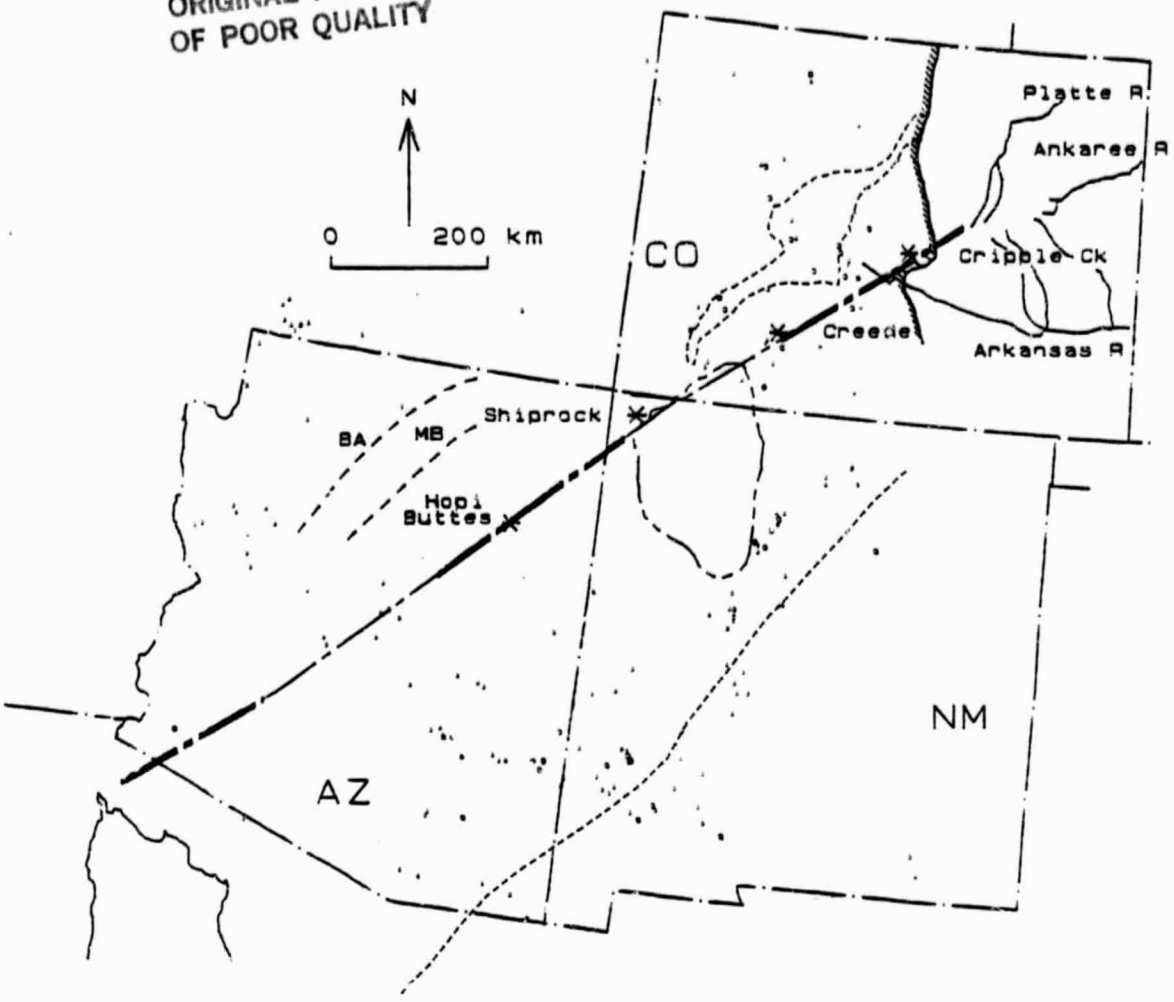

---------- Mineral belts: New Mexico (Jerome and Cook, 1967)
Colorado (Tweto and Sims, 1963)
- - - - - - - Fault systems: BA Bright Angel, MB Mesa Butte (Shoemaker et al., 1978)
——— San Juan Basin
——— Lineament (line broadens where feature detected on HCMM data)
. . Hot and warm springs (Berry et al., 1980)
Eastern boundary of the Front Range

Figure 22.--Map of the proposed lineament from Arizona through Colorado. Features discussed in the text are shown.

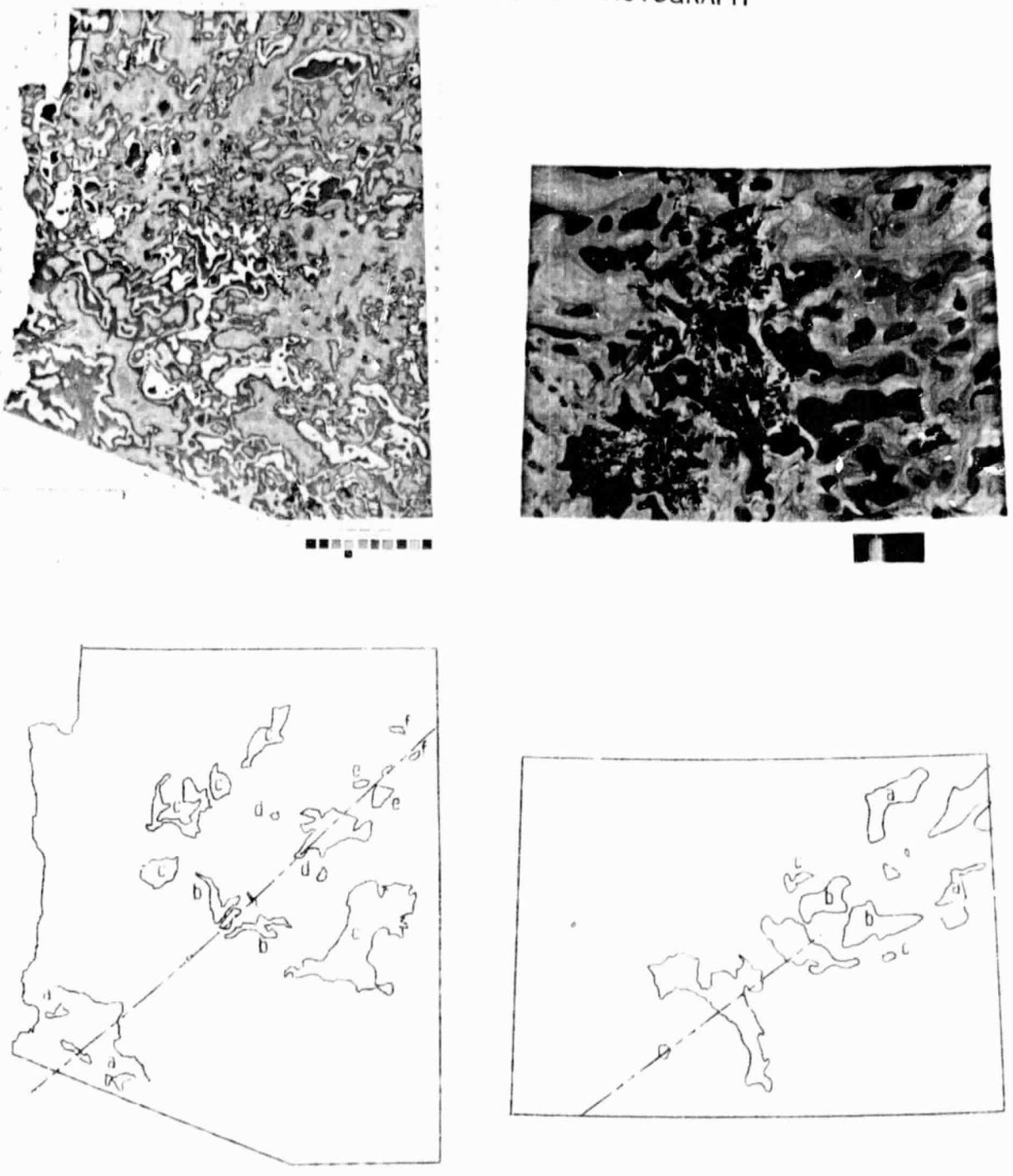

Figure 23.--Aeromagnetic maps of Arizona (Sauck and Sumner, 1970) to the left and Colorado (Zietz and Kirby, 1972) to the right. Letters are used on the bottom figures to indicate anomalies with matching contour values. The lineament described in the text is also shown.

symmetry in the aeromagnetic patterns is evident (Sauck and Sumner, 1970). Zietz and Kirby, 1972. The feature is also present in spatially filtered regional gravity data (Hildenbrand and others, 1982), wavelengths less than 1,000 km (Figure 24). Peripheral evidence includes coincidence with significant topographic breaks, drainage divides, other proposed lineaments (Cordell, 1978; Titley, 1981; Knepper, 1982), and parallelism to prominent lineament, joint (Badgley, 1962), and mineral district trends. The distribution of hot springs in the southwestern U.S. (Figure 22) has a primary trend that follows the general outline of the Colorado Plateaus province, but there are sporadic coincidences of hot springs along the lineament in southwestern Arizona and southwestern Colorado. Seismic refraction data (Warren, 1969) in the vicinity of where the feature passes from the Basin and Range to the Colorado Plateau indicate a crustal thickening and can be interpreted as evidence for a "keel" in the crust along the proposed structure.

2.4 BASIN and RANGE PROVINCE

2.4.1 Silver City Quadrangle in Arizona/New Mexico

The Silver City quadrangle of the Basin and Range (Figure 1) is at the southern edge of the Colorado Plateau province and the western edge of the Rio Grande rift zone. Rocks of Precambrian to Tertiary age crop out in the quadrangle, and geologic structures associated with both the Sevier orogeny (Laramide) and Rio Grande rift (middle to late Cenozoic) are present. In addition, the southern edge of the middle to late Cenozoic Datil-Mogollon volcanic field extends into the extreme northern part of the quadrangle.

The area is a mineral producer and is currently being studied by the U.S. Geological Survey as part of the CUSMAP (Conterminous U.S. Mineral Appraisal Program) program. Economic interest in the quadrangle is centered around copper, and to some extent gold and silver. Gold and silver are present in

ORIGINAL PAGE
COLOR PHOTOGRAPH

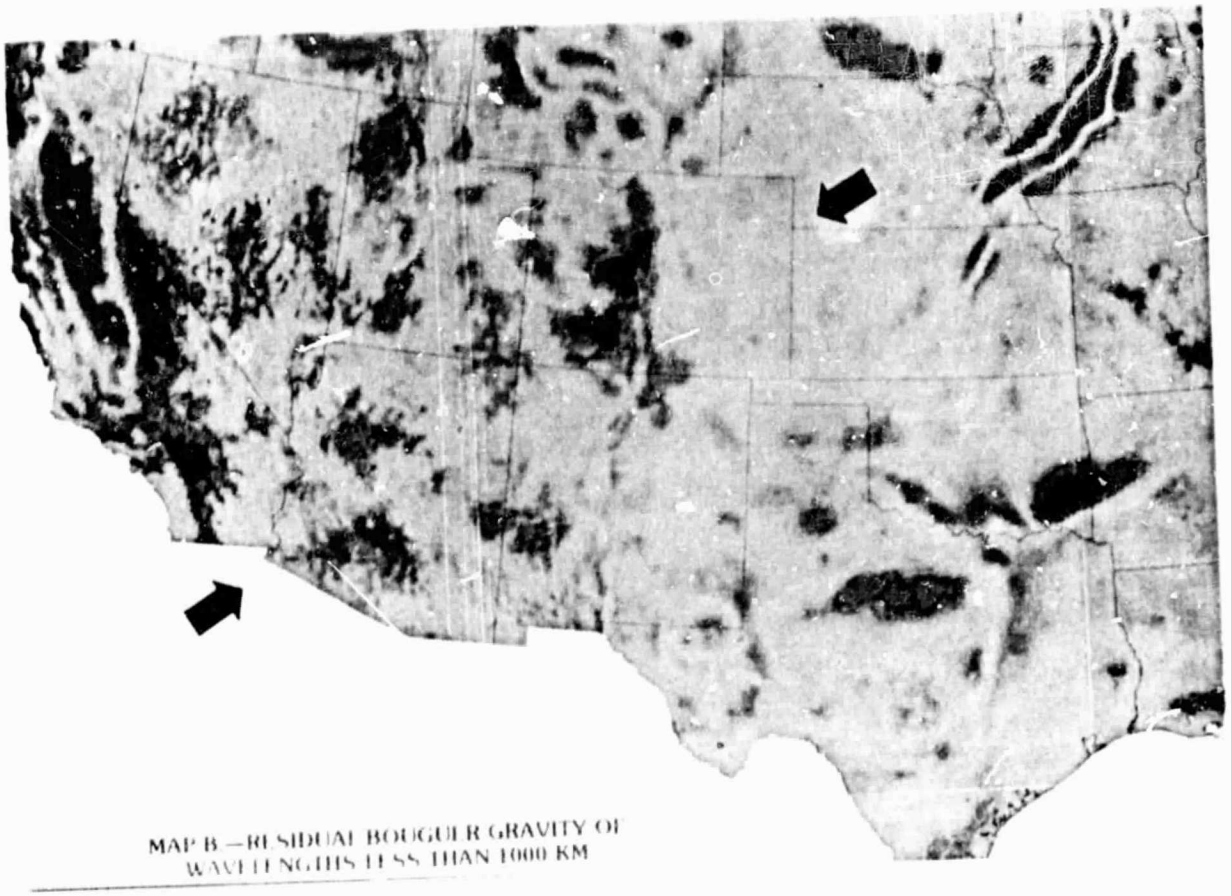

Figure 24.--Spatially filtered regional gravity map (Hildenbrand and others, 1982). Position of lineament shown by facing arrows.

the quadrangle in a wide variety of vein and replacement deposits. Gold is also found in a number of small placer deposits and both metals are very significant secondary commodities in porphyry Cu(Mo) deposits. The gold and silver resource in the quadrangle is limited almost entirely to the latter deposits (Richter and others, in press).

The copper porphyry deposits can be divided into two types: a Safford type, which occurs high in the crust within the volcanic pile, and a Santa Rita-Tyrone type, which occurs deeper and is confined to the source pluton. The Safford type is characterized by classical clay and sericite dominated alteration zones, and the Santa Rita type by massive replacement deposits in the Paleozoic carbonate rocks peripheral to the source pluton. Both deposit types are cut by pronounced northeast- to east-northeast-trending fault-fracture zones. At Santa Rita, the stock occurs at the intersection of a northeast-trending zone with a less pronounced north- to northwest-trending zone.

For this phase of the investigation, we decided to examine the use of thermal-inertia mapping both to detect structural control, particularly northeast trends, and also to discriminate geologic materials and, if possible, to correlate them with limonitic materials that had been detected previously using Landsat MSS data. A thermal-inertia image (Figure 25a) of the Silver City quadrangle area (location map, Figure 25b) was constructed using data acquired on October 13/14, 1978 (AA0170-09160-3 and AA0171-20240-1,2), and plotted at a scale of 1:250,000 using an ink jet color plotter. This is somewhat enlarged for HCMM data (1 pixel is 2mm x 2mm), but it is a convenient scale for comparison with existing geologic, geophysical, and topographic maps.

ORIGINAL PAGE
COLOR PHOTOGRAPH

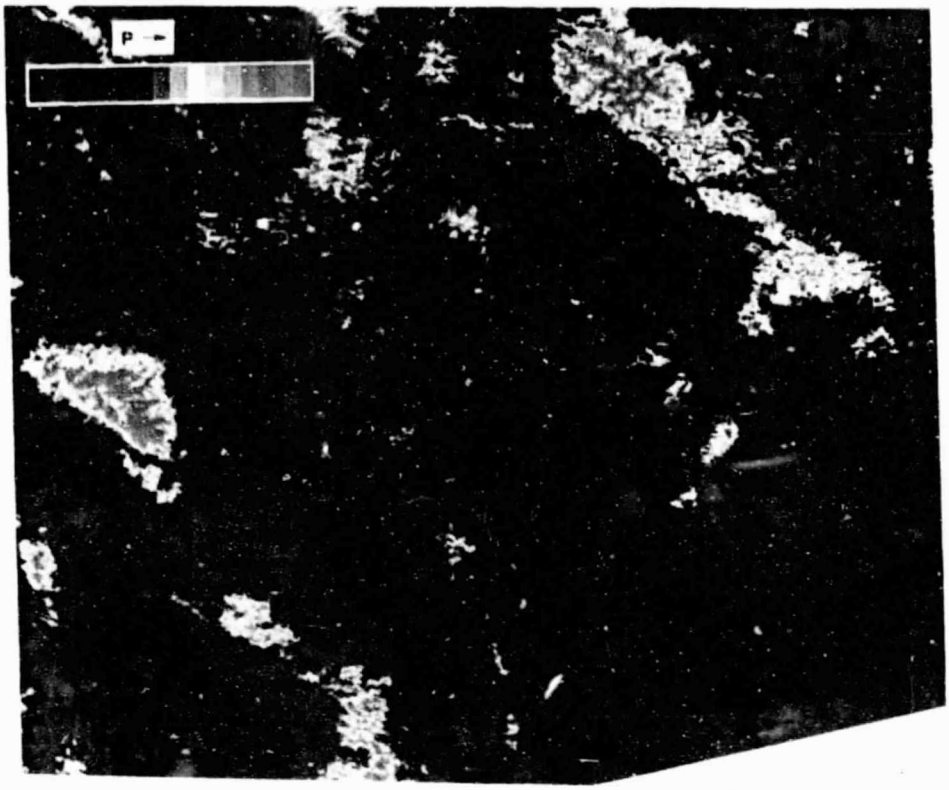

Figure 25a.--Thermal-inertia image of the Silver City 2° quadrangle (New Mexico and Arizona). Tick marks indicate the corners of the quadrangle.

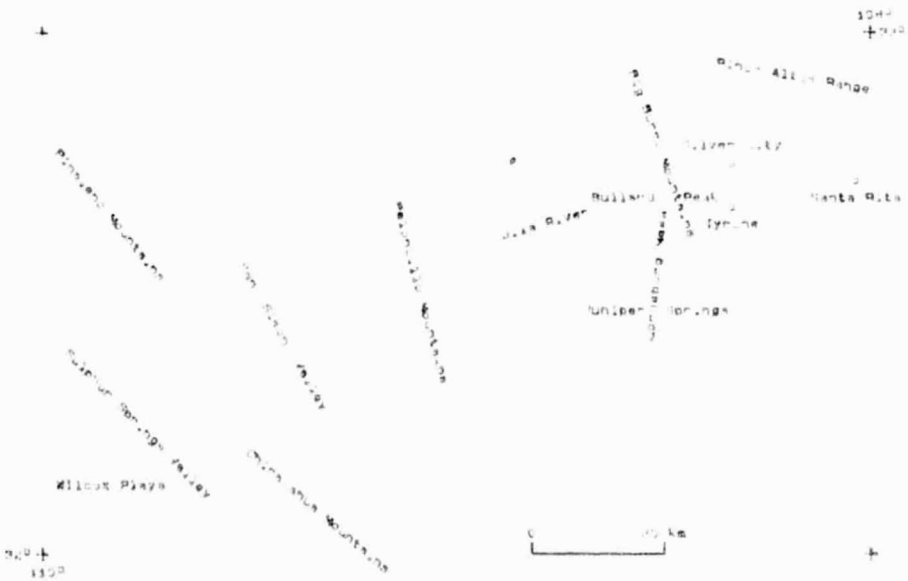

Figure 25b.--Location map of physiographic features in the Silver City 2° quadrangle (New Mexico and Arizona).

Generally, the thermal-inertia lows coincide with the valleys and the highs with the exposed bedrock. A linear features map (Figure 26) was constructed largely on the basis of evident thermal-inertia contrasts seen in the valleys. In some cases, the linear features were extended into the bedrock areas, and in a few cases, linear features were drawn in vegetated areas where they appear to coincide with resistant ridges. The pervasive northeast direction is the recognized Basin and Range trend in this area. The northeast direction is quite prominent on the map, and several long features were detected, including several that coincide in part with 30-kilometer-long straight segments of the Gila River (Figures 26 and 27) and a third that roughly coincides with the Santa Rita Trend and the New Mexico mineral belt line (Jerome and Cook, 1967).

The thermal-inertia contrasts within the alluvial valleys and within the exposed bedrock suggest possibilities for discrimination that may be geologically useful. The color thermal-inertia display shows three distinct units within the alluvium. The lowest thermal-inertia unit was found within the Wilcox Playa (Figure 28). It is contained within an area of high albedo as seen on Landsat data and suggests that a finer level of discrimination can be achieved by combining Landsat data with thermal-inertia data. The intermediate thermal-inertia unit within the alluvium was generally confined to the axes of the valleys or, where the regional slope is low, to the lowest elevations. In two areas this thermal-inertia unit, which we believe is associated with the finest grain materials, appears to be offset from the valley axis. One is in the northern Sulphur Springs Valley, where the thermal-inertia patterns are disrupted by cultivated fields. The other is in the southern San Simon Valley between the Chiracahua Mountains and the southern Peloncillo Mountains, where the thermal-inertia unit is offset towards the west, closer to the most mountainous area in the region. The

Figure 26.--Linear features map of the Silver City 2° quadrangle (New Mexico and Arizona) drawn from the black and white thermal-inertia image. Scale and boundaries are the same as on Figure 25b. Tick marks indicate the corners of the quadrangle.

ORIGINAL PAGE
COLOR PHOTOGRAPH

Figure 27.--Landsat color infrared composite (June 16, 1976) of the Silver City 2^{o} quadrangle (New Mexico and Arizona). Vegetated areas appear red.

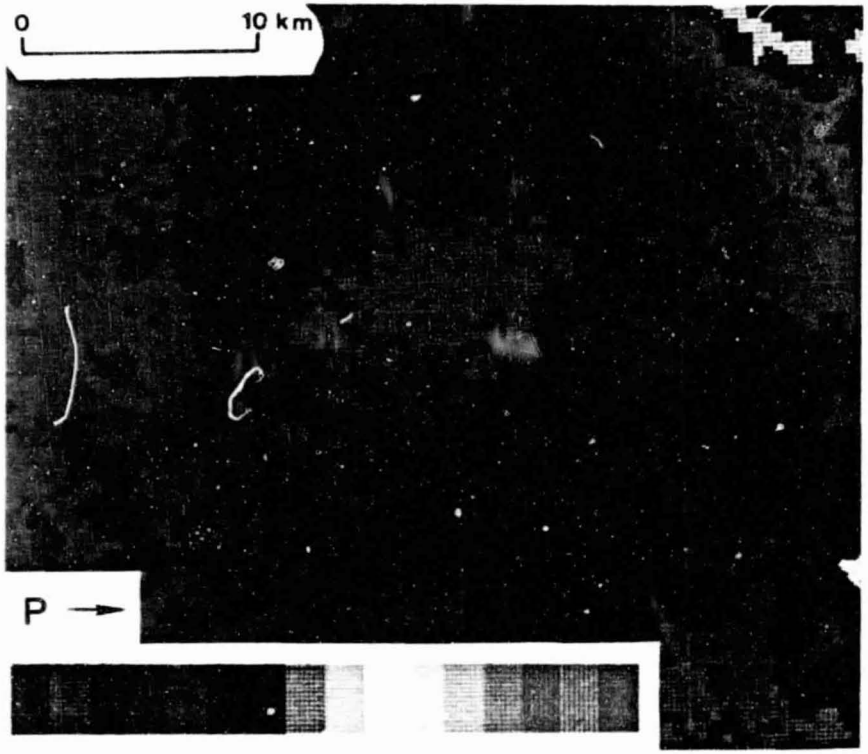

Figure 28a.--Outline of Wilcox Playa, Arizona on a thermal-inertia image. North is to the top of the image. A thermal-inertia low occurs within the playa.

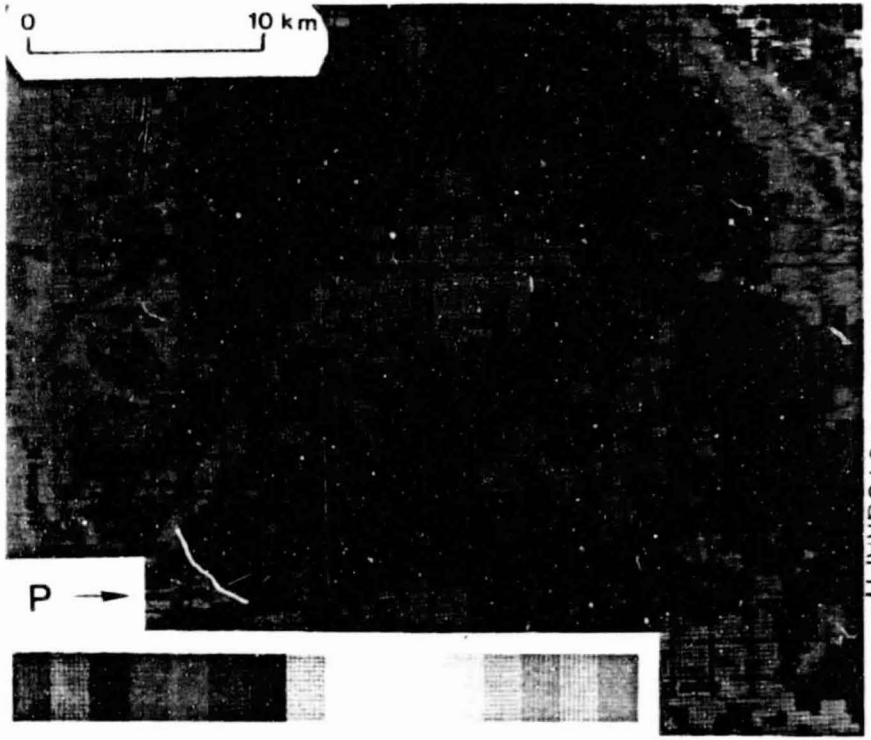

Figure 28b.--Topographic contours (interval 200 ft.) are superimposed on the thermal-inertia image.

offset may be related to the previous position of the drainage.

We next examined a large anomalous limonitic area that Raines and others (in press) previously identified in Quaternary and Tertiary gravels on Lordsburg Mesa from Landsat data and interpreted, using geophysical and geochemical data, as the surface expression of a chemical trap that may contain uranium concentrations similar to calcrete-uranium deposits. They speculate that ground water would be higher near the surface of a buried bedrock ridge. The thermal-inertia image of this feature (Figure 29) shows a northwest-trending zone (light-blue) of moderately higher thermal inertia. The western side of the limonite anomaly is roughly coincident with a disruption in the trend of both the thermal-inertia patterns and the topographic contours. Generally, lower thermal-inertia values bound the feature on the northeast, northwest and southwest sides. Although there is some local correlation between thermal inertia and topography, the topographic contours only show a bend in the vicinity of the anomaly and to the north thermal-inertia contrasts cross topographic contours. Possibly the subtle thermal-inertia changes reflect surface material differences or changes related to the ground water flow patterns across a buried bedrock ridge.

The thermal-inertia patterns within the bedrock units are not well understood at this time. In general, we believe that the highs correlate with the more resistant rock masses. Because these occur at higher elevations in this region, which is also vegetation covered (Figure 27), it is necessary to consider the effects of vegetation cover and elevation on the thermal-inertia map. Our main support for assuming these effects are not dominant is based on the analysis conducted using co-registered digital data sets for the Richfield quadrangle, Utah. There, we determined that, in the tree-covered bedrock areas above 2000 m, the correlation coefficient for thermal inertia versus

ORIGINAL PAGE
COLOR PHOTOGRAPH

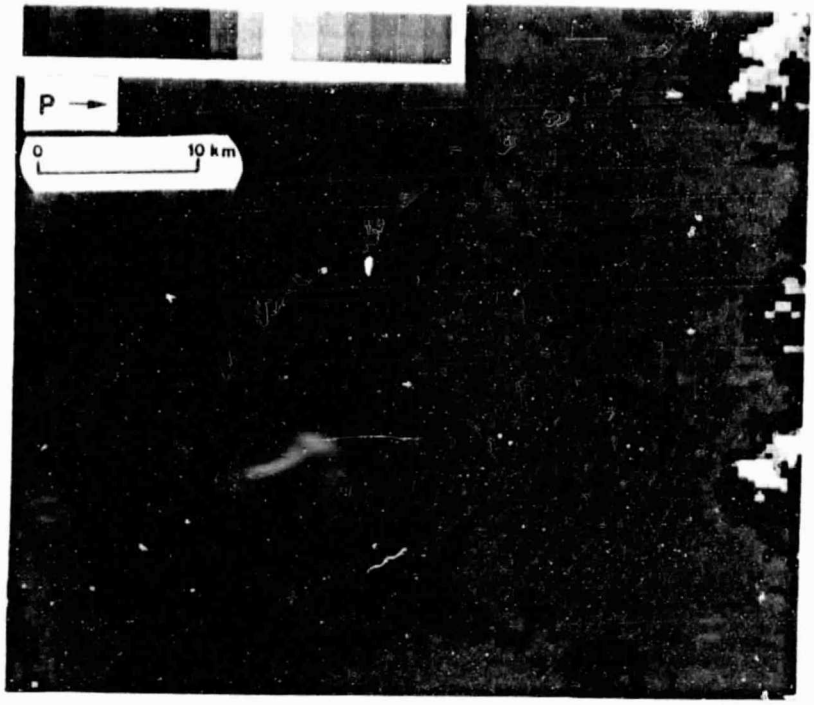

Figure 29a.--A limonitic area described in the text is outlined on a thermal-inertia image of the Lordsburg, New Mexico, area.

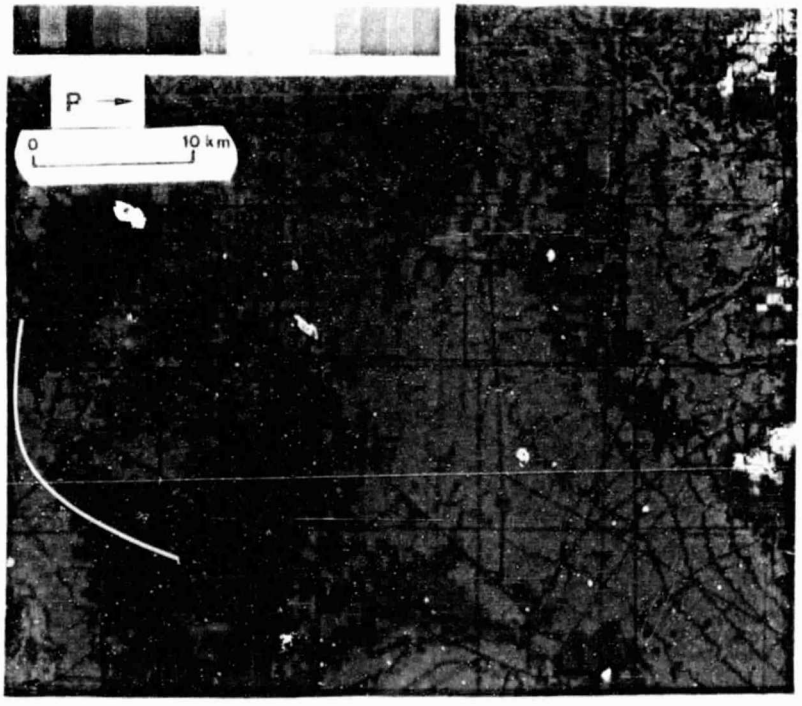

Figure 29b.--Topographic contours are superimposed on the thermal-inertia image.

vegetation was .08 and that for thermal inertia versus elevation was .009. We concluded that in terrain somewhat similar to that of the Silver City quadrangle, the thermal-inertia changes were not caused primarily by elevation or vegetation cover. We then examined the local correlations between the thermal-inertia image and the geologic and topographic maps within the areas of bedrock.

In the Big Burro Mountains, in the northeastern part of the quadrangle, the highest thermal-inertia values lie within an unfaulted zone of Precambrian granitic rocks. The south and southeastern boundaries of the zone appear to coincide with faults rather than topographic contours (Figure 30). Other thermal-inertia highs in the area occur at lower elevations. Southwest of this area, near Juniper Springs, an anomaly is located on rocks that are about 700 m lower than the granitic rocks and lie roughly along a ridge. Northwest of the main area, near Bullard Peak, thermal-inertia highs occur within the Precambrian metasedimentary and metaigneous rocks, about 300 m lower than the main area. The areas adjacent to this anomaly are at similar elevations and appear to have similar vegetation cover. About 7 km northwest of Bullard Peak is another zone of thermal-inertia highs within the Precambrian metasedimentary and metaigneous unit that appears to be fault bounded in several places. Accurate registration to the base maps and precise feature identification of all anomalies is not possible at the resolution of the HCMM system, but, in general, the anomalous patterns do seem to correlate with resistant ridges, knolls, and peaks.

On the western side of the quadrangle, within the Pinaleno Mountains, northeast- and east-trending thermal-inertia highs also correlate with ridges and knolls (Figure 31). In addition, a thermal-inertia anomaly seems to match an inlier of younger Precambrian granitic rocks within older Precambrian

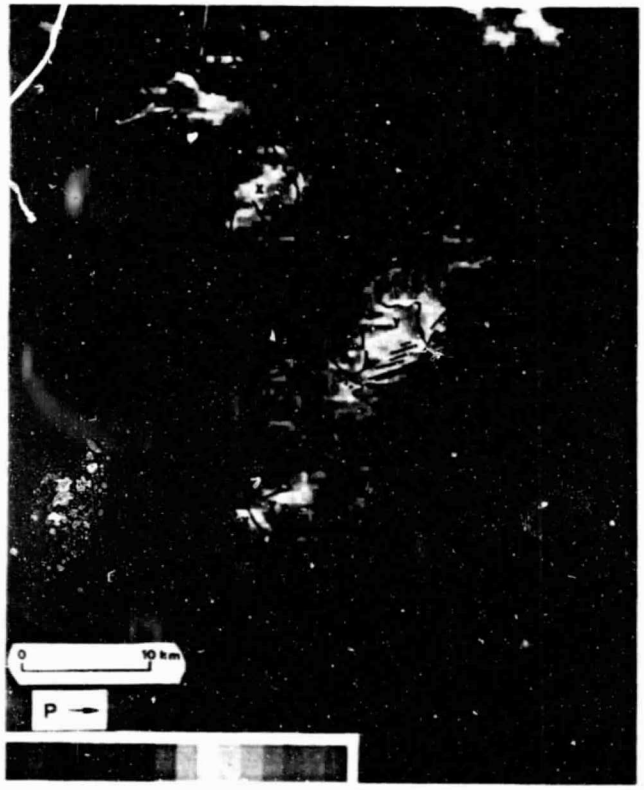

Figure 30a.--Thermal-inertia image of the Big Burro Mountains, New Mexico. Near the center of the image, the highest thermal-inertia values (red) lie within an unfaulted zone of Precambrian granite (Y). In other areas, the thermal-inertia boundaries between the green and yellow units often correspond to lithologic boundaries or faults. Map symbols are: X - Precambrian metamorphics, Y - Precambrian granite, TK - Tertiary and Cretaceous rhyolite, TKa - Tertiary and Cretaceous andesite, T - Tertiary rhyodacite and rhyolite, and Q - Quaternary alluvium.

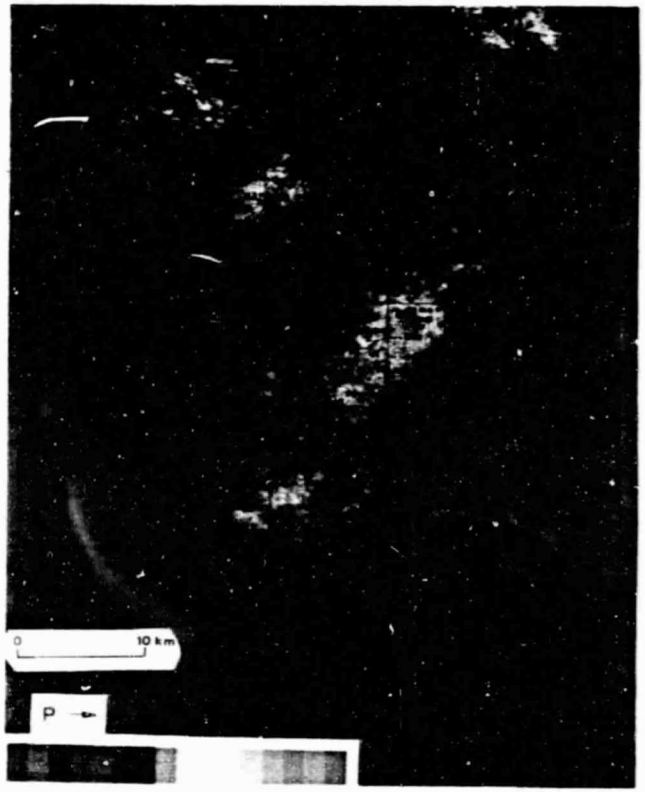

Figure 30b.--Topographic contours are superimposed on the thermal-inertia image. In general, the anomalous patterns seem to correlate with resistant ridges, knolls, and peaks.

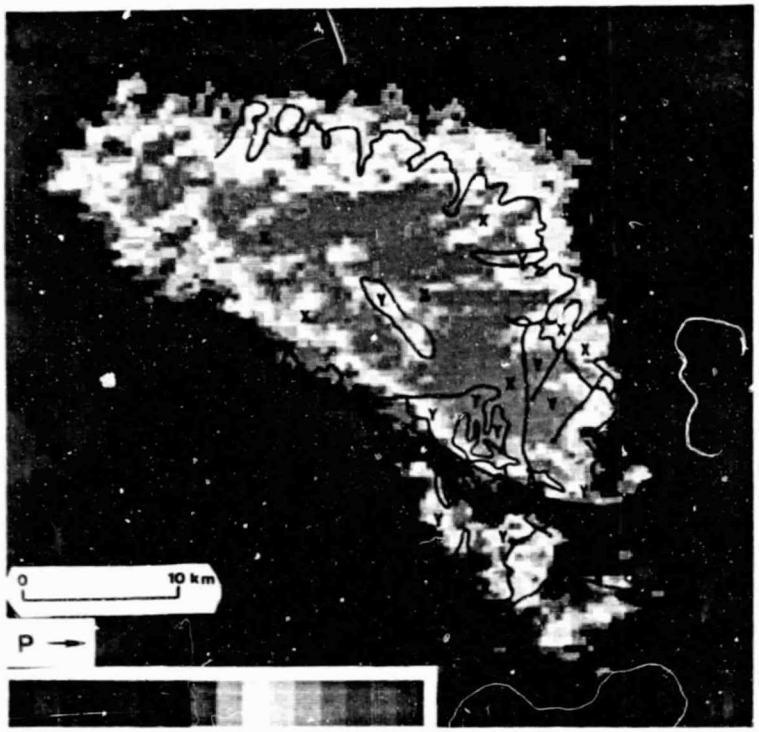

Figure 31a.--Thermal-inertia image of the Pinaleno Mountains, Arizona. The mountains are densely vegetated and appear completely red on a standard color-ratio composite Landsat image. Thermal-inertia differences can be seen, however, within the heavily vegetated areas. A thermal-inertia low seems to correlate with a Precambrian granite inlier (Y) within Precambrian metamorphics (X).

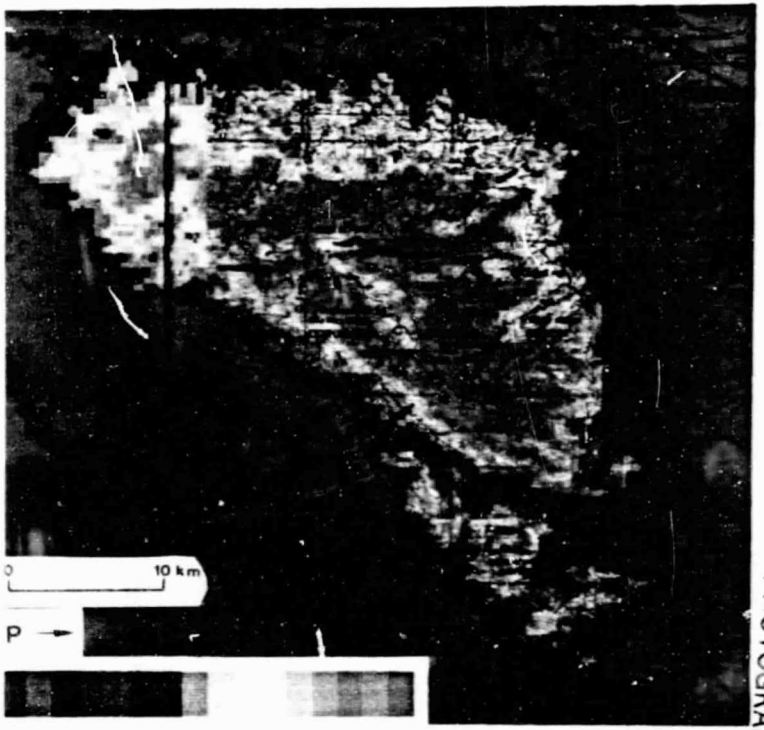

Figure 31b.--Topographic contours are superimposed on the thermal-inertia image. Thermal-inertia highs seem to correlate with resistant ridges.

terrain. In the Mogollon Mountains, north of Silver City, New Mexico, prominent thermal-inertia anomalies trending northwest and west can also be observed (Figure 25a). These are believed to be expressions of resistant units and may be related to regional structural fabric.

Analysis of the thermal-inertia image of the Silver City quadrangle indicates that geologically useful discriminations can be achieved. Several thermal-inertia units were discriminated within unconsolidated materials at lower elevations, and a contrast was detected that correlates with an area previously identified as a chemical trap possibly containing uranium concentrates. In the bedrock areas, which are generally obscured on the Landsat images due to vegetation cover, thermal-inertia anomalies have been detected that we believe correlate with resistant rock masses, and in one identified case, with a lithologic change. We tentatively conclude from these results, tempered somewhat by the resolution limits of the HCMM system, that thermal-inertia mapping may have significant value for geologic studies in moderately-well vegetated areas.

2.4.2 Walker Lake Quadrangle in California/Nevada

The other portion of the Basin and Range province studied was Walker Lake quadrangle, California and Nevada (Figure 1). The eastern three-fourths of this area is in the Great Basin, and the western one-fourth is in the Sierra Nevada Mountains. The Great Basin part is transected by the Walker Lane, a major northwest-trending zone of right-lateral, strike-slip faulting. Cenozoic volcanic and related intrusive rocks ranging in composition from rhyolitic to basaltic dominate this part of the area, but Mesozoic granodioritic plutonic, metasedimentary, and metavolcanic rocks are scattered throughout the area. Paleozoic metasedimentary rocks are locally exposed. Broad pediments form the transition from the ranges to the basins, which are

the sites of playas and, locally, salt marshes. Most of the known mineral deposits in the quadrangle are associated with Cenozoic epithermal veins and Mesozoic skarns formed at the contacts of the granodioritic plutons. The Yerington, Nevada, porphyry copper deposit is an exception.

The Sierra Nevada part of the study area consists mainly of Mesozoic granodioritic rocks with scattered roof pendants of metasedimentary rocks and metavolcanics and locally extensive remnants of Cenozoic volcanic rocks, chiefly andesite. Alpine glaciation carved deep canyons and provided excellent fresh exposures throughout most of this uplift block, but deeply weathered granodioritic rocks are present in the southwestern corner of the area. Although the volcanic rocks are extensively altered in some places, mineralization is much less extensive than in the Great Basin section.

A thermal-inertia image (Figure 32) was constructed of the Walker Lake quadrangle area from HCMM data acquired July 17, 1978 (AA0082-10160-3 and AA0082-21090-1,2). The area was selected for study in order to ascertain whether HCMM data would show any expression of lineaments and areas of hydrothermally altered rock that had been interpreted from Landsat MSS data and extensively field checked by T. L. Purdy and L. C. Rowan (written commun., 1983).

The two main lineament directions seen on the HCMM data (Figure 33) correspond in direction to two prominent lineament systems detected on Landsat images (Rowan and Wetlaufer, 1981): the northeast-trending Midas system and the northwest-trending Walker Lane system. In general, it appears that the linear features detected on the thermal-inertia image do not coincide with the mapped Landsat lineaments and may represent different aspects of the tectonic expression.

A superficial correlation between the thermal-inertia highs and areas of

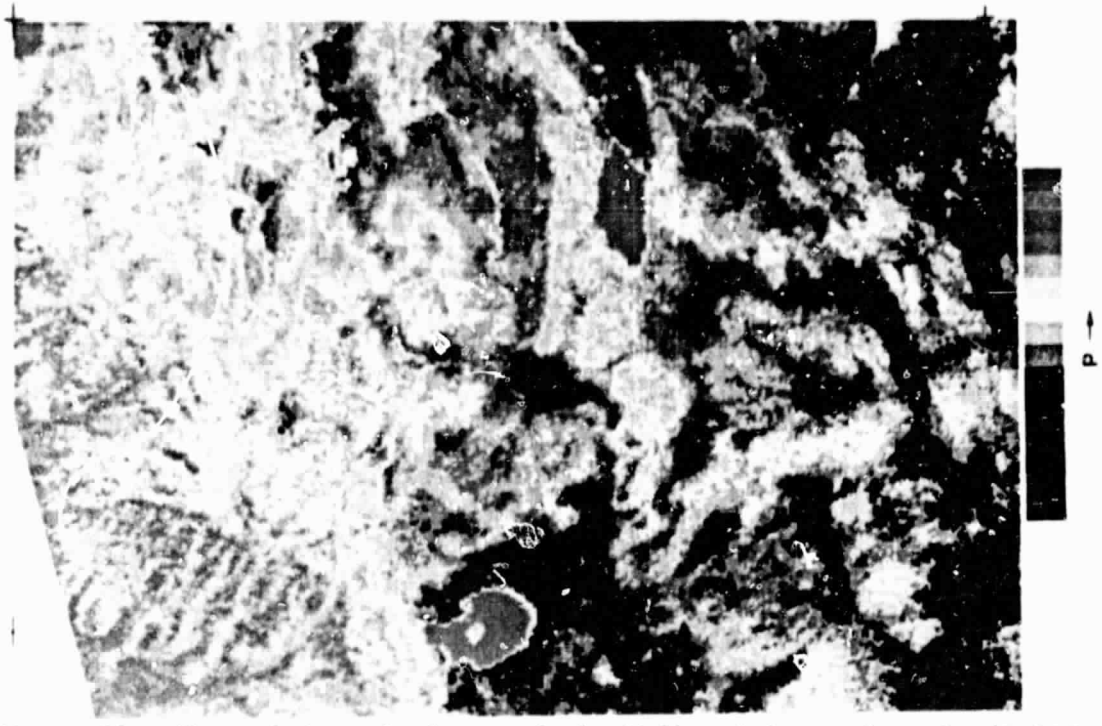

Figure 32.--Thermal-inertia image of the Walker Lake quadrangle (California and Nevada). Tick marks indicate the quadrangle corners. Mono Lake is to the south, Walker Lake to the north, and the Sierra Mountains to the west. The color bar chart shows thermal inertia increasing to the top.

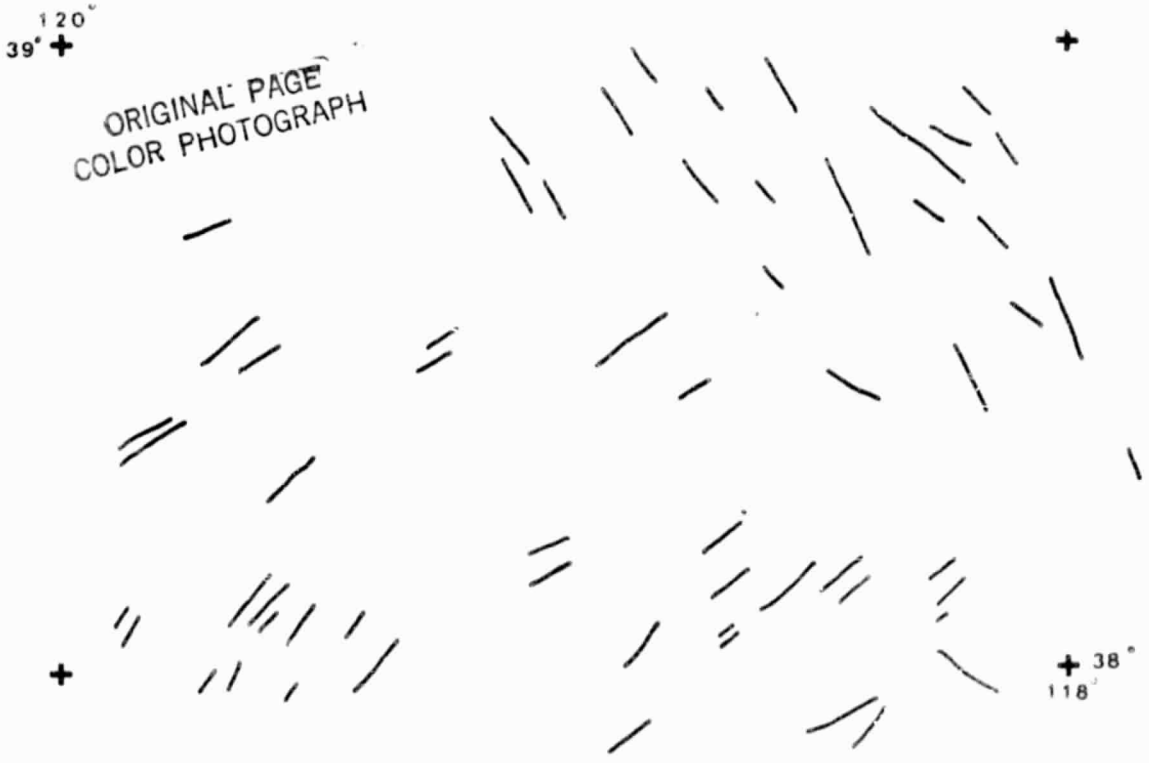

Figure 33.--Selected linear features of the Walker Lake 2^{o} quadrangle (California and Nevada) drawn from the black and white thermal-inertia image. Two prominent lineament directions (northwest and northeast) can be seen.

alteration can be seen in several areas, but this seems to be largely the result of the generally higher thermal inertia in areas of bedrock. To consider this aspect of the problem, we examined in more detail one zone of alteration, the Walker Lane Alteration Belt (Figure 34). As described by Rowan and Purdy (1982), the belt is a zone roughly 20 km wide and at least 65 km long in the northeastern part of the quadrangle, covering most of the Cubbs Valley Range. The belt coincides with the northwest-trending Walker Lane fault zone, and the rocks are rhyolitic ash-flow tuffs and flows and associated intrusive rocks. Those areas of altered rocks that are large enough to be resolved on HCMM data are: silicified (S), silicified and argillized, silicified dominant (SAg), argillized and silicified, argillized dominant (AgS), argillized (Ag) and altered undifferentiated (A). A bedrock map at HCMM resolution was drawn by generalizing from the surficial geologic map of the quadrangles (Dohrenwend, 1982). There is a striking similarity between the higher thermal-inertia values (yellows and light green) and the areas of bedrock. The correlation with altered areas is much less. In between parts of the alteration boundary and the thermal-inertia contours, and in a general sense, the altered areas tend to be associated with somewhat higher thermal-inertia values. However, most areas of high thermal inertia do not coincide with mapped alteration.

We then examined the remaining larger areas of alteration in the quadrangle as identified by T. L. Purdy and L. C. Rowan (written commun., 1983) to determine if any general relationship could be observed in thermal inertia between altered rocks and their surroundings and among the different types of alteration.

Markleeville Alteration Belt

Of the three major areas of alteration (Figure 35), the silicified unit

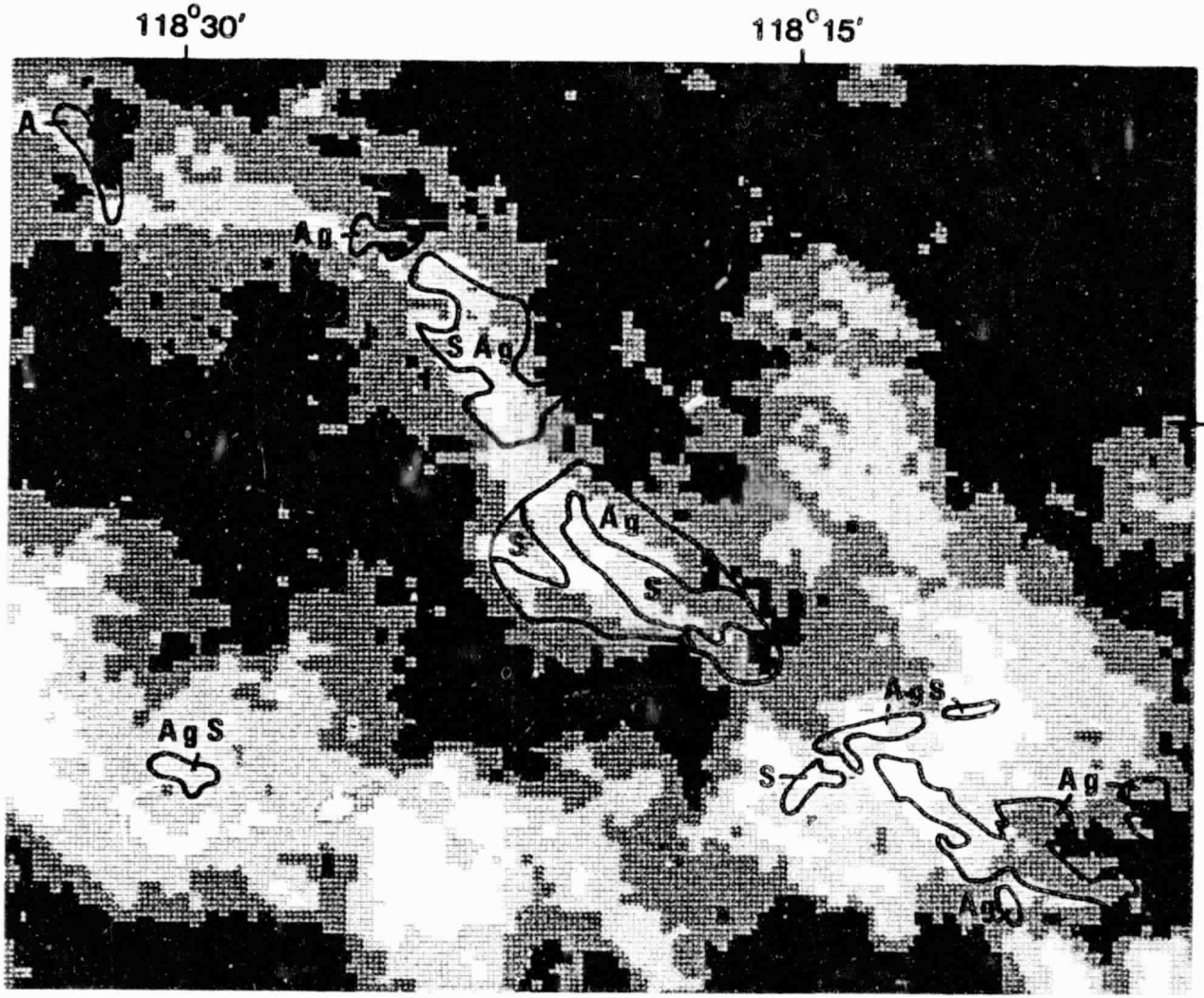

ORIGINAL PAGE
COLOR PHOTOGRAPH

Figure 34.--Thermal-inertia image of the Walker Lane Alteration Belt. Areas of altered rocks are labeled as silicified (S), silicified and argillized, silicified dominant (SAg), argillized and silicified, argillized dominant (AgS), argillized (Ag), and altered undifferentiated (A). Scale 1:250,000.

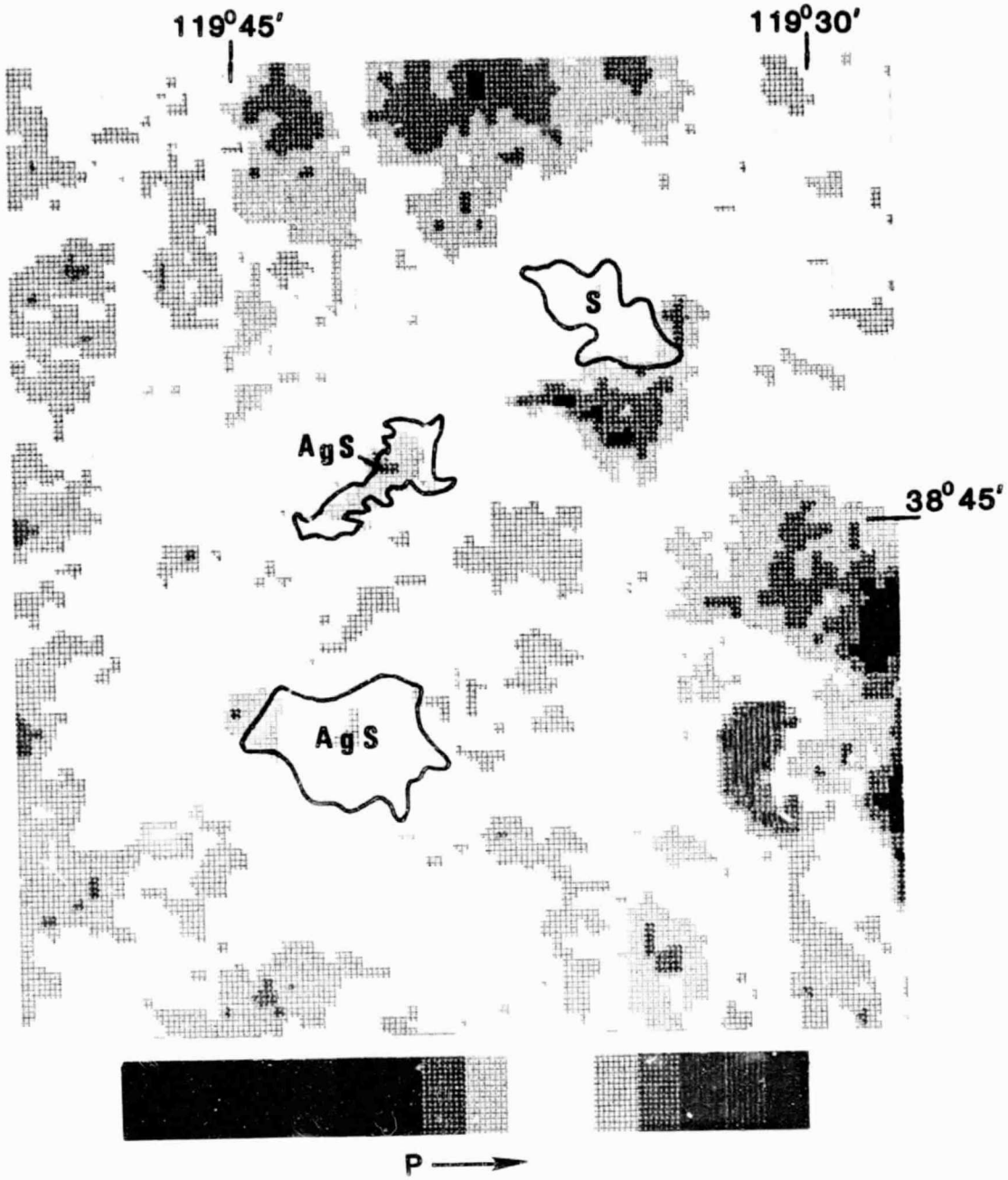

Figure 35.--Thermal-inertia image of the Markleeville Alteration Belt. Symbols are the same as Figure 34. Scale 1:250,000.

(S) roughly coincides with increased thermal inertia (bright yellow), the more northerly argillized silicified unit (AgS) with a reduced thermal inertia contrast (green), and the southerly unit (AgS) is indistinguishable from its surroundings.

Sweetwater Mountains-Garfield Flat Alteration Belt

The main area of alteration (AgS) in the Sweetwater Mountains (Figure 36a) has lower thermal inertia (green) to the west and higher thermal inertia (yellow) to the east. The main area, in Garfield Flat (Figure 36b), is distinguishable only because it is partially bounded by a bedrock-alluvium contact. A smaller silicified unit (S) and an argillized unit (Ag) both are associated with higher thermal inertia (bright yellow).

Aurora-Bodie Hills Alteration Belt

In this area (Figure 37) north of Mono Lake, the most westerly argillized unit (Ag) is associated with lower thermal inertia, a smaller unit (Ag) to the east with higher thermal inertia, and the largest unit (AgS) is indistinguishable from its surroundings.

Summary of observations in the Walker Lake quadrangle:

1. Areas of bedrock have high thermal inertia; unconsolidated materials have low thermal inertias. In a test area in the northeastern corner of the quadrangle, the bedrock alluvium contact was found to coincide quite well with the thermal-inertia contact between the light and dark green colors corresponding to a thermal-inertia value of approximately 2100 TIU's.
2. No clear example was found of a thermal-inertia anomaly matching an altered bedrock area. Many instantces were found of a partical match between a thermal-inertia color pattern and an altered area. This result may express both the heterogeneity of the thermal-inertia variations of altered areas and the variable nature of the boundary between altered and unaltered bedrock.

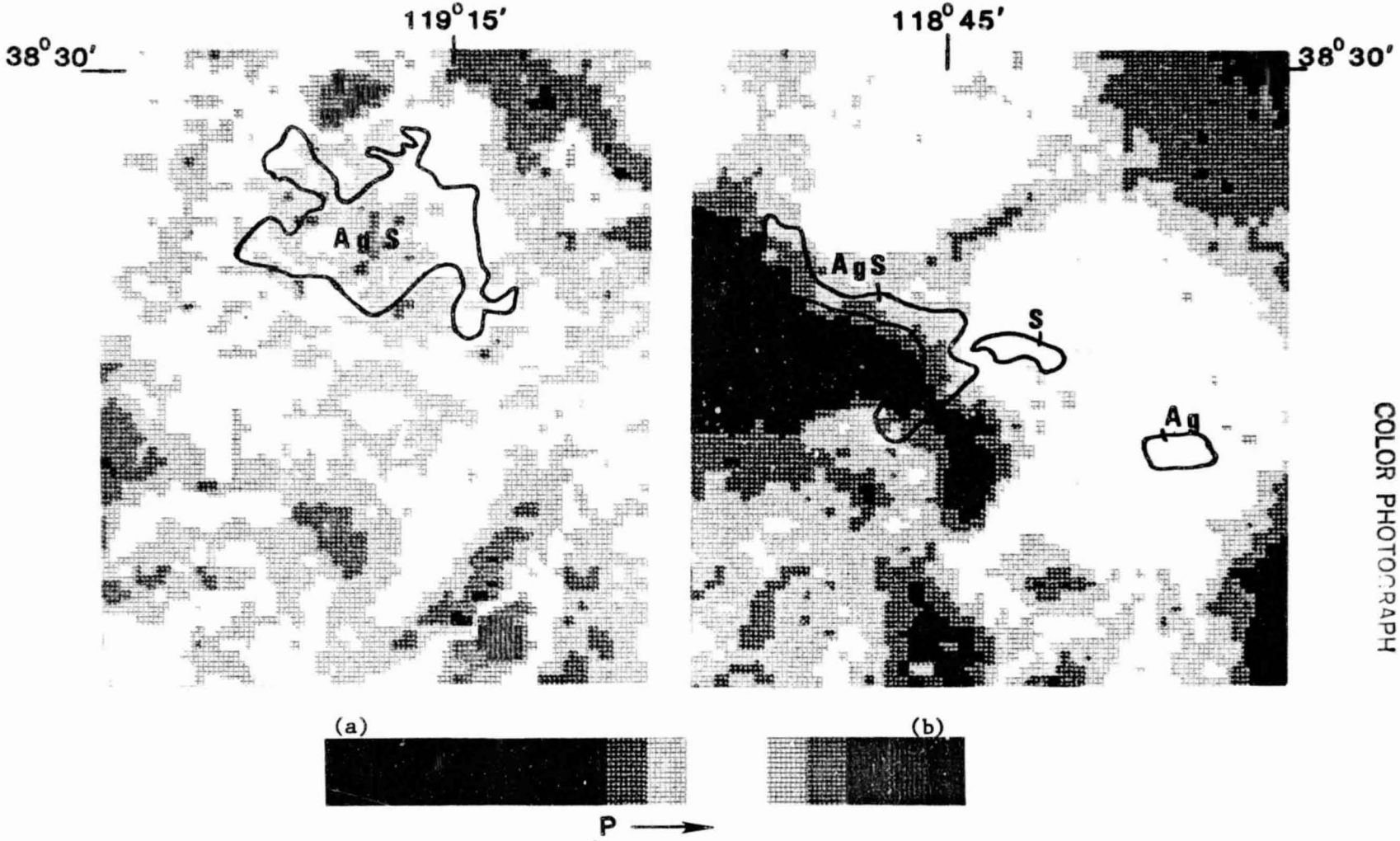

ORIGINAL PAGE
COLOR PHOTOGRAPH

Figure 36.--Thermal-inertia images of parts of the Sweetwater Mountains-Garfield Flat Alteration Belt. (a) is approximately 30 km to the west of (b). Symbols are the same as Figure 34. Scale 1:250,000.

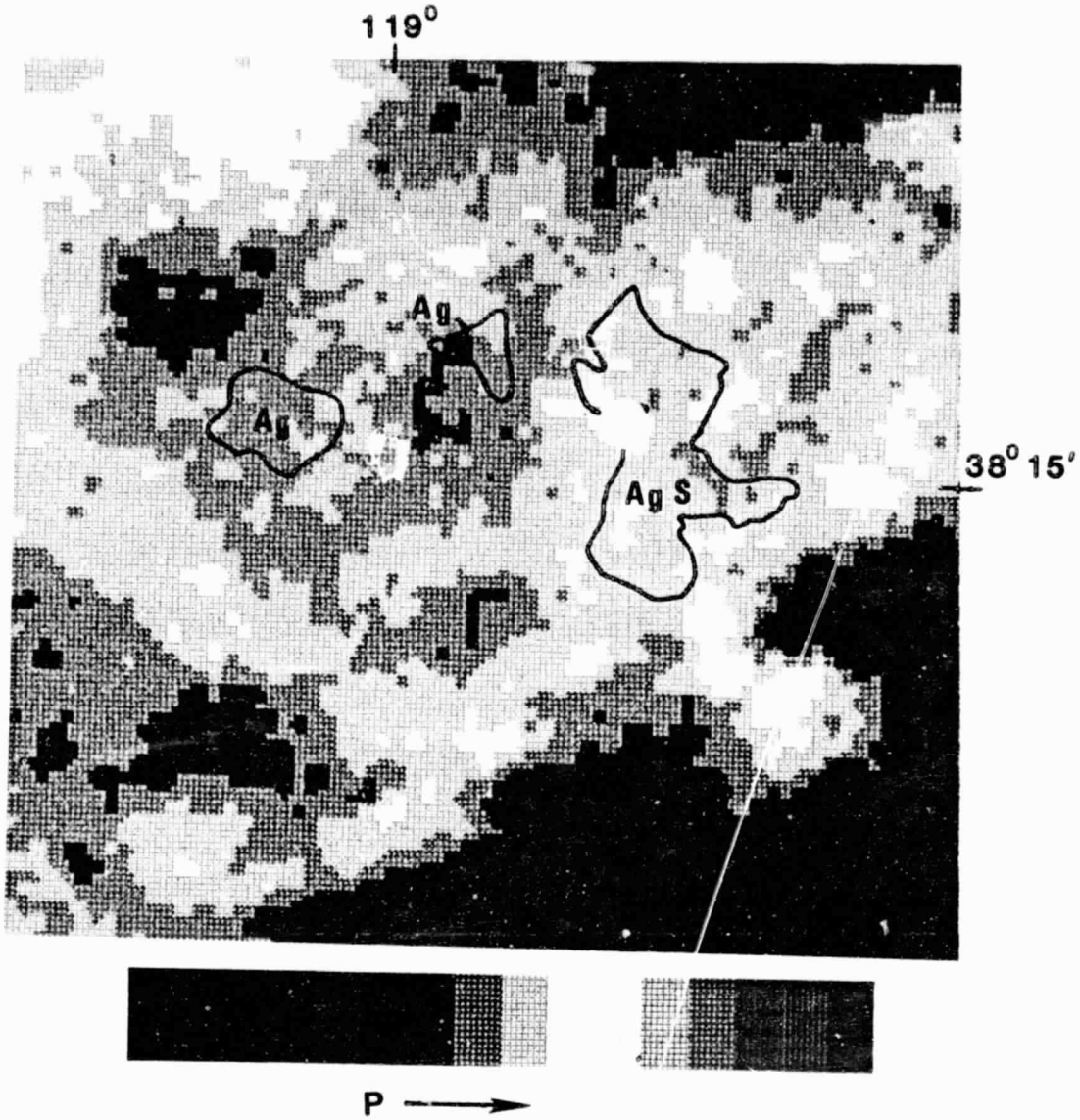

Figure 37.--Thermal-inertia image of the Aurora-Bodie Hills Alteration Belt. Symbols are the same as Figure 34. Scale 1:250,000.

3. No obvious correlation was found between the thermal inertia of altered areas and their surroundings, and no consistent thermal-inertia behavior was observed among the various types of alteration.

In these areas the altered siliceous rocks have undergone extensive cation leaching, generally producing a porous, fine-grained mass (T. L. Purdy and L. C. Rowan, written commun., 1983). We conclude that the increased thermal inertia that occurs due to silicification is offset by the reduced thermal inertia associated with the highly porous, low density altered rocks. Thus, no consistent pattern of either high or low thermal inertias can be expected. The competing effects can be illustrated with a numerical model.

Assume that the material surrounding an altered area has the thermal inertia of an "average" rock. The primary effect of silicification is to increase the thermal conductivity to a value of quartz, while the primary effect of leaching is to remove mass and thus reduce the density.

$$P = \sqrt{K.p.c}$$

Using differentials $dP = .5[\sqrt{K.c/p}\, dp + \sqrt{p.c/K}\, dK] = .5P(dp/p + dK/K)$

where P is thermal inertia, K is conductivity, c is specific heat capacity, and p is bulk density. Thus, little or no change in thermal inertia will occur if the proportional decrease in density roughly equals the proportional increase in conductivity. We can estimate the conductivity increase at about a factor of 2 using literature values (Roy and others, 1981) for quartzites versus igneous (volcanics, intrusives) and metasedimentary rocks, and, thus, we require that the density decreases by a roughly similar factor. A density decrease of this magnitude is not unlikely for rocks described as having undergone extensive cation leaching to form a porous mass. This result illustrates a restriction in the use and interpretation of thermal-inertia data. Where density variation effects are large they can significantly change

or even mask variations due to rock composition.

Density variations are also an important factor (the other being moisture content) in controlling the thermal inertias of unconsolidated materials. In the thermal-inertia image of the Walker Lake quadrangle (Figure 32), the lowest values are primarily in the area northeast of Mono Lake, and there and elsewhere in the quadrangle the lows coincide largely with Quaternary eolian deposits (Dohrenwend, 1982).

In general, we can detect fairly directly bedrock and linear features, and we can discriminate some surficial units on the thermal-inertia image of the Walker Lake quadrangle. The study has also indicated that within altered bedrock material the increased thermal inertia associated with silicification can be masked by reduced density induced by leaching. The result is highly variable, unpredictable patterns between altered and unaltered terranes.

2.5 ALLEGHENY PLATEAU and APPALACHIAN MOUNTAINS

2.5.1 Allegheny Plateau and Valley and Ridge provinces of north-central Pennsylvania

The Valley and Ridge province is characterized by moderately to intensely folded siltstones, sandstones, and limestones of Cambrian through Devonian age. At the surface, these rocks are cut by numerous faults, most of which strike parallel to the trend of bedding. A few faults are at an oblique angle or are normal to the strike of the beds. The Allegheny Plateau (Figure 1) province is characterized by gently folded siltstone and sandstones of Devonian through Pennsylvanian age. The plateau rocks are cut by occasional faults both parallel and oblique to the strike of the beds. The transition between the Valley and Ridge and the Allegheny Plateau provinces is characterized by gently tilted to intensely folded siltstones and sandstones of Devonian age that are unfaulted to highly faulted.

Two experiments were originally envisioned using the HCMM data (AA0153-07160-4,5,6,8 - September 26, 1978). The first, which met with limited success, was to identify zones of faulting in the Valley and Ridge. Although the individual folds are readily recognized on all the images, the individual faults or groups of faults are clearly too narrow to be resolved. Even faults with thousands of meters of displacement in the subsurface are seen at the surface as zones which are only a few meters to tens of meters wide. We had anticipated that a large contrast in moisture in these zones might produce a concomitant high thermal-inertia difference, which might be detected due to the contrast and the length of features. Unfortunately, a condition where the surrounding region was dry, with high moisture confined to fault zones, did not occur during the overpass.

Of greater success was the discrimination of lithologic units by the HCMM system. At least four different groups of lithologies can be easily (but not always uniquely) discriminated using the HCMM thermal-inertia data (Figure 38a).

The most conspicuous lithology portrayed is the Tuscarora Formation (T), (Figure 38b) which is predominantly composed of orthoquartzite. The unit is a conspicuous ridge-former throughout the Valley and Ridge province due to its high resistance to weathering. Where the Tuscarora Formation is weathered, it produces scree slopes composed of meter- to house-sized blocks that have much the same thermal properties as the unweathered formation. The thermal inertia of such an orthoquartzite ought to be quite high and, in fact, the outcrops of Tuscarora Formation are by far the brightest (highest thermal inertia) rocks in the imag The next most conspicuous lithologies are the combined Gatesburg Formation and Warrior Limestone (G) of Cambrian age, the Pocono Formation (Pc) of Mississippian age, and the Pottsville Group (Pv) of Pennsylvanian age. The Warrior and Gatesburg are limestones, the Pocono

Figure 38a.--Thermal-inertia image of the Allegheny Plateau and Valley and Ridge. The lithologies labeled are the combined Gatesburg Formation and Warrior Limestone (G) of Cambrian age, the Tuscarora Formation (T) of Silurian age, Devonian siltstones (S), Devonian, Mississippian, and Pennsylvanian sandstones and conglomerates (D), the Pocono Formation (Pc) of Mississippian age, and the Pottsville Group (Pv) of Pennsylvanian age.

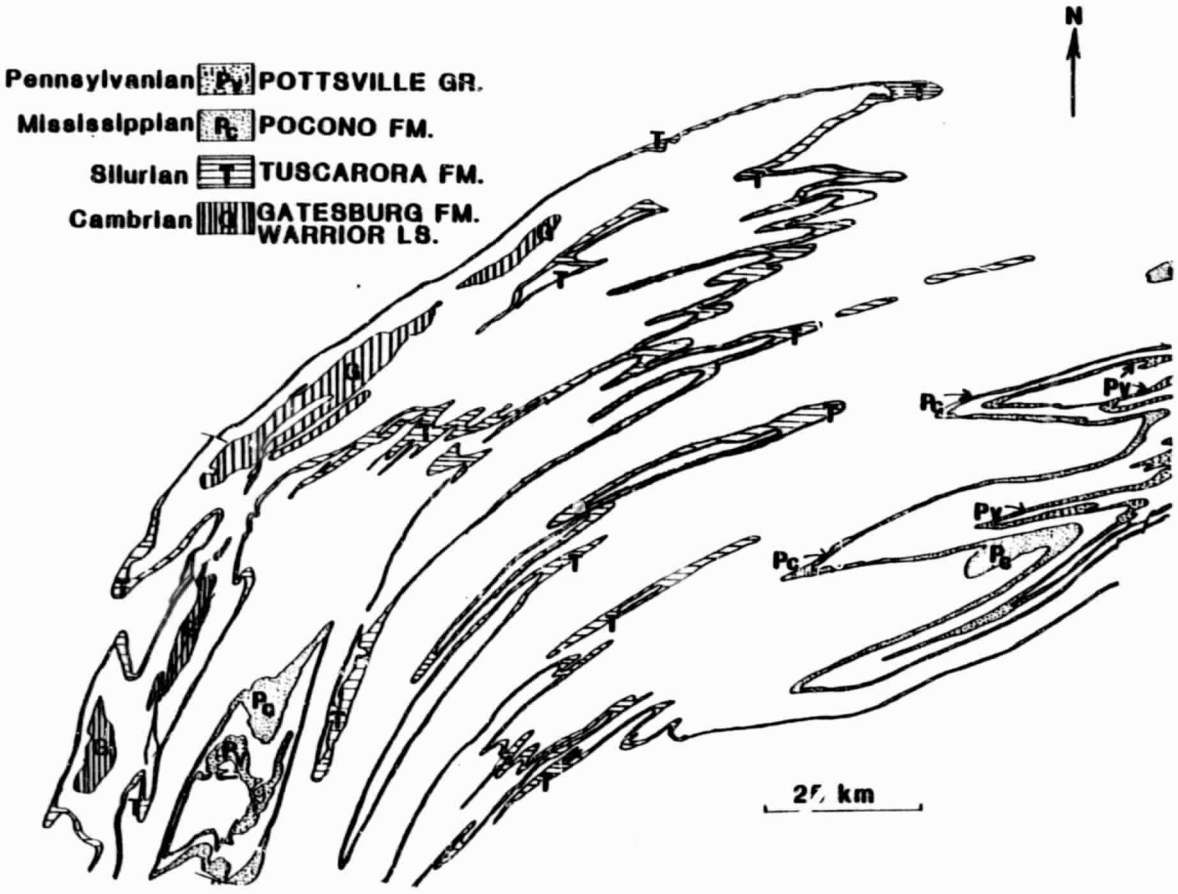

Figure 38b.--Geologic map of a portion of the Valley and Ridge province. Location of map is shown as box 1 in Figure 38a. Only the geologic units discussed in the text are shown.

Formation is sandstone, and the Pottsville Group varies from sandstone to conglomerate. All of the units have approximately the same apparent thermal inertia. This is not unreasonable considering that the sandstones and conglomerates are moderately well-cemented and might easily have similar thermal inertias similar to the limestones.

The fourth group of lithologies involves the Devonian, Mississippian, and Pennsylvanian sandstones and conglomerates (D) that cap the synclines in the Appalachian Plateau of central Pennsylvania (Figure 38c). These rocks are less bright in the thermal-inertia image than the previously mentioned units, but they are of higher thermal inertia than the Devonian siltstones (S) of the intervening anticlines that are conspicuous in the thermal-inertia image.

It is interesting to note that thermal-inertia values of all of the previously mentioned units have the same relative ranking as the literature-computed values (Miller and Watson, 1977).

We have conducted preliminary analyses and found that there is not a strong correlation between the nature of the tree canopies of the dominant vegetation types and various lithologic units. This conclusion supports the hypothesis developed in other geographic areas (see section 3.2) that vegetation type and extent does not seem to correlate with thermal inertia and, hence, thermal-inertia variations are not likely to be controlled by variations in vegetation.

2.5.2 Eastern Appalachian Mountains

The other part of this eastern test area encompasses the Appalachian Mountains in central Virginia and lies totally within the Piedmont and Coastal Plain geologic provinces. The Piedmont is a complex sequence of metamorphosed Paleozoic clastic and igneous rocks, and may be entirely allochthonous according to recent studies in the eastern Overthrust Belt. The Coastal Plain is a sequence of flat-lying, loosely consolidated Cenozoic clastic

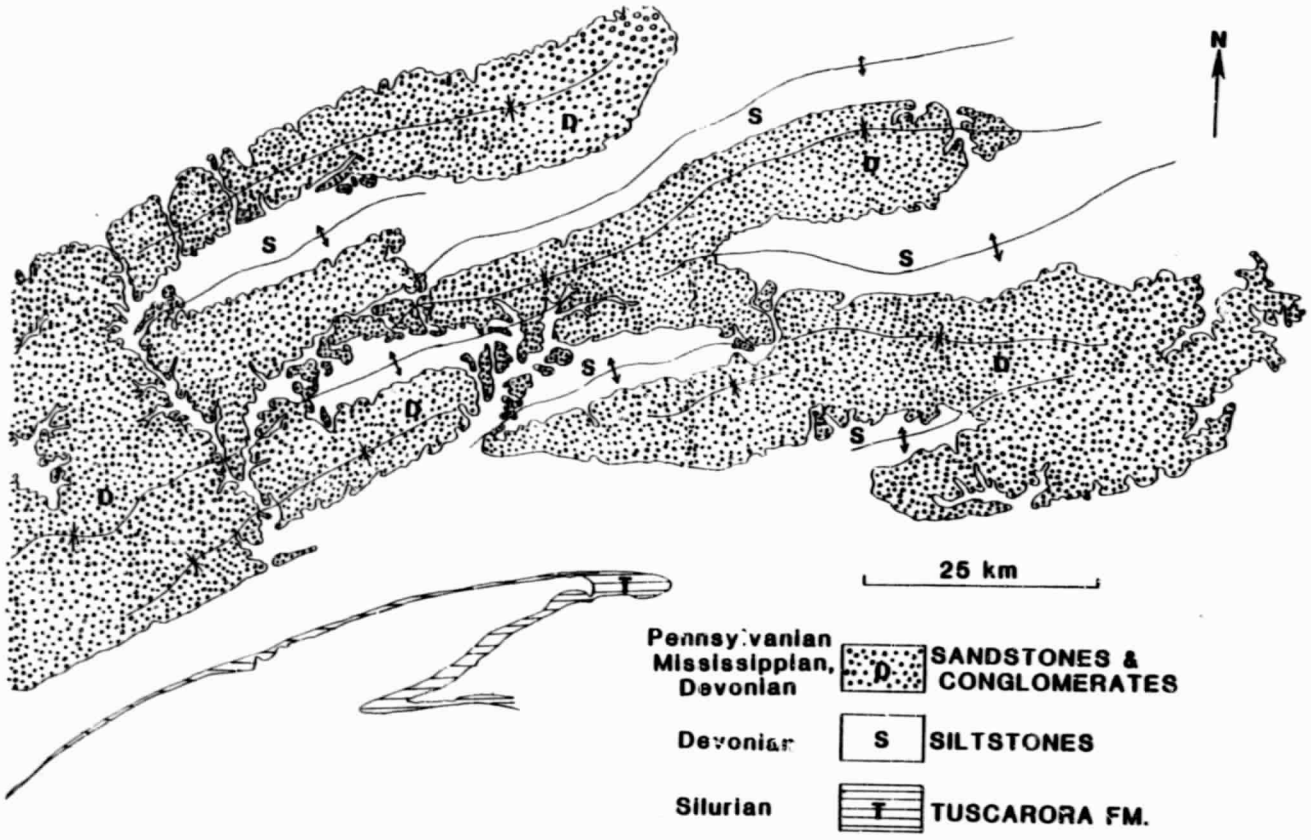

Figure 38c.--Geologic map of a portion of the Allegheny Plateau. Location of map is shown as box 2 in Figure 38a. Resistant sandstones and conglomerates crop out along the synclinal axes and siltstones crop out along the intervening anticlinal axes.

sediments. Interspersed in the Piedmont and buried beneath the Coastal Plain are several small rift basins associated with igneous intrusives formed during Triassic and Jurassic time. An east-west zone of seismicity and the discovery of several young reverse faults are evidence of recent tectonic activity in an area that is not well understood.

In conjunction with our HCMM study, other remote sensing studies in the eastern Appalachians have been conducted to observe geobotanical relationships of the forest canopy to structural and lithologic features in the Piedmont and Coastal Plain. Single band HCMM images were compared to existing remote sensing data sets to determine whether common or supplementary geobotanical features are being observed. Only two of the six available images were suitable for evaluation, primarily because of less cloud cover. The two images analyzed were a day/night pair from October 22/23, 1978 (AA0179-07050-3 and AA0180-18150-2). The discussion will be divided into two parts: (1) comparison of HCMM to SIR-A (Shuttle Imaging Radar) data in coastal areas of North Carolina, and (2) comparison of HCMM to enhanced Landsat Multispectral Scanner (MSS) data in the Virginia Piedmont.

In the coastal area, the HCMM daytime thermal image of October 23, 1978, (Figure 39a) seems to show good differentiation of wetland areas, particularly in the vicinity of Pamlico and Albemarle Sounds in North Carolina (location map, Figure 39b). The wetland areas appear darker, hence cooler, than the surrounding land masses, but not as dark as the ocean. The HCMM data show more extensive wetland areas than either SIR-A or MSS Band 7 Landsat images. As the SIR-A radar generally shows areas of standing water, the HCMM appears to be indicating some type of moist soil environment in between standing water and dry upland soil. Comparison of HCMM images to aerial photography does not show a direct correspondence to the vegetation canopy. The HCMM images appear to define areas of moist soil under both marsh and forest canopies in the area

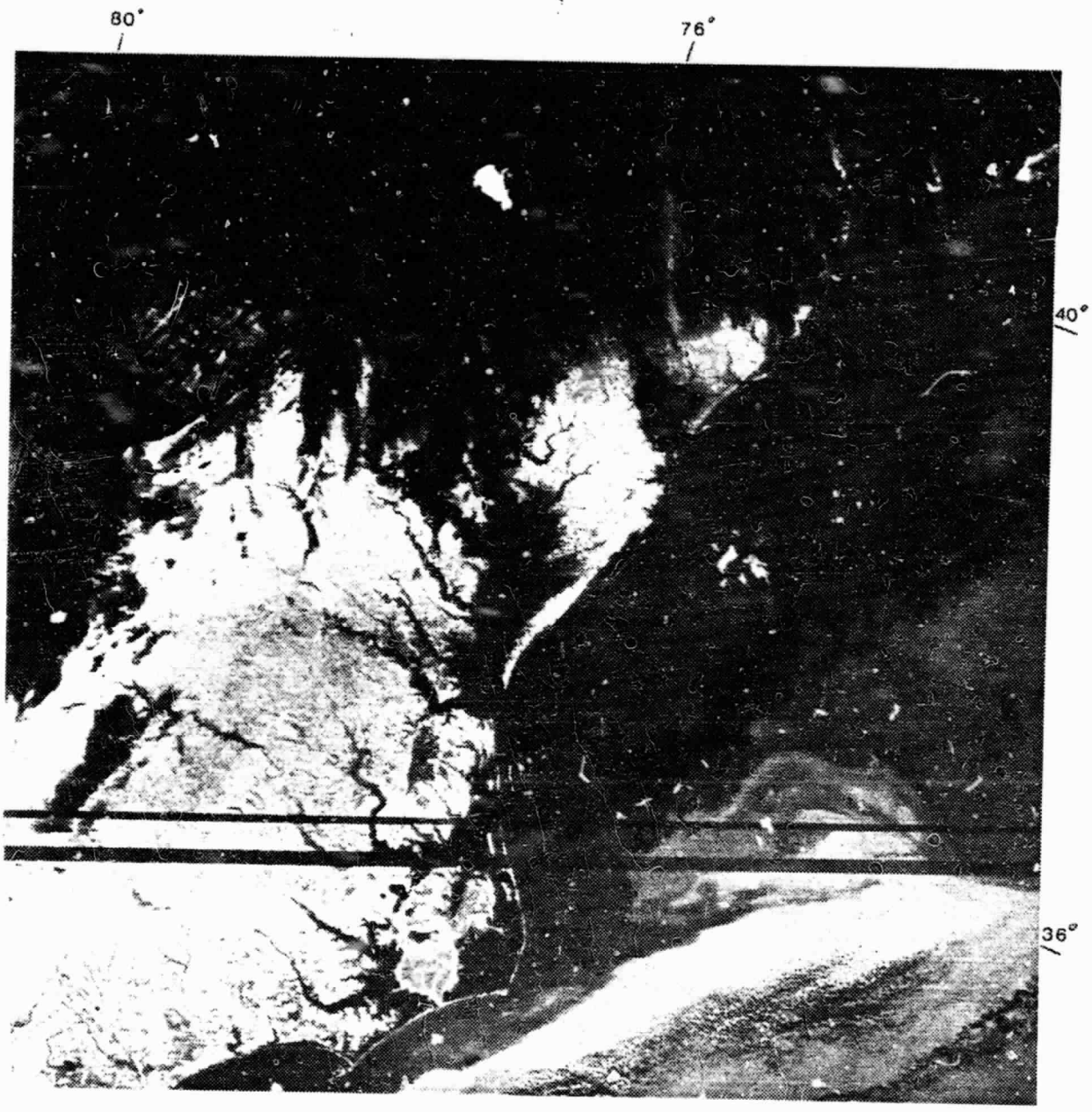

Figure 39a.--HCMM day thermal image of the Atlantic Coastal Plain. Clouds (dark) cover most of the northern portion of the scene. Scanline dropouts are seen in the southern portion. Scale 1:4,000,000.

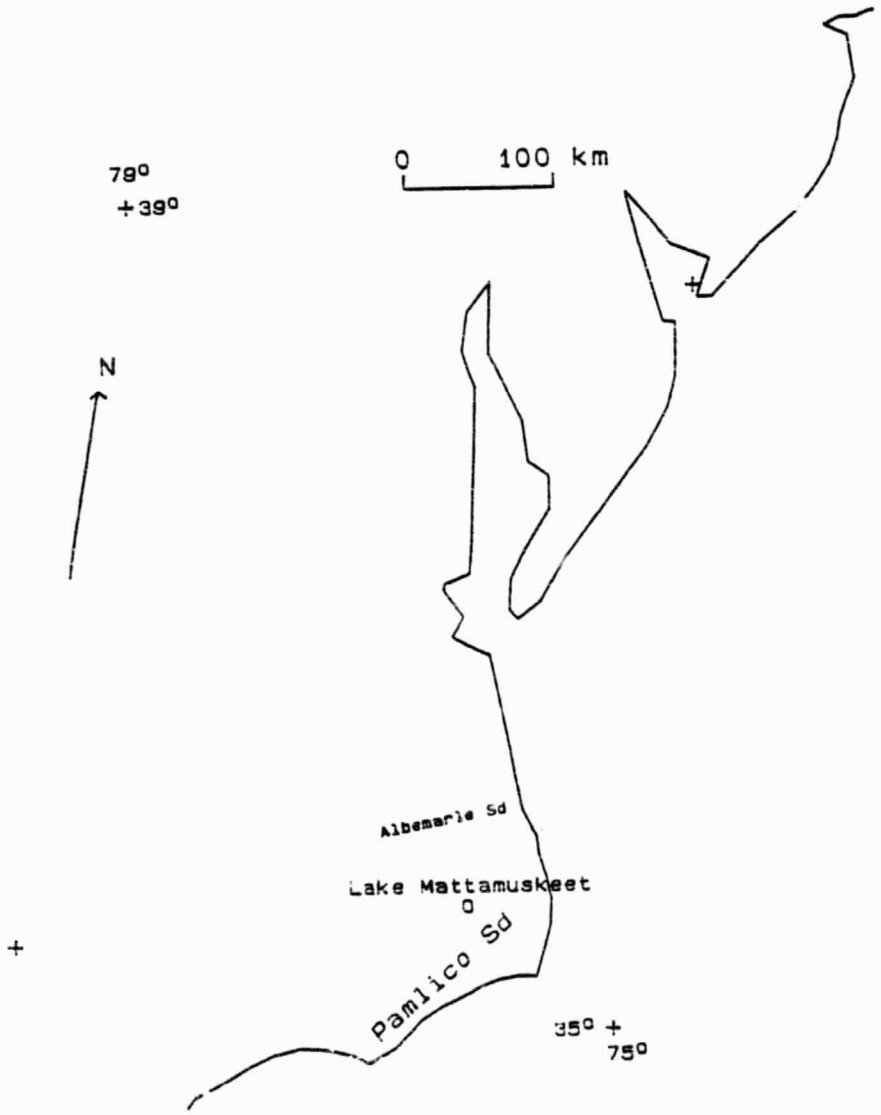

Figure 39b.--Location map of features in the Atlantic Coastal Plain described in the text.

around Lake Mattamuskeet, North Carolina, and show a close, but not an exact correspondence to the mapped distribution of Pocosin wetland areas (Richardson, 1981). The HCMM image appears to be a useful supplement to radar and Landsat images for vegetated wetland mapping, for it appears to be distinguishing a different physical phenomenon than the other two sensors.

The second part of our study was an examination of the Virginia Piedmont using the nighttime thermal image of October 22, 1978 (Figure 40a). This image is 90% cloud-free and shows the stream drainages as darker (cooler) and the mountainous areas as lighter (warmer). Stream drainages are well-defined in the Piedmont area, but only a few major drainages are distinguishable in the Coastal Plain. North of Lake Gaston, the divide between the Piedmont and the Coastal Plain drainages can be seen on the night image, trending N. 5° E. This approximates the Fall Line rather than the mapped lithologic contact (Figure 40a and 40b). The lithologic contact between Miocene and Paleozoic units is sinuous due to erosion of the Coastal Plain sedimentary cover. Recent outcrop evidence for a zone of reverse faults along the Fall Line (Mixon and Newell, 1982) supports it as the contact between the Coastal Plain and Piedmont.

The reason why Piedmont drainages appear better defined on the HCMM images than do the Coastal Plain drainages is not explainable at this time. The lowland vegetation along the stream banks is fairly similar between the Coastal Plain and Piedmont; the largest differences are between lowland and upland vegetation. Water temperature does not appear to be the reason since the inland lakes appear warmer than the surrounding land areas. Topography may be involved in the explanation as the Piedmont drainages are generally more incised than Coastal Plain drainages. The Meherrin River (Figure 40b), an east-west trending river in southern Virginia just north of the North Carolina border, is particularly well expressed on the image. The Meherrin

Figure 40a.--HCMM night thermal image of the eastern Appalachian Mountains and the Atlantic Coastal Plain. Scale 1:4,000,000.

Figure 40b.--Location map of features in the eastern Appalachian Mountains and Atlantic Coastal Plain described in the text. The Fall Line (straight line, dashed where approximate) and the sinuous contact between Tertiary sediments and Paleozoic rocks (King and Beikman, 1974) is also shown.

River is incised approximately 20 m below the level of surrounding Piedmont upland near Lawrenceville, Virginia.

Two lineaments are seen in the HCMM image that are not apparent in a Landsat MSS Band 7 mosaic (Trask and others, 1977). A prominent east-west lineament that cuts across the general trend of the Piedmont foliation is observed north of the connected Lake Gaston and John Kerr Reservoir. The northern boundary of the lineament is defined by the sharp boundary of the Meherrin River. The lineament appears to extend to the Blue Ridge to the west and almost to Albemarle Sound to the east, a distance of 300 km. The lineament is also expressed as a bending and truncation of highs in the horizontal-gradient gravity map of the United States (Simpson and others, 1982). The N.75°W.-trending lineament is subparallel to another lineament further north along the James River (Krohn and Phillips, 1982), which is apparent on enhanced Landsat images, onshore gravity maps, and offshore aeromagnetic maps.

A second HCMM lineament is parallel to the orientation of the Piedmont metamorphic foliation. The lineament originates at one of the projecting arms of Lake Anna, Virginia, continues south-southwest past one of the big bends of the James River near Arvonia, Virginia, and can be traced in segments at least as far south as the lineament just described. The lineament is expressed as an alignment of the generally dark stream drainages in the Piedmont and seems to correspond to a feature observed in the aeromagnetic map of Virginia called the Spotsylvania lineament (Pavlides, 1981). The HCMM counterpart to the Spotsylvania lineament does not appear north of Lake Anna, the area where the aeromagnetic Spotsylvania lineament was initially defined. The small scale and emphasis of the drainages of the HCMM images helps to enhance the lineament while only portions of it are observed on Landsat MSS band 7 mosaics.

This evaluation of thermal data in the eastern Appalachians shows that the HCMM images display some features also observed elsewhere in other remote sensing (spectral reflectance, radar) data sets, but, in addition, gives evidence for new, larger geologic features, only portions of which were observed previously.

3 GENERAL ANALYSIS

This section will examine some of those general aspects of our study that are not site specific. They cover: estimation of the heating flux terms used in the thermal model to map thermal inertias, examination of vegetation effects, development of a thermal-inertia model for igneous rocks, and a discussion of the registration of images. In all these aspects of the analysis we have adopted a "simplest is best" philosophy. In modelling the heating fluxes, we assume a simple time varying function, spatial invariance of the coefficients, and linear corrections for topography. A more detailed model, which might employ ground station data, field measurements, and complex analytical expressions, would be more accurate for a limited set of circumstances, but would run the risk of introducing unintended correlations that could bias our analysis of the thermal-inertia variations. For the registration of images and maps, we use a simple bilinear form, which has computational advantages. We have also found, in some cases, that the residuals have a parabolic variation along the scanline. In these cases the "simplest" solution is thus somewhat more complex.

3.1 REGIONAL FLUXES

Interpretation of thermal images as well as their use in thermal-inertia mapping is complicated by the various types of natural heating and cooling processes which influence surface temperature variations. Of necessity, the interpretation of thermal infrared data has been based on theoretical models that involve assumptions about these regional fluxes. The focus of our research has been to determine the simplest valid expressions for these processes and to develop techniques for estimating their magnitude based solely on remote sensing data.

For example, our method of estimating the effective regional atmospheric

parameters for thermal-inertia mapping (Watson and Hummer-Miller, 1981) assumes that the atmospheric fluxes are spatially--but not temporally--invariant and that the solar, sky, and sensible heat fluxes can be approximated by a simple mathematical form. Coefficients can then be determined from a least-squares method by fitting observational data to our thermal model. The technique permits analysis of data such as HCMM for which few or no meteorological data exist and examination of subareas to test the homogeneity of the effective regional atmospheric parameters. Additionally, the method is less susceptible to distortions produced by local meteorological anomalies that may influence a single ground-observation station.

Most recently, we have examined HCMM data, acquired over a period of 17 months, which included a variety of geologic sites in the western United States. In addition to our study of the geologic expression discussed elsewhere in this report (section 2.4.2), large statistical samples of temperature (day/night) and reflectance data were obtained to estimate the fluxes that heat the ground on a regional scale. Trends could thus be examined for developing more detailed thermal models and identifying anomalous meteorological conditions, so that appropriate care is exercised in the interpretation of thermal-inertia images.

Temporal variations in the incident solar flux due to changing atmospheric conditions can be examined by monitoring the reflectance statistics of the same area at different times. A simple model can be developed by assuming that the surface albedo and the satellite detector response are invariant, that the reflectance function is governed by Lambert's Law, and that the atmospheric backscattering is negligible. In this case, the reflectance (R) is given by

$$R=A\cdot Tau(z)\cdot COS(z)$$

where Tau(z) is the atmospheric transmission at zenith angle z, and COS(z)=COS(Lat)•COS(Dec)•COS(wt)+SIN(Lat)•SIN(Dec), where Lat is the site latitude, Dec is the solar declination, and wt is the product of diurnal frequency and solar time.

This model was applied to reflectance data acquired at 12 different solar declinations from May 1978 to September 1979 in two adjacent areas located in Nevada between Lake Tahoe and Walker Lake. The statistics for each area are based on 33,000 pixels. Area 1 covers part of the Sierra Nevada Range and part of the Basin and Range Province and has a significant vegetation component; area 2 is east of area 1 and falls entirely within the Basin and Range Province. The mean, deviation, and modal values for the two areas are plotted versus the zenith angle in Figure 41. The dashed line shows the simple theoretical form used in our thermal modelling studies. The general fit seems quite good and most of the mean values are within one or two Dn of the theoretical curve. Two mean values are several Dn above the curve and are indicated on the figure by month and year. All values are for 1978 data unless indicated otherwise.

A further illustration of the method to examine variation of the heating fluxes was made by examining day/night pairs of data. We can estimate variations in the regional fluxes by modelling the heating flux as a half wave of specified amplitude (A) and offset (B) (Watson, 1982a), compute the values of A and B by employing our thermal model algorithm based on a Laplace transform solution (Watson, 1982b), and match the observed temperatures. A and B values for various sites were plotted versus latitude and solar declinations in Figure 42. In general, the offset or constant parameter B remains fairly invariant with both latitude and solar declination, but the amplitude term, A, varies considerably, reflecting anomalous transient

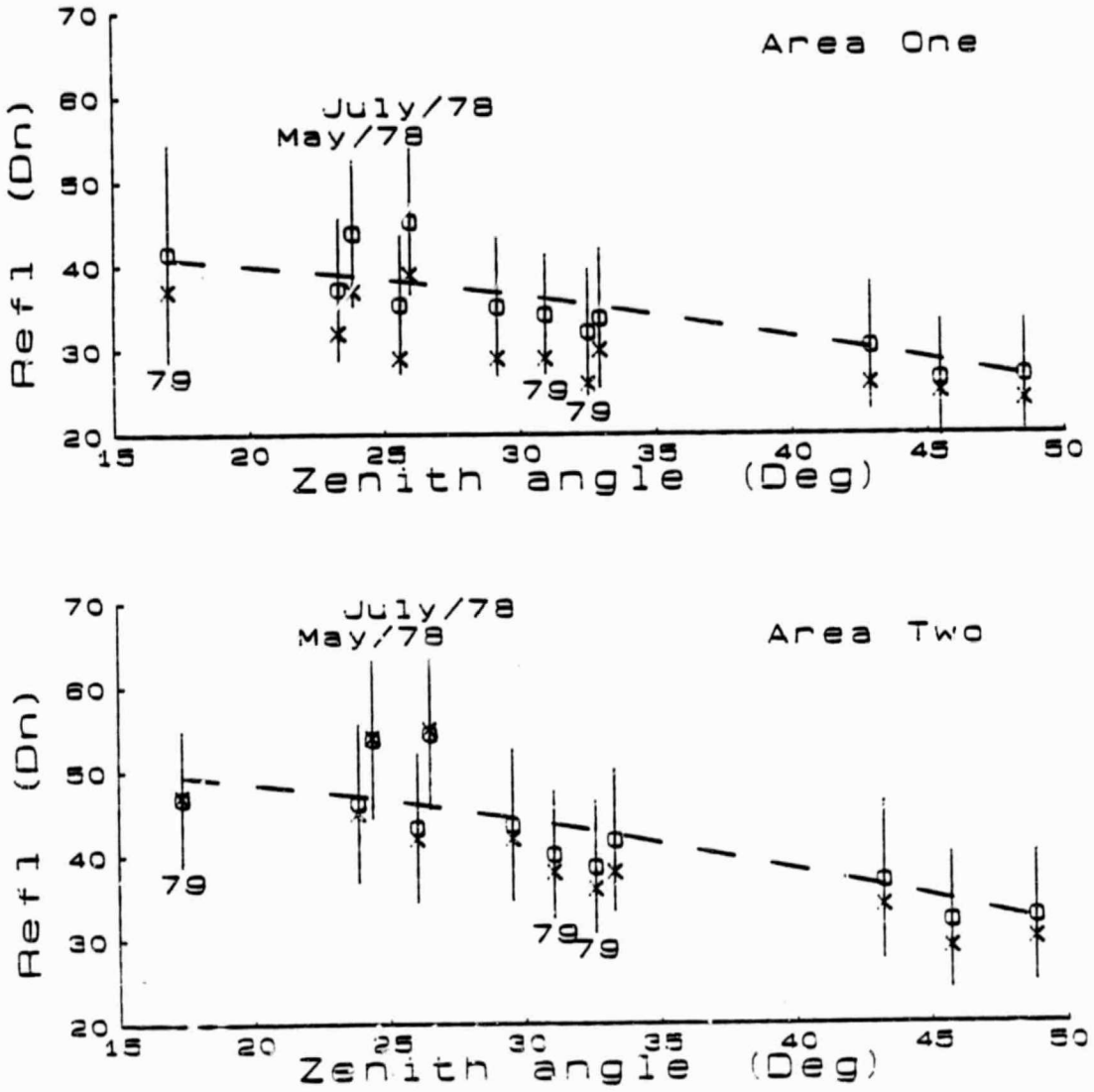

Figure 41.--Reflectivity versus zenith angle (z) using 12 solar declinations. Mean values are indicated by o, modes by x, and deviations by vertical lines. Two slightly anomalous values are indicated by month and year. All values are in 1978 unless indicated otherwise. The dashed line is for Tau = $1 - .2\sqrt{\text{Sec } z}$. See text for description of the two areas.

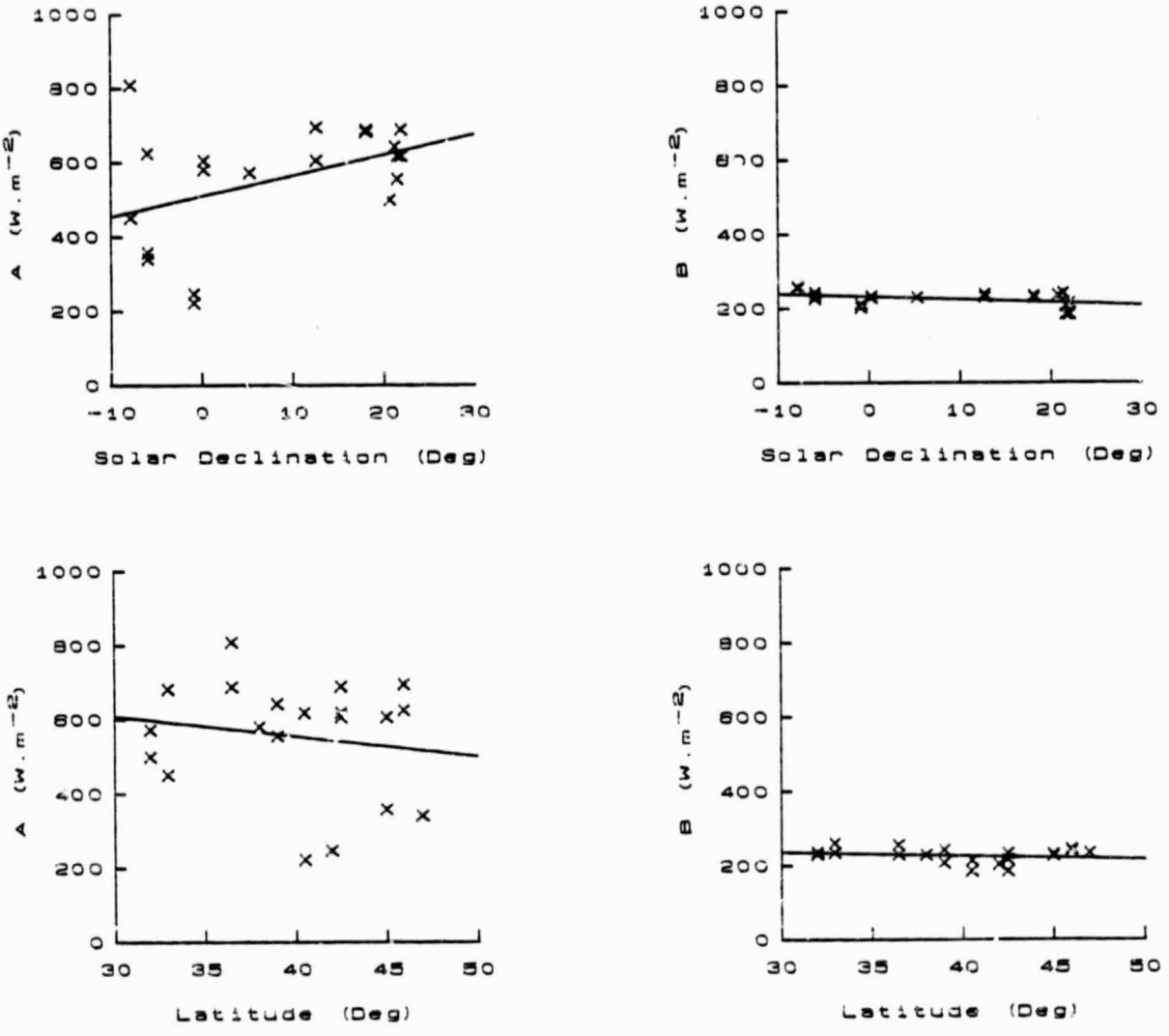

Figure 42.--Meteorological flux parameters A and B are plotted as functions of solar declination and latitude for several sites in western United States. The flux is approximated by a half wave of amplitude A and offset B. The lines shown are least-squares fits.

conditions superimposed on a general trend. As with the reflectance analysis, the method assumes that the thermal properties of a site and the detector responses are invariant. Although anomalous conditions can be identified by this method, their causes are often complex and difficult to diagnose. Rainfall will substantially affect the thermal properties of the surface as well as introduce an additional heat loss term due to evaporation. Windy conditions will appreciably increase the sensible heat flux term and produce a spatial variability within the site depending on such factors as the vegetation canopy and the terrain topography.

As part of our modelling studies, we investigated a technique for correcting thermal-inertia data for topographic effects. To perform this we assumed a simple linear relationship between temperature and topographic slope components and elevation. We determined the coefficients by using a least-squares fit. The method was evaluated using the registered HCMM and digital terrain data for the Richfield, Utah, quadrangle. For these data we found that the elevation term for the day data roughly matches the theoretical adiabatic lapse rate. The night scene indicated that the slope effects were negligible and the elevation term was quite low. We also determined that the topographic effects were only observable above 1.83 km, so the topographic correction was only applied above this elevation. The resulting correction to the day-night temperature difference is:

$$DT_{corr} = DT_{obs} + 7.2\ (E - 1.83) + 9.8\ d \cos q + 1.99\ d \sin q$$

where DT_{obs} is the observed temperature difference, E is the elevation in kilometers, d is the dip in radians, and q is the azimuth angle. This "simple" linear correction to our thermal-inertia image has the advantage that, although it cannot prevent some influence of geology on the correction

(higher thermal-inertia materials will often be exposed at the highest elevations), it does average out most geologic variations, agrees with the expected adiabatic lapse rate, and mutes some of the more obvious topographic effects that mask thermal-inertia variations. This is also a necessary first step in analyzing the effects of vegetation.

3.2 VEGETATION STUDY

In our past HCMM studies, we have been concerned with the possible effects of vegetation masking the thermal inertia of the underlying material. In this study, our concern arose following a visual comparison of a the thermal-inertia image with a topographic map of Richfield, Utah, quadrangle. The green areas of the topographic map, indicating vegetation (trees-brushwood), appear to have a high coincidence with areas of high thermal inertia. For this particular site most of the vegetation cover occurs at high elevations where resistant rocks having high thermal inertias are exposed. Thus, we need to address the effect on our thermal-inertia images of vegetation cover.

A previous study by Siegal and Goetz (1977) found that vegetation can significantly affect the observed spectral reflectance of rocks. They observed that low albedo materials were the most strongly affected and could be completely unrecognizable with only 10% vegetation cover. Dry or dead vegetation, however, did not greatly affect the spectral reflectance but rather changed only the albedo.

We decided to investigate the possible effects of vegetation on the observed thermal inertia using a variety of data sets of the Richfield quadrangle. This site has an arid climate, and the vegetation ranges from sparse in the western lowlands to more dense in the eastern, higher elevation areas. Typically in lowlands, which are not cultivated or irrigated, the

vegetation consists primarily of several species of rabbitbrush, sagebrush, and scattered grasses. Some salt desert shrubs are in the more alkaline soils in the lowlands. The uplands and flanks of the hills (higher than 1830 m) support stands of pinyon pine and Utah juniper, with ponderosa pine and mountain mahogany occurring at higher elevations where rainfall is greater. Gambel oak, bigtooth maple, and quaking aspen are predominately found at high elevations.

The data used in this vegetation study is of a unique set of co-registered data. The following products were all registered to a topographic base: HCMM reflectance, HCMM day and night thermal, the four Landsat bands, and digital elevation data. These data were used to form a topographically-corrected thermal-inertia image, a Landsat "albedo" image (a combination of the four bands), and a vegetation index image.

The Landsat data were acquired on June 22, 1974 (Figure 43). Since the HCMM data of Richfield were acquired four years later during a different growing season, the validity of using such a data set had to be tested. We constructed a Landsat "albedo" image using a weighted sum of the four bands and cross-plotted this value against the HCMM reflectance (Figure 44). The correlation coefficient of 0.83 (for 58,512 samples) between the two data sets is a measure of (1) the registration accuracy, (2) the adequacy of the albedo model, and (3) the general similarity of the vegetation state of the two images. Seasonal differences between the two images do not appear to be highly significant. We also examined the effects of illumination differences on the correlation by topographically correcting both HCMM reflectance and Landsat bands. The correlation coefficient increased by less than one percent, indicating that illumination effects were not significant in the vegetated areas and that a topographic correction was not necessary.

C-2

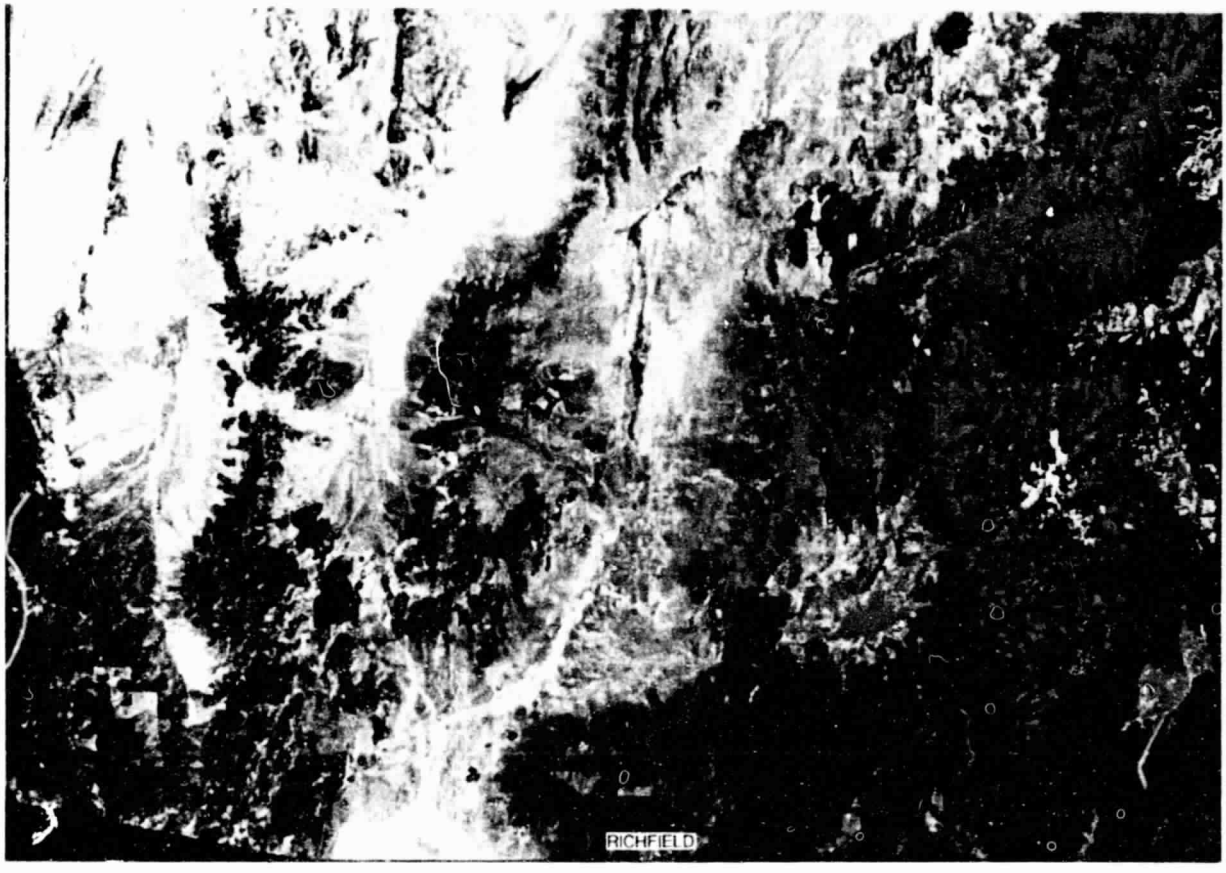

Figure 43.--Landsat color infrared image of the Richfield 2^{o} quadrangle (Utah). The corners of the photograph are approximately the quadrangle boundaries. See Figure 16a for the location map.

ORIGINAL PAGE
COLOR PHOTOGRAPH

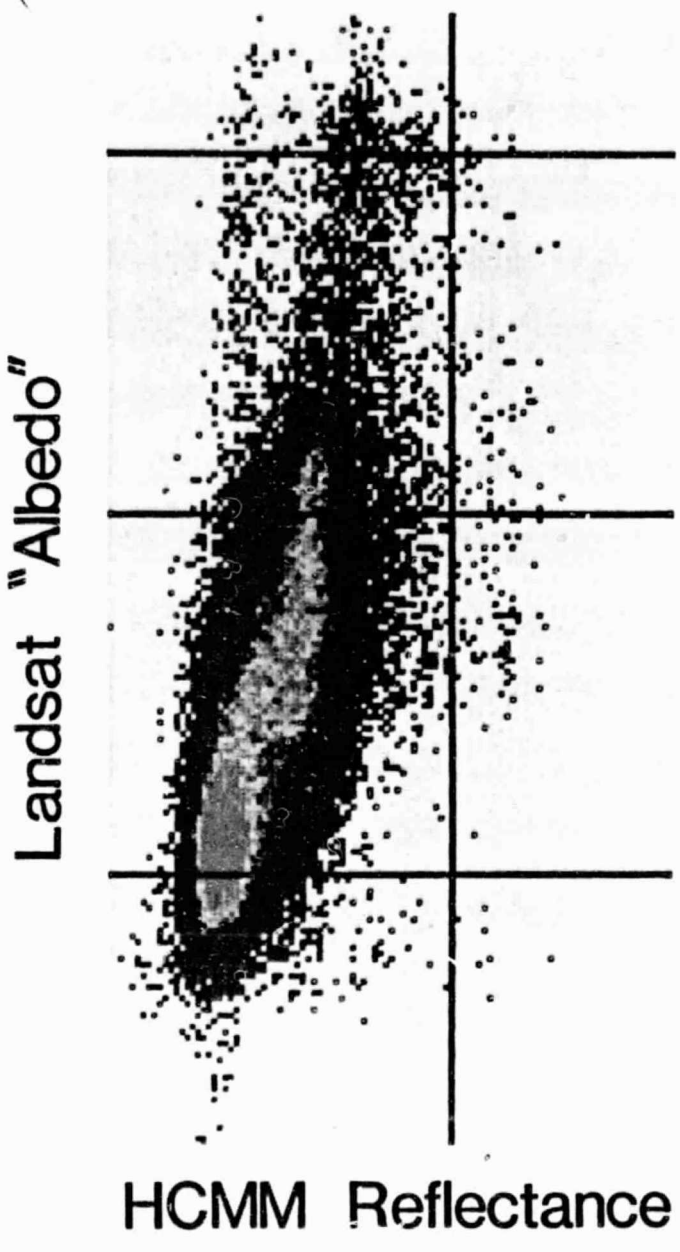

Figure 44.--Landsat "albedo" versus reflectance (HCMM) of Richfield 2° quadrangle (Utah). The "albedo" is computed from a weighted sum of the individual Landsat bands (see text). The black grid is drawn with a spacing of 64 Dn's. The colors represent varying densities of pixel values, red representing the highest densities and blue low densities. This scheme is employed for figures 44 - 47.

The vegetation index used in this study was formed as a ratio of the difference between the infrared and red Landsat bands to their sums (MSS7 - MSS5)/(MSS7 + MSS5). The ratio was first developed by Rouse and others, 1973; 1974) using Landsat MSS data, and was shown to be "sensitive primarily to the green leaf area or green leaf biomass", and "can be employed to monitor the photosynthetically active biomass of plant canopies" (Tucker, 1979).

A plot of the vegetation index with the thermal inertia showed no apparent trend and a correlation coefficient of only 0.08 (Figure 45). Even though this coefficient is low, it does not preclude a weak correlation. To evaluate the significance of the correlation coefficient and to test our assumption that the Landsat image reflected the state of the vegetation at the time of the HCMM data acquisition, we extended our study. A plot of reflectance versus vegetation index (Figure 46a) was made. This graph shows two populations with separate reflectivity groupings and an overlapping range in vegetation index. These two data sets were cross-plotted for various elevations and it was determined that the two distributions occur at different elevations (Figure 46 b,c) One population occurs below roughly 2000 m, where the vegetation is primarily rabbitbrush, sagebrush, scattered grasses, and isolated, irrigated crops and is associated with low thermal inertia. The other population occurs above 2000 m, where the vegetation consists of coniferous and deciduous forests and the thermal-inertia values are high and vary over a large range (Figure 47).

Having established that the vegetation separates into two classes, we examined each class individually. Two local areas (about 25 km^2 each) at elevations below 2000 m were chosen to test the correlation for irrigated sites, where the correlation should be high. One of the sites was in Beaver Valley and the other near Upton Siding. The resulting correlation

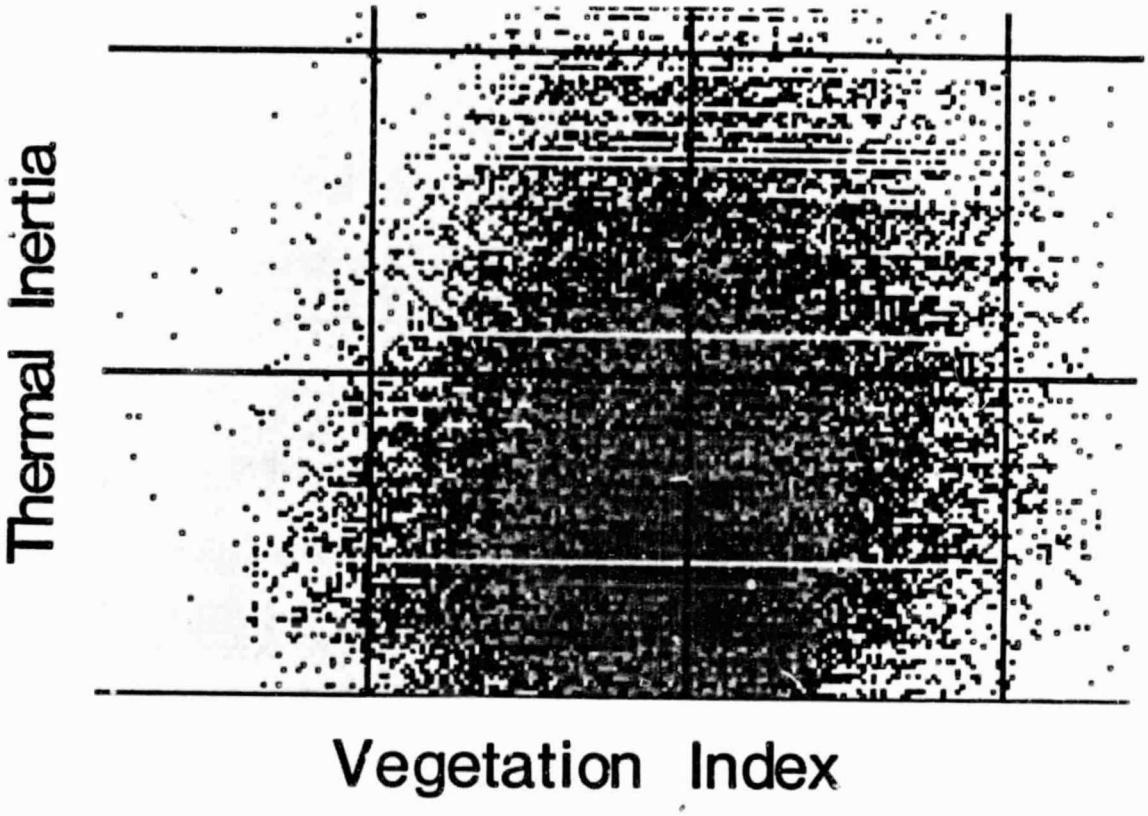

Figure 45.--Thermal inertia (HCMM) versus vegetation index (Landsat) of the Richfield 2^{o} quadrangle (Utah). A correlation coefficient of only 0.08 was observed for this set of over 60,000 points.

ORIGINAL PAGE
COLOR PHOTOGRAPH

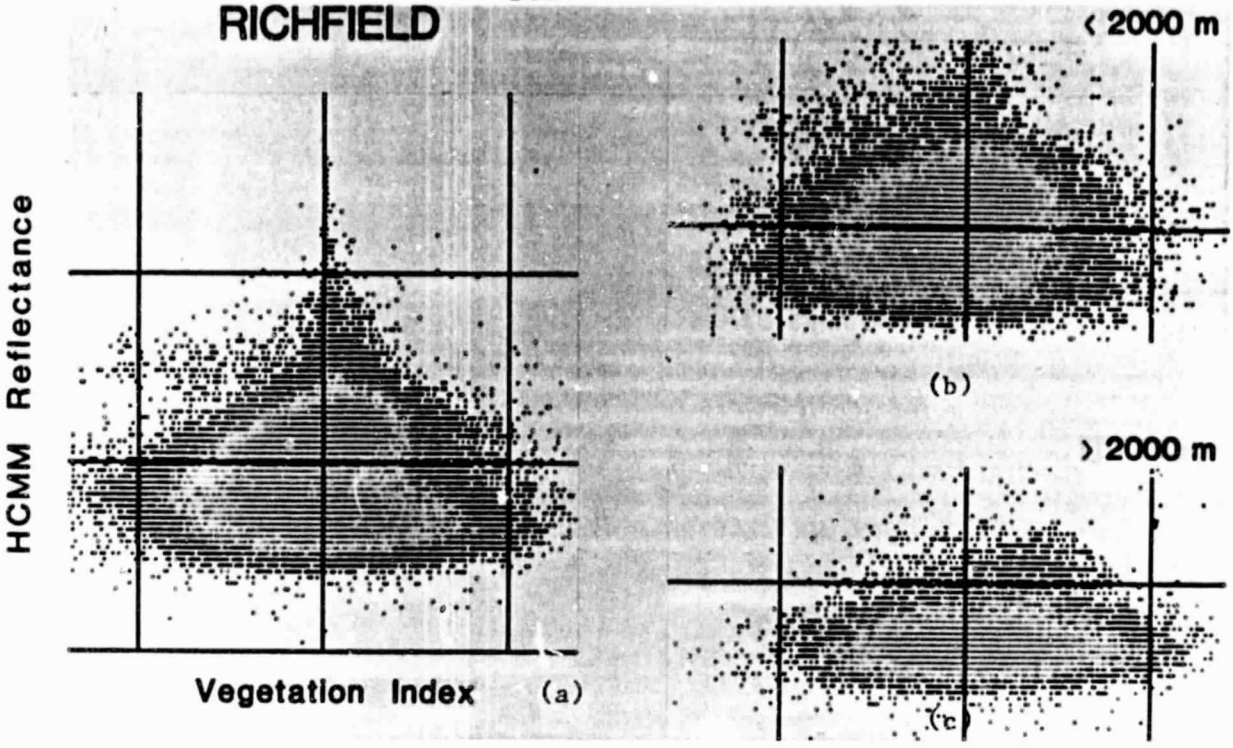

Figure 46.-- Reflectance (HCMM) versus vegetation index (Landsat) of Richfield 2° quadrangle (Utah). (a) entire data set, (b) elevations < 2000 m, (c) elevations >2000 m. Two clusters can be seen in (a), separating at 2000 m, which corresponds roughly to the lowest limit of the trees.

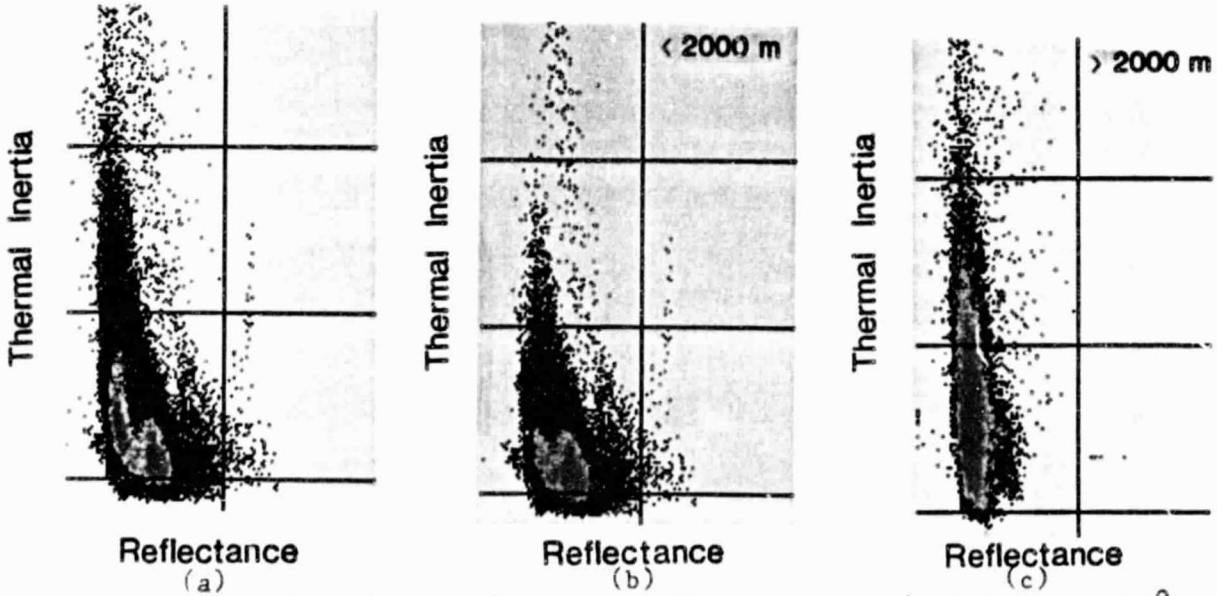

Figure 47.--Thermal inertia (HCMM) versus reflectance (HCMM) of Richfield 2° quadrangle (Utah). (a) entire data set, (b) elevations < 2000 m, (c) elevations > 2000 m. Two clusters can be seen (as in Figure 46) separating at 2000 m. The tree covered areas above 2000 m appear red on the Landsat color infrared composite (see Figure 43), are tightly clustered in reflectivity (HCMM), and display a large variation in thermal inertia (HCMM).

coefficients of 0.33 and 0.40 indicate a detectably higher correlation between thermal inertia and vegetation--most probably due to the irrigation. In general, higher moisture content is expected to increase both thermal inertia and vegetation index and, thus, produce a detectable correlation.

Two other areas at elevations above 2000 m, which also appeared irrigated on the June Landsat image, showed a low correlation with the September thermal-inertia image: 0.08 and 0.09 for 100 samples. We suspect, based on common practice in these areas at higher elevations, that they were not being irrigated by late September, the time of the HCMM data acquisition, and thus no correlation would result. We also examined other vegetation covered areas in non-cultivated areas of similar size at higher elevation. They showed a very low correlation coefficient, 0.04, again providing supporting evidence for our hypothesis that vegetation does not correlate with thermal inertia when irrigation is not a controlling factor. This has important implications regarding the detection of thermal-inertia differences in vegetated terrain and the effect of vegetation on the observed thermal-inertia variation of geologic materials. We still cannot pick out an effect of vegetation indeed it must play a role in modifying the heat fluxes, but the effect must be much more uniform than we had previously expected.

3.3 THERMAL-INERTIA VARIATION OF IGNEOUS ROCKS

We have observed that the thermal inertias of igneous rocks in both Cabeza Prieta, Arizona (Watson and others, 1981) and Richfield, Utah, (this study) exhibit variations which, although having considerable overlap, nevertheless follow a consistent pattern. The granites have the highest thermal inertias, basalts are intermediate, and rhyolites, andesites and quartz latites have the lowest thermal inertias. A study of the thermal inertias of igneous rocks, computed from literature thermal property values,

generally shows no discernable trend (Watson, 1981), in part due to the incompleteness of the data sets needed to compute the values. To compute thermal inertia it is necessary to have thermal conductivity and either thermal diffusivity or density and specific heat capacity. Because there does not seem to be any significant or recognizable variation of heat capacity with igneous rock type, thermal-inertia values can be approximated using thermal conductivity and density values. In most cases in the literature, however, only thermal conductivity values are provided, and estimates of thermal inertia using assumed density values can lead to errors which are comparable to the variations that we have observed in the satellite data.

A simple estimate of the type of thermal-inertia variation to be expected among igneous rocks can be provided by considering the thermal inertias of quartz, olivine, and fused silica glass (Figure 48). For comparison the thermal inertias of a granite, a basalt, a gabbro, and a rhyolite are plotted; they exhibit somewhat similar characteristics. This suggests that the thermal inertias of igneous rocks can be characterized, to a large degree, by three variables: quartz, mafic minerals, and glass content. Felsic intrusives, being high in quartz, would have the highest thermal inertias, mafic rocks would have intermediate values, and felsic extrusive rocks the lowest values. This model is useful for predicting the thermal inertias of the end member rock types and is in agreement with the satellite observations. For rocks of intermediate composition, we can use empirical models of thermal conductivity and density to estimate the shape of the thermal-inertia variation. A linear fit of thermal conductivity versus quartz content based on 100 samples of granites and quartz monzonites (Roy and others, 1981) was combined with a correlation fit of density versus a felsic-mafic index (Young and Olhoeft, 1976). The thermal inertia was then determined assuming a

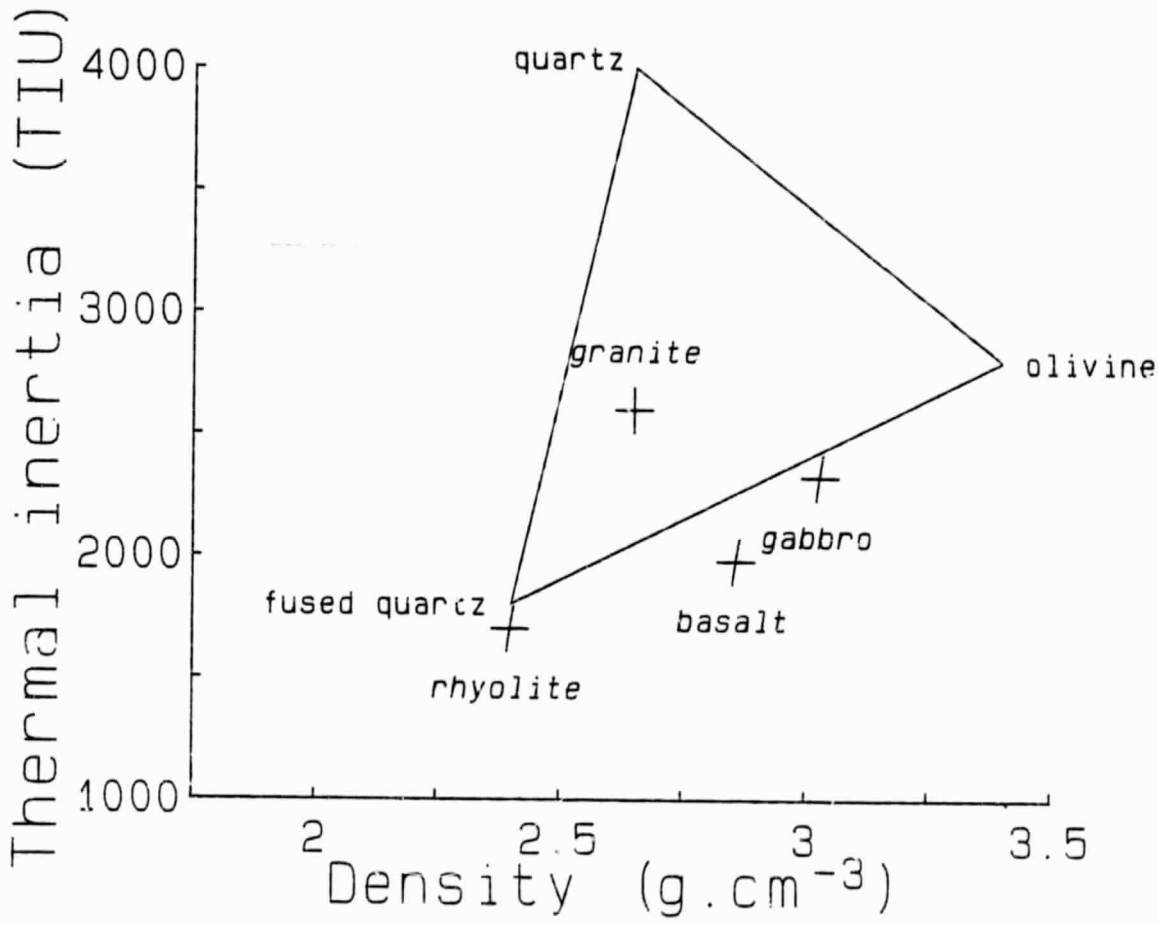

Figure 48.--Thermal-inertia and density values. Quartz, fused quartz, and olivine are shown at the vertices of a triangle. Selected igneous rock types are shown with crosses.

constant specific heat capacity, and the results were plotted (Figure 49) assuming a proportional relationship between the felsic-mafic index and quartz content. The curve indicates that a minimum is likely to occur at an intermediate composition, its exact position being somewhat dependent on the relationship between the felsic-mafic index and quartz content. This variation then is the behavior we would predict for intermediate composition intrusive rocks, and we might expect a somewhat similar behavior for extrusive rocks. This latter behavior will be complicated, however, not only by the presence of glass, which has a lower thermal conductivity than quartz, but also by the effects of higher (and variable) porosities, which will reduce the thermal inertia, and by devitrification (crystallization of the glass), which will increase the thermal inertia.

Glasses result from extreme undercooling and high viscosities of magmas. Because magmas that are rich in silica and alkalies tend to be more viscous than those poor in silica and rich in lime and iron, the glass content is generally much higher in felsic than mafic lavas (Williams and others, 1954). As glasses have a thermal inertia much lower than quartz, the thermal inertias of felsic rocks, such as rhyolites, dacites, and trachytes, would be expected to be lower than those of granites, and the thermal-inertia differences between extrusive and intrusive rock types should diminish for more mafic rocks due to both lower quartz and glass content. Because glass is "metastable", however, and tends to crystallize or devitrify, the glass content of extrusive rocks will diminish with increasing geologic age and cause the thermal inertia to rise. The age factor is illustrated by the observation that ancient glasses are very rare, particles of volcanic glass are rarely found in pre-Tertiary rocks, and no ancient glasses have been found of pre-Carboniferous age (Williams and others, 1954; Tyrrell, 1929).

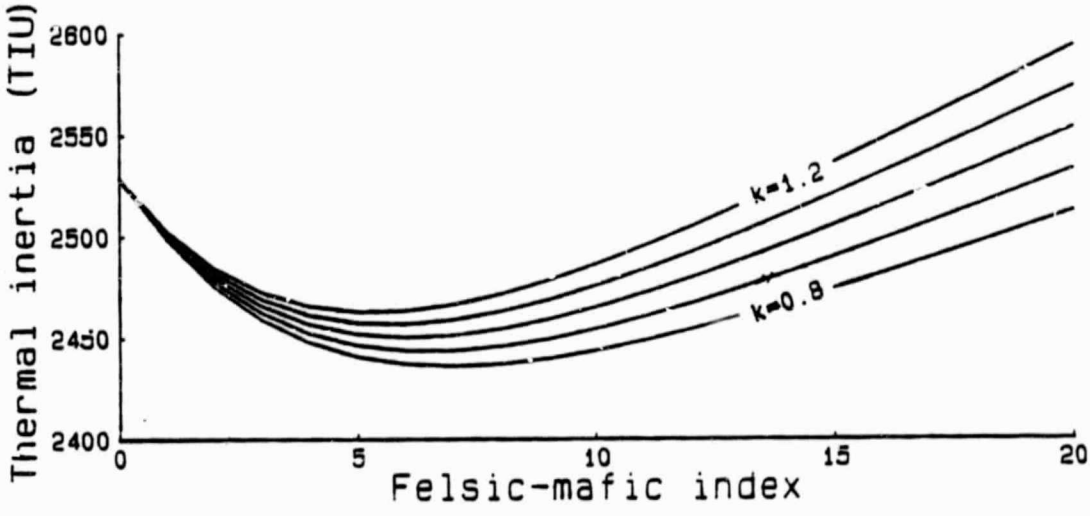

Figure 49.--Empirical thermal inertia versus a felsic-mafic index. The empirical value is computed by assuming a constant specific heat capacity, a model of density versus felsic-mafic index (Young and Olhoeft, 1976), and a model of conductivity versus quartz content. The quartz content is assumed to be proportional to the felsic-mafic index with a proportionality constant, k. Results are plotted for various values of k. A thermal-inertia minimum is predicted for intermediate compositions.

An illustration of the proposed model of the thermal-inertia behavior of igneous rocks is shown in Figure 50.

3.4 REGISTRATION

One of the major tasks in processing HCMM data is to co-register images acquired at different times. Thermal images, however, have some unique characteristics which make this registration process more complex than registration of standard photographs and Landsat images. The diurnal surface temperature variations, which depend primarily on topography (slope, elevation) and thermal inertia and secondarily on a variety of effects including vegetation and emissivity, make day images appear substantially different than the night images. Texture and topography often are portrayed in an entirely different manner on thermal images acquired at different solar times (Sabins, 1969; Rowan and others, 1970; Offield, 1975), and features that might be easily identified on one image appear quite different on images acquired 12 hours later. The selection of reproducible control points associated with various features can thus be a difficult task and one subject to substantial error. HCMM data also present an additional problem because the 500 m digital resolution masks many distinctive features--primarily cultural--that can be seen on the 80 m resolution Landsat data.

We have experimented with several potentially promising techniques and this has led to our selection of a fairly simple scheme for registration (Watson and others, 1982). We discovered that a satisfactory registration could be accomplished by careful selection of control points and a single affine transformation. This method is somewhat similar to the scheme employed by NASA (Price, 1982), which involves creating triangular regions with the control points at the vertices and an affine transformation applied to each region. Because the coefficients of the transformation of each triangle are

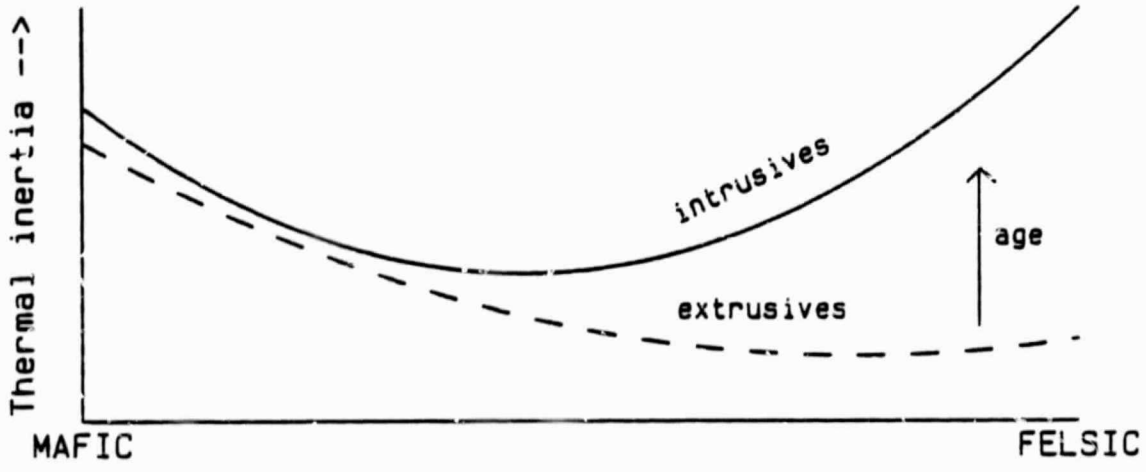

Figure 50.--Proposed model of the therm l-inertia behavior of igneous rocks. It is developed from a need to explain HCMM observed values and tested using selected laboratory data in the literature.

independent, this method minimizes the propagation of errors. It does have the disadvantage, though, that errors caused by inaccurate control points cause non-linear distortions which the user cannot correct without the original data set. In our scheme inaccurate control point effects are minimized because of the least squares fitting employed. In addition any errors that are introduced are linear and thus can be corrected by applying another affine transformation to the data without having access to the original data set.

We are now using an interactive image display system with four image planes in our registration procedure. This system allows us not only to improve the quality of our registrations, but also to significantly reduce the time required to produce them. The procedure employed is to first "rough register" the night to the day image. This is done quickly with a minimum of points (6-8) selected from the images. A simple affine transformation is then applied to the nighttime data, resulting in an image that is approximately in registration with the daytime data. The three "rough registered" images, day visible, day thermal, and night thermal, can then be viewed on our image display system. We then enlarge a selected portion of each image using a magnification of four. The nighttime image is translated using a "roam" capability until the day scene and the night scene do not seem to move when we alternately view the images on the screen. We are not limited to isolated features for control in this method but employ the entire pattern. Even in areas lacking distinct features, control can still be obtained by "matching shapes" (a sort of visual cross-correlation), and a single control point is then selected from the area to represent this optimum match. Another advantage of our display system is that it can be used to obtain the coordinates of any point using an illuminated cursor, thus eliminating

inaccuracies from mechanical scale measurements. Because of the capabilities of zooming and roaming images and cursor digitizing, we can--with little difficulty--obtain a fairly evenly spaced grid of control points over an entire image. These control points are used to determine the coefficients of the final transformation, which is then directly applied to the "roughly registered" nighttime data.

The technique appears to be fairly successful. In many cases the residual errors are a pixel or less and our processing time has been reduced to a fourth that of the old technique. We have successfully employed this technique to register HCMM images to digital terrain data and the Landsat data. We have also discovered in some cases the need for a quadratic correction along scanlines from examination of residual plots.

4 CONCLUSIONS

In a somewhat general sense we have found that a thermal-inertia image provides an approximate "outcrop" map. This applies to vegetation covered terrain as well, where we observe resistant ridges, peaks and knolls to have characteristically higher thermal inertias. In outcrop areas where the vegetation cover is not too extensive, we see substantive differences among the thermal inertias of some sedimentary rock types, ranking from highest to lowest values: quartzites and orthoquartzites > dolomites > limestones and shales. This is in agreement with predictions based on laboratory thermal property values (Miller and Watson, 1977). The thermal inertias of igneous rock outcrops are more closely grouped, with granites having the highest values. We have developed a model of the behavior of igneous rocks that is consistent with the observed satellite thermal inertias and selected laboratory data based on three constituents: quartz, glass and mafic minerals.

The lower elevation, non-bedrock areas examined in our western test sites in the Basin and Range have little vegetation cover and appear to display thermal-inertia differences which we believe are primarily due to density and/or moisture content differences, a conclusion based largely on literature data (Watson, 1981). We have noted that the lowest thermal-inertia values observed are generally associated with the lowest elevations except where anomalies due to surface water occur. In some areas we have found that the low thermal-inertia areas have a higher sand content, which will cause a lower density and a higher permeability (to aid in water run off). We also see thermal-inertia contrasts in alluvium that suggest relationships to deeper features, such as pediments and faults.

In terms of the potential for obtaining new geologic information, the HCMM images have been more useful in detecting linear features than in discrimination of materials. We have now discovered three long (>100 km), previously unrecognized linear features in the Powder River Basin, the Colorado Plateau-Basin and Range, and the Overthrust Belt. These are features that were initially detected on HCMM data and not identified on geologic maps. Supporting evidence for geologic control was found on a variety of other maps, such as gravity, magnetic, topographic, and detailed geologic. In addition, lineament studies in the several regions indicate that HCMM data are complementary to Landsat data, providing a more synoptic look, emphasizing different azimuthal directions, and sensing geologic aspects in vegetated terrain that are obscured in Landsat data.

A number of techniques have been developed or refined from previous studies. A simplified thermal model, employing a half wave heating approximation, has been extended to include the effects of topographic slope and elevation. A lineament distribution plot has been developed which has general application to the analysis of linear features, including fault maps, and aircraft and space images. Registration procedures to match HCMM, Landsat, digital terrains, and various geologic and geophysical maps have been refined and the limitations identified for several diverse areas of complex geology and terrain. This has turned out to be an essential element in support of the HCMM studies because we have discovered that interpretation of the thermal-inertia images and, in particular, the evaluation of new features has required cross comparisons with many types of data at widely varying scales.

5 REFERENCES

Anderson, A. L., 1948, Role of the Idaho batholith during the Laramide orogeny, Economic Geology, v. 43, p. 84-99.

Badgley, P. C., 1962, Analysis of structural patterns in bedrock: Society Mining Engineers Transactions, v. 223, no. 4, p. 381-389.

Berry, G. W., Grim, P. J., and Ikelman, J. A., (compilers), 1980, Thermal springs list for the United States: NOAA Key to Geophysics Records Documentation, No. 12, Boulder, Colorado.

Cater, F. W., Pinckney, D. M., Hamilton, W. B., Parker, R. L., Welding, R. D., Close, T. J., and Zilka, N. T., 1973, Mineral resources of the Idaho Primitive area and vicinity, Idaho: U.S. Geological Survey Bulletin 1304.

Connard, G., Couch, R., and Gemperle, M., 1983, Analyses of aeromagnetic measurements from the Cascade Range in Central Oregon: Geophysics, v. 48, n. 3, p. 376-390.

Christiansen, R. L., and McKee, E. H., 1978, Late Cenozoic volcanic and tectonic evolution of the Great Basin and Columbia Intermontane regions, in Smith, R. B., and Eaton, G. P., eds., Cenozoic tectonics and regional geophysics of the western Cordillera: Geological Society of America Memoir 152, p. 283-311.

Cordell, Lindrith, 1978, Regional geophysical setting of the Rio Grande Rift: Geological Society of America Bulletin, v. 89, p. 1073-1090.

Dohrenwend, J. C., 1982, Surficial geologic map of the Walker Lake 1^{o} by 2^{o} quadrangle, Nevada-California: U.S. Geological Survey Miscellaneous Field Studies Map, MF-1382-C.

Goodyear Aerospace, 1973, Developing earth resources with synthetic aperture radar, GIB-9290D: Littefield Park, Arizona, 35 p.

Hildenbrand, T. G., Simpson, R. W., Godson, R. H., and Kane, M. F., 1982, Digital colored residual and regional Bouguer gravity maps of the Conterminous United States with cut-off wavelengths of 250 km and 1,000 km: U.S. Geological Survey Geophysics Investigations Map GP-953-A, 2 sheets, scale 1:7,500,000.

Jerome, S. E., and Cook, D. R., 1967, Relation of some metal mining districts in the western United States to regional tectonic environments and igneous activity: Nevada Bureau of Mines, Bulletin 69, 35 p.

King, B. P., and Beikman, H. M., compilers, 1974, Geologic map of the United States (excluding Alaska and Hawaii): U.S. Geological Survey, 2 sheets, scale 1:2,500,000.

Knepper, D. H., 1982, Lineaments derived from analysis of linear features mapped from LANDSAT images of the Four Corners Region of the southwestern United States: U.S. Geological Survey Open-File Report, 82-849, p. 79.

Konizeski, R. L., McMurtrey, R. G., and Brietkrietz, A., 1968, Geology and ground-water resources of the Deer Lodge Valley, Montana, with a section on Gravimetric Survey by E. A. Cremer III, U.S. Geologic Survey Water-Supply Paper 1862, 55 p.

Krohn, M. D., and Phillips, J., 1982, A principal component enhancement for Landsat images: possible structural application in vegetated Virginia Piedmont (abs.): American Association of Petroleum Geologists Bulletin, v. 66, no. 5, p. 590.

Lyden, Charles, J., 1948, The gold placers of Montana: Montana Bureau of Mines and Geology, Memoir 26, 152 p.

McMannis, W. S., 1959, Salient tectonic features of western Montana: Guidebook to field trips, Geological Society America, Rocky Mountain Section (Pub. by Montana State University, Missoula), p. 71-75.

Miller, S. H., and Watson, K., 1977, Evaluation of algorithms for geological thermal-inertia mapping: Proceedings 11th International Symposium on Remote Sensing of Environment, v. 2, p. 1147-1160.

Mixon, R. B., and Newell, W. R., 1982, Mesozoic and Cenozoic compressional faulting along the Atlantic Coastal Plain margin, Virginia: in P. T. Lyttle, ed., Central Appalachian Geology Field Trip Guidebooks NE-SE, Geological Society of America, p. 29-54.

Offield, T. W., 1975, Thermal-infrared images as a basis for structure mapping, Front Range and adjacent plains in Colorado: Geological Society of America Bulltein, v. 86, p. 495-502.

O'Neill, J. M., and Lopez, D. A., 1983, Great Falls lineament, Idaho and Montana (abs.): APPG-SEPM-EMD Rocky Mountain Section Meeting, Billings, MT, September 18-21.

Pavlides, L., 1981, The Central Virginia Volcanic-Plutonic Belt: An island arc of Cambrian(?) Age: U.S. Geological Survey Professional Paper 1231-A, 34 p.

Price, J. C., 1982, Registration of Heat Capacity Mapping Mission day and night images-Forum: Photogrammetric Engineering and Remote Sensing, v. 48, no. 9, p. 1466-1467.

Purdy, T. L., and Rowan, L. C., 1983, written communication.

Raines, G. L., Erdman, J. A., McCarthy, J. H., and Reimer, G. M., in press, Remotely sensed limonite anomaly on Lordsburg Mesa, New Mexico: possible implications for uranium deposits: United Nations Special Publication.

Richardson, C. J., 1981, Pocosin Wetlands, Hutchinson Ross Publishing Co., Stroudsburg, PA, 364 .

Richter, D. H., W. N. Sharp, K. C. Watts, G. L. Raines, B. B. Houser, and D. P. Klein, 1983, Mineral resource assessment of the Silver City 1° x 2° quadrangle, New Mexico-Arizona: U.S. Geological Survey Open-File Report 83-924.

Rouse, J. W., Haas, R. H., Schell, J. A., and Deering, D. W., 1973, Monitoring vegetation systems in the great plains with ERTS: Third ERTS Symposium, NASA SP-351, v. 1, p. 309-317.

Rouse, J. W., Haas, R. H., Schell, J. A., Deering, D. W., and Harlan, J. C., 1974, Monitoring the vernal advancement and retrogradation (greenwave effect) of natural vegetation: NASA/GSFC Type III Final Report, Greenbelt, Md, 371 p.

Roy, R. F., Beck, A. E., and Touloukian, Y. S., 1981, Thermophysical properties of rocks, in Chap. 12 in Physical Properties of Rocks and Minerals: McGraw Hill Book Co., 548 p.

Rowan, L. C., Offield, T. W., Watson, Kenneth, Cannon, P. J., and Watson, R. D., 1970, Thermal infrared investigations, Arbuckle Mountains, Oklahoma: Geological Society of America Bulletin, v. 81, p. 3549-3562.

Rowan, L. C., and Wetlaufer, P. N., 1981, Relation between regional lineament systems and structural zones in Nevada: American Association of Petroleum Geologists Bulletin, v. 65, no. 8, p. 1414-1432.

Rowan, L. C., and Purdy, T. L., 1982, Remote sensing studies in the Walker Lake, California-Nevada 1° x 2° quadrangle: U.S. Geological Survey Miscellaneous Field Studies Map, MF-1382-P.

Ruppel, E. T., 1982, Cenozoic block uplifts in east-central Idaho and southwest Montana: U.S. Geological Survey Professional Paper 1224, 24 p.

Ruppel, E. T., O'Neill, J. M., and Lopez, D. A., 1982, Preliminary geologic map of the Dillon 2° quadrangle, Montana and Idaho: U.S. Geological Survey Open-File Report, 83-168, 2 sheets.

Sabins, F., 1969, Thermal infrared imaging and its application to structural mapping, southern California: Geological Society of America Bulletin, v. 80, pp. 397-404.

Sauck, W. A., and Sumner, J. S., 1970, Residual aeromagnetic map of Arizona: University of Arizona, Tucson, Arizona, scale 1:1,000,000.

Shoemaker, E. M., Hackman, R. J., and Eggleton, R. E., 1962, Interplanetary correlation of geologic time: Advances in the Astronautical Sciences, v. 8, Published by Plenum Press, Inc., 227 West 17 St., New York.

Siegal, B. S., and Goetz, A.F.H., 1977, Effect of vegetation on rock and soil type discrimination: Photogrammetric Engineering and Remote Sensing, v. 43, no. 2, pp. 191-196.

Simpson, R. W., Hildenbrand, T. G., Godson, R. H., and Kane, M. F., 1982, A description of colored gravity and terrain maps for the conterminous U.S.: U.S. Geological Survey Open-File Report 82-0477.

Society of Exploration Geohysicists, 1982, Gravity anomaly map of the United States exclusive of Alaska and Hawaii: Scale 1:2,500,000, 2 sheets.

Steven, T. A., and Morris, H. T., 1983, Geologic map of the Richfield 1° by 2° quadrangle, west-central Utah: U.S. Geological Survey Open-File Report 83-583, scale 1:250,000.

Titley, S. R., 1981, Geologic and geotectonic setting of porphyry copper deposits in the southern Cordillera, 1981: Arizona Geological Society Digest, VXIV, (N. R. Dickenson and W. D. Payne, eds.), Tucson, Ariz., p. 79-94.

Trask, N. L., Rowan, L. C., and Krohn, M. D., 1977, Lineament map of parts of Virginia, North Carolina and South Carolina: U.S. Geological Survey Open-File Report 77-434.

Tucker, G. J., 1979, Red and photographic infrared linear combinations for monitoring vegetation: Remote Sensing of Environment, v. 8, pp. 127-150.

Tyrrel, F. W., 1929, The principles of petrology, second edition: Datan and Co., Inc., p. 82.

Wallace, C. A., Schmidt, R. G., Waters, M. R., Lidky, D. J., and French, A. B., 1981, Preliminary geologic map of parts of the Butte 1 degree x 2 degree quadrangle, Central Montana: U.S. Geological Survey Open File Report 81-1030.

Wallace, R. E., Griggs, A. B., Campbell, A. B., and Hobbs, S. W., 1960, Tectontic setting of the Coeur d' Alene District, Idaho: U.S. Geological Survey Professional Paper 400, p. B25-27.

Warren, D. H., 1969, A seismic refraction survey of crustal structure in central Arizona: Geological Society America Bulletin, v. 80, p. 257-282.

Waters, M. R., 1982, oral communication.

Watson, K., 1981, Application of HCMM data to regional geologic analysis for mineral and energy resource evaluation: NASA proposal, HCMM Investigations, 49 p.

_____ 1983, Thermal-inertia mapping from space (abs.): International Colloquium on Spectral Signatures, Bordeaux (France), 12-16 September 1983, p. G.11.6.

Watson, K., Hummer-Miller, S., and Offield, T. W., 1981, Geologic applications of thermal-inertia mapping from satellite: U.S. Geological Survey Open-File Report, 81-1352, 72 p.

Watson, K., Hummer-Miller. S., and Sawatzky, D. L., 1982, Registration of heat capacity mapping mission thermal satellite images: Photogrammetric Engineering and Remote Sensing, v. 48, no. 2, pp. 263-268.

Watson, Kenneth, 1982a, Radiative transfer from a homogeneous half-space: A fast algorithm solution: U.S. Geological Survey Open-File Report 82-986, 7 p.

Watson, Kenneth, 1982b, Regional thermal-inertia mapping from an experimental satellite: Geophysics, v. 47, no. 12, p. 1681-1687.

Weidman, R. M., 1965, The Montana lineament: Billings Geological Society 16th Annual Field Conference, p. 137-143.

Williams, H., Turner, F. J., and Gilbert, C. M., 1954, Petrology: Freeman and Co., Inc., p. 15 and 308.

Young, E. J., and Olhoeft, G. R., 1976, Relations between specific gravity and chemical composition for a suite of igneous and metamorphic rocks: U.S. Geological Survey Open-File Report 76-809, 14 p., 2 pls.

Zietz, I., and Kirby, J. R., 1972, Aeromagnetic map of Colorado: U.S. Geological Survey Geophysics Investigations Map GP-880, scale 1:1,000,000.

Zietz, I., Gilbert, F. P., and Kirby, J. R., Jr., 1978, Aeromagnetic map of Idaho: Color coded intensities: U.S. Geological Geophysical Investigations Map GP-920, scale 1:1,000,000.

Zietz, I., Gilbert, F. P., and Snyder, S. L., 1980, Aeromagnetic map of Montana: In color: U.S. Geological Survey Geophysical Investigations Map GP-934, scale 1:1,000,000.